DISSERTATION

CHAINED SWEET: NANOCONFINEMENT OF CARBOHYDRATES

Submitted by

Benjamin P. Wiebenga-Sanford

Department of Chemistry

In partial fulfillment of the requirements

For the Degree of Doctor of Philosophy

Colorado State University

Fort Collins, Colorado

Fall 2017

Doctoral Committee:

Advisor: Nancy Levinger

Ellen Fisher
George Barisas
Carmen Menoni
James Graham

ABSTRACT

CHAINED SWEET: NANOCONFINEMENT OF CARBOHYDRATES

Sugars and other carbohydrates play critical roles in a vast array of chemical and biological systems. In biological systems, the carbohydrates' environments are highly heterogeneous, including interfaces in cells and subcellular organelles, and on proteins. Nanoconfined aqueous environments also feature in these naturally and artificially occurring systems. The studies reported here explore glucose and other carbohydrate molecules, specifically ethylene glycol, glycerol, meso-erythritol, xylitol, sorbitol, myo-inositol, and trehalose, in the nanoconfined environments offered by reverse micelles, also referred to as water-in-oil mocroemulsions. I investigate how the nanoconfinement affects the carbohydrate behavior and how the carbohydrates affect the reverse micelles. I report the effect of carbohydrates on report the loading-ability of carbohydrates into the reverse micelles, demonstrate the location of the carbohydrates in the reverse micelle water pools, and show an unexpected effect where the carbohydrates to add to the reverse micelle volume without appearing to take up space. I use EXSY or Z-Z exchange spectroscopy to show that that the exchange rate between water and carbohydrate hydroxyl groups is substantially slower than it is in bulk aqueous solution and that it does not depend on hydrogen bonding between the carbohydrate and surfactant headgroup. These reverse micellar environments can provide unique platforms for confinement and as model systems for biological constructs. Results from these studies provide fundamental information to help us understand, predict and control carbohydrates, in particular glucose, in biological systems. Finally, I report on experiments utilizing steady-state fluorescence spectroscopy to characterize the nature of the reverse micellar interior, specifically the local "viscosity" via the response of a dye probe molecule. I also detail experiments that aimed to measure the aggregation number, that is, the number of surfactant molecules in the reverse micelles of varying water and carbohydrate loading. Although interesting, these studies did not yield the desired results.

ACKNOWLEDGEMENTS

Thanks to Dr. Nancy Levinger

For beliving in me when I didn't.

And teaching me more than I thought possible.

Additional Thanks to:

Mr. Benjamin Kohn

Dr. CW Rithner

Dr. Joseph DiVerdi

Dr. Debbie Crans

Dr. Rich Cole

Jack and Brett, Eddie and Derek

Tania, Daniel, Trevor

Kristen, Tuck, Ryan

Thank you mom and dad

DEDICATION

for jon

gone, not forgotten

TABLE OF CONTENTS

Chapter 1

Sweet As Can Be

1.1 Walking On The Sweet Road

Sugars and carbohydrates are ubiquitous in biology. Sugars usually serve as metabolic fuel sources, or generic polymer subunits for structural elements like cellulose in plant cell walls. In addition, sugars play an active role in biological processes, including cell-cell communication and signaling[1], as a forest of glycoproteins on cell surfaces, particularly cancer cells[1–3], modulating cell function[4], or acting as cryo- or lyoprotectants[5]. Researchers have explored many different properties of bulk carbohydrate-water solutions finding, for example, that interactions with sugars strongly affects water dynamics[6–10], but not water structure[7,11]. However, in the crowded environment inside cells or on the surface of proteins, the nature of the water-sugar interaction is much less clear. Complicating the desire to investigate the interior of a cell organelle is the exceptionally diverse, complex, crowded and confining environment that all biomolecules in living cells occupy. This is unfortunate for studies focused on these environments because crowded systems, including biologically relevant ones like cells, cell organelles, and hydrophilic pockets in macromolecular structures (like proteins), molecular dynamics - translation and rotation - can differ significantly from bulk solution and impact reaction rates[12]. This means that insights gained from experiments with carbohydrates in bulk solution are not at all guaranteed to transfer to their behavior in confined systems. Thus, measuring the interaction of sugars with water directly in a confined or croweded environment provides insight to help understand the role of sugars in biology.

To bring the complications of a confined environment down to a manageable level, I use a model confined system to explore the behavior of carbohydrates, particularly glucose, in a confined aqueous environment. My model system of choice is the reverse micelle (RM, see Fig. 1.1). These are spontaneously self-assembled nanoscopic polar droplets stabilized by a surfactant in a bulk non-polar liquid[13]. RMs provide a convenient and flexible platform to explore the effect

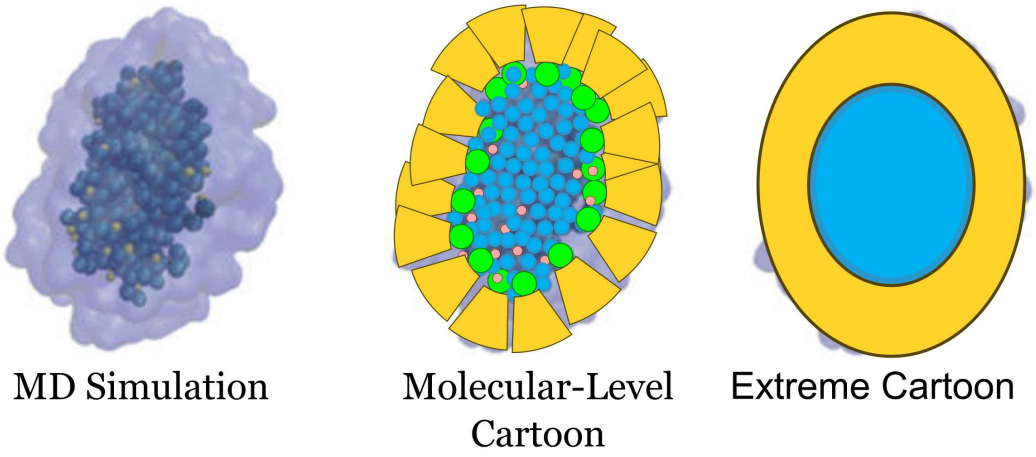

Figure 1.1: Three different depictions a reverse micelle. In all cases, the nonpolar solvent is omitted for clarity. Left: molecular dynamics simulation of a w_0=7.5 RM with 64 AOT molecules from Eskici and Axelsen.[15] Middle: a cartoon of individual water molecules, surfactant head and tail groups, and counterions overlaid on the MD simulation. Right: an extreme cartoon of a water pool surrounded by surfactant. Each depiction of RM differs wildly in detail, but they all maintain the essential character of an inner water pool stabilized by surfactant within a (implied) nonpolar phase and each can be interchanged with another depending on which level of detail is both necessary and sufficient for the current discussion.

of confinement because their particle size distributions are relatively monodisperse and they have many parameters that can be adjusted such as particle size, concentration, and surfactant character. In the majority of the following studies, I will be using a popular RM system consisting of water and AOT surfactant in isooctane (2,2,4-trimethylpentane), whose molecular structures are shown in (Fig. 1.2). RM size is characterized with the parameter w_0=[H_2O]/[AOT];[13,14] if the particles are spherical on average, w_0 is directly proportional to the particle diameter. Water pool diameters for AOT RMs range from approximately 0.5 to 5 nm.

These artificial RM confined environments have advantages and disadvantages (like almost everything in life). On the plus side, these systems are very easy to prepare and handle (great for passing to undergraduates). They quite literally make themselves, and are stable over exceptionally long periods*. This is especially true for RMs prepared using using AOT (sodium di-ethylhexylsulfosuccinate) surfactant[14], considered the bulletproof gold standard for RM pro-

*Anecdotally RM samples, properly stored, have been found stable and unchanged nearly a decade after being placed in storage. Considering the primary enemy of an AOT/H_2O/Isooctane RM is evaporation, proper storage is a relatively easy task.

duction. A plethora of experimental and simulation studies provide a wealth of information about them[12,14–25] that makes it easy to find information you need, as well as easy to get overconfident about the depth of knowledge available for them. The disadvantages are not as obvious to those just seeking a confining environment. RMs have minuscule proportions, from 2-20 nm in diameter. Putting the very largest RMs on the same scale as the smallest while virus capsids[26], or mitochondrial cristae.[27] They are much smaller than biological cells where intracelluar water displays many properties similar to bulk water.[28–32] Because the amphiphilic surfactant layer dividing polar and nonpolar phases is just a monolayer, it lacks the order seen in lipid bilayers comprising cell membranes, or even AOT at a planar interface[33]. Perhaps more importantly, permeation across the amphiphilic layer differs from passive transport across cell membranes because water soluble species cannot escape across the interface into the nonpolar solvent.

With the limitations of the RM model considered, we report the creation and characterization of AOT RMs encapsulating aqueous carbohydrate solutions, especially D-glucose, as well as ethylene glycol, glycerol, meso-erythritol, xylitol, sorbitol, myo-inositol, and trehalose, whose molecular structures are shown in Fig. 1.5. For the purposes of this dissertation, I will use a broad umbrella definition of carbohydrate to include saccharides (general molecular formula, $C_n(H_2O)_m$), and their reduced sugar alcohol cousins, (generally $HOCH(C_n(H_2O)_m)CHOH$). I explore how these carbohydrates, particularly glucose, impact the RMs and how the RMs impact the carbohydrates. I present information about the effect of carbohydrates on the size of the RMs, the loading limit or "solubility" of the carbohydrates in AOT RMs, their location in the samples determined from one and two dimensional (1D and 2D) NMR experiments, the effect of nanoconfinement on proton exchange between water and carbohydrates, and the effect of glucose on water pool viscosity as well as aggregation number. From this wide range of data, I can develop a comprehensive picture of carbohydrates in confining environments that makes significant implications for the nature of carbohydrates in biological confinement.

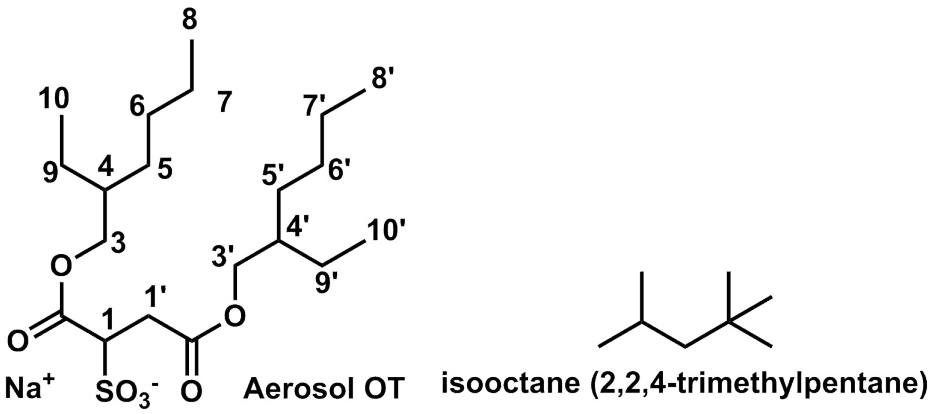

Figure 1.2: AOT and isooctane; the gold standard of reverse micelle formulation[34].

1.2 A Quick Introduction to Reverse Micelles

Reverse micelles present easily prepared and well characterized model systems to invoke nanoconfinement. And[14,21,35] At a minimum, RMs comprise a ternary mixture of insoluble polar and nonpolar phases bridged by an amphiphilic layer. Traditionally, water is the polar phase but often other molecules are introduced into the RM polar phase, such as proteins[36] or molecular reporters whose light absorption and emission,[37] or interaction with magnetic fields[37,38] report details through various spectroscopies. Other non-aqueous polar liquids such as ethylene glycol, glycerol, formamide, dimethylformamide, aqueous mixtures[39–41], and some ionic liquids[42] can also form RMs. In some cases, RM formation requires more than three components, e.g. a cosurfactant, to form a stable microemulsion with isolated polar solvent droplets. This is particularly true for single chain surfactants that are highly effective for normal micelle formation but have an unsuitable geometryt for forming RMs e.g. sodium dodecylsulfate (SDS) and cetyltrimethylammonium bromide (CTAB).

Reverse micelles are characterized by the term w_0, defined as the mole ratio of water to surfactant which, if the two components are in the same solution, is also equal to the ratio of concentrations in molarity or molality. As the interior volume of an RM is comprised of water molecules while the outer surface is surfactant, the w_0 term is proportional to $\frac{Volume}{Area}$. Assuming that reverse micelles are spherical allows w_o to be related to particle radius via:

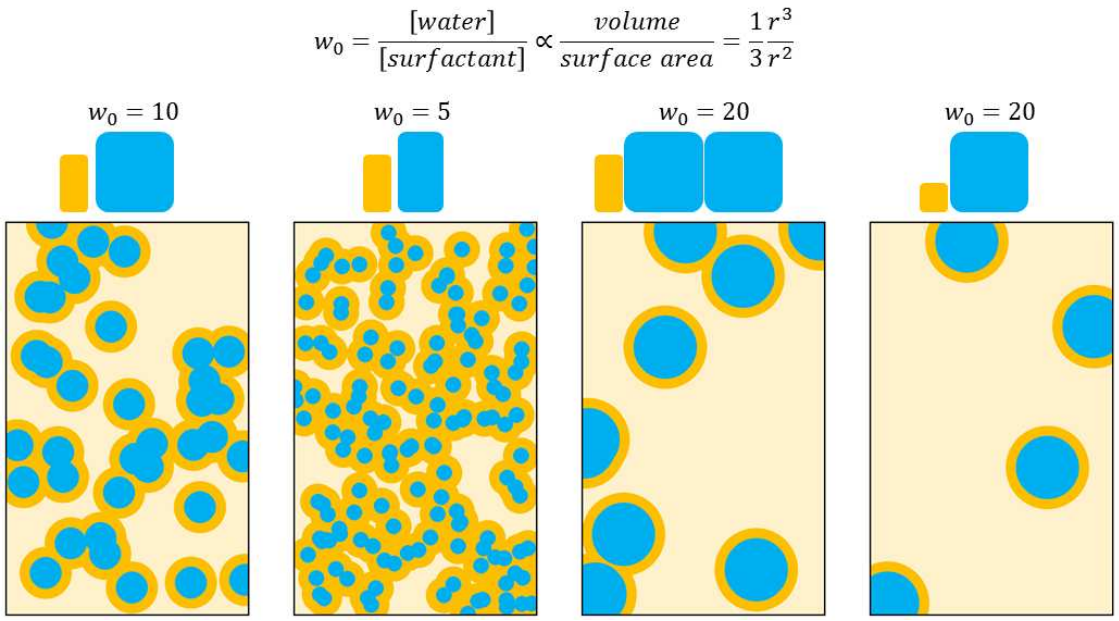

Figure 1.3: Changing w_0 changes more than just RM size, it also changes the particle concentration. Halving the w_0 from 10 (far left) to 5 (middle left) with a constant surfactant concentration reduces particle surface area while keeping total surface area constant, resulting in 4x increase in RM concetration. Doubling the w_0 from 10 to 20 results in 1/4 the RM concentration if surfactant concentration (e.g. total surface area) is kept constant (middle right), or 1/8 if water (total volume) is kept constant (far right).

$$w_o = \frac{N_{water}}{N_{surf}} = \frac{[H_2O]}{[AOT]} = \frac{N_{H_2O}\overline{V}_{H_2O}}{N_{AOT}\overline{A}_{AOT}} = \frac{V_{sphere}}{A_{sphere}} = \frac{\frac{4}{3}\pi r^3}{4\pi r^2} = \frac{1}{3}r$$

where $\overline{V}_{H_2O}$ and $\overline{A}_{AOT}$ being the molar volume and molar area of water and AOT, respectively. Using the density of bulk water provides an estimate for $\overline{V}_{H_2O}$ of 30 $\mathring{A}^3$, while the average head-group area of an AOT molecule is calculated to be 55 $\mathring{A}^2$[15]. These numbers give an average radius of 5.45 $\mathring{A}$ for a w_0 =10 AOT RM. Importantly, this is the diameter of the water pool and does not include the outer layer of surfactant tails and is therefore smaller than the hydrodynamic diameter, which is what dynamic light scattering (covered in Chapter 2) measures. RM solutions are quite dynamic and changing w_0, surfactant concentration, or water concentration has an effect on both particle size and number of particles in solution (Fig. 1.3)

1.2.1 AOT, Isooctane, and Water: Why This Mixture in Particular?

The simple answer is cost and ubiquity. Aerosol OT (AOT) is common food additive and emulsifier, one of the most widely used laxatives in the world (check any bottle of stool softener pills and it's likely to list docusate sodium, another name for AOT, as the active and only ingredient), and actual tons of AOT were dumped into the gulf of Mexico during the 2010 Deepwater Horizon oil spill to hide BP's shame[43]. Isooctane is the petroleum industry standard to which gasoline is compared when determining octane ratings. And finally, water is water: the most common molecule on Earth's surface and one of the most important biomolecules[44]. The more complicated answer is that AOT is an ideal surfactant for making reverse micelles (RMs) due to its shape... and it's cheap. AOT can form stable RMs at concentrations as high as 1 M AOT and a w_0 = 0.5-50[45]while other surfactants may only be stable at concentrations below 0.05 M and w_0 = 2-12, or even a maximum of 4[42]. This is due to AOT's highly branched aliphatic tail structure and conical molecular shape which makes it ideal for packing into spherical shapes with the polar head group pointing inward, as shown in fig 1.4. Surfactant geometry directly contributes to suitability for different purposes. Narrow, long chain surfactants such as cetyltetraamoniumbromide (CTAB) have difficulty forming structures other than micelles. Blockier surfactants such as DOPC can form micelles and reverse micelles, but are ideal for lamellar structures (such as cell walls). AOT and other conical surfactants form stable reverse micelles due to being naturally shaped like a section of a spherical shell. Surfactants with geometries similar to AOT work just as well[34] and there is no special significance to the surfactant tails branching at carbon 4 and 4' vs 4 and 5', or being 2 carbon chains vs 3 carbon, or a 2 and a 3; it just happens that AOT is the most easily available surfactant and gets the job done.

1.2.2 Properties of Reverse Micelles

There are thousands of papers that have been written about the physical characteristics of RMs, their ability to act as nanoreactors[39,47], confinement of biomolecules[48,49], computer modeling[15,50].

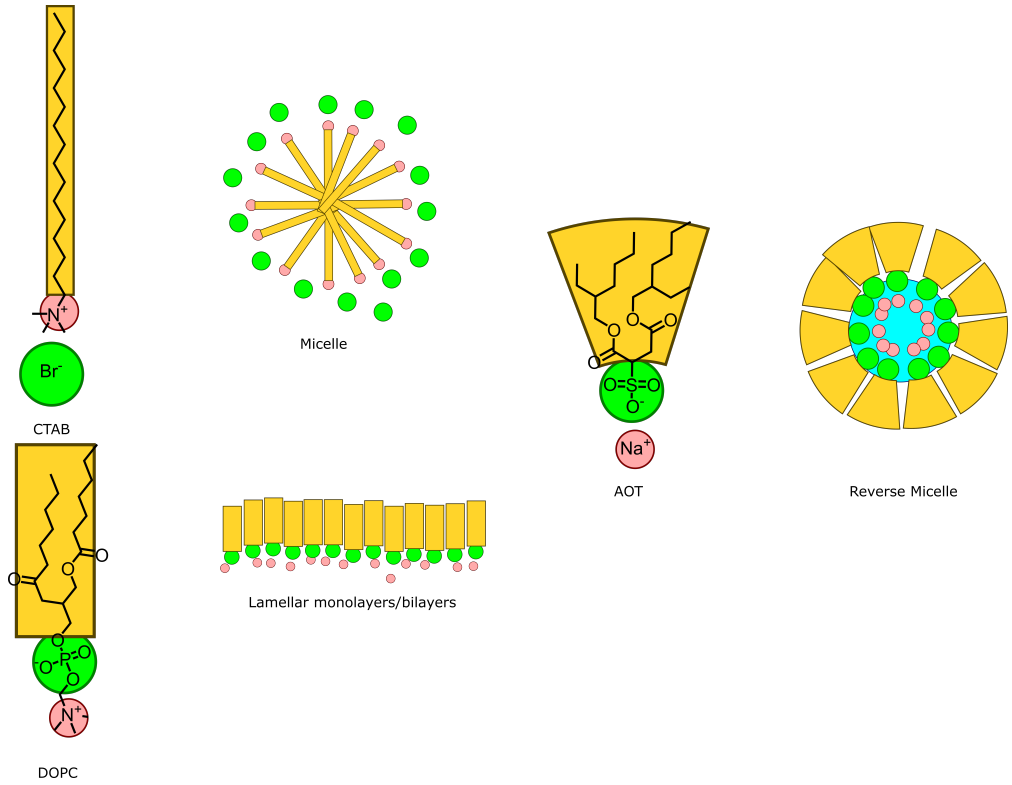

Figure 1.4: Long, narrow, surfactants such as CTAB are suitable for forming micelles, but are unstable when attempting to make RMs. Conical surfactants form much more stable RMs due to having a suitable geometry. DOPC and similar surfactants occupy a middle ground.

Out of this massive body of work, there are three characteristics of AOT RMs that are especially important to the data presented in the following chapters:

1. Water in the RM interior is divided between a "core" of with similar rotational dynamics to bulk water[18,24,51] and "shell" water near the water-AOT interface with highly restricted motion dynamics.

2. AOT counterions are primarily located at the RM interface due to electrostatic interactions with the sulfonate headgroups[12,19,22].

3. There is a strong proton gradient consisting of high proton density at the interface tapering to something approaching neutral water at the core of an AOT RM. This could be called a pH gradient save that pH is not a meaningful term when the H_3O^+ concentration may only approach one hydronium ion per ten reverse micelles.[16,52]

This change in water behavior through the interior of a RM is important when dealing with carbohydrates (or any other molecule put into the RM environment, really) as there is a significant difference between merely being "in the water pool" and being in the central "core" region of the RM vs being adsorbed to the surface dealing with "shell" water and the high ionic strength of a proton gradient, sulfonate headgroups, and sodium counterions.

1.3 Carbohydrates

Carbohydrates are defined by their molecular formula "motif" of$C_m\left(H_2O\right)_n$ and iconic carbohydrates such as glucose, sucrose, and fructose all follow this formula. Of the molecules I present in Figure 1.5 glucose, trehalose, and myo-inositol are all "true" carbohydrates, while sorbitol and the rest all slightly violate the carbohydrate "motif". Despite this these molecules can all be considered a single carbohydrate "family" linked to each other through glucose. Glucose can take many conformations, but in aqueous solution it is in either the α or β pyranose (six membered ring) form 99.95% of the time[53] with a ~40/60 ratio of α to β. Glucose can also take a furanose (five membered ring) or open chain form but does so only fleetingly. With this in mind,

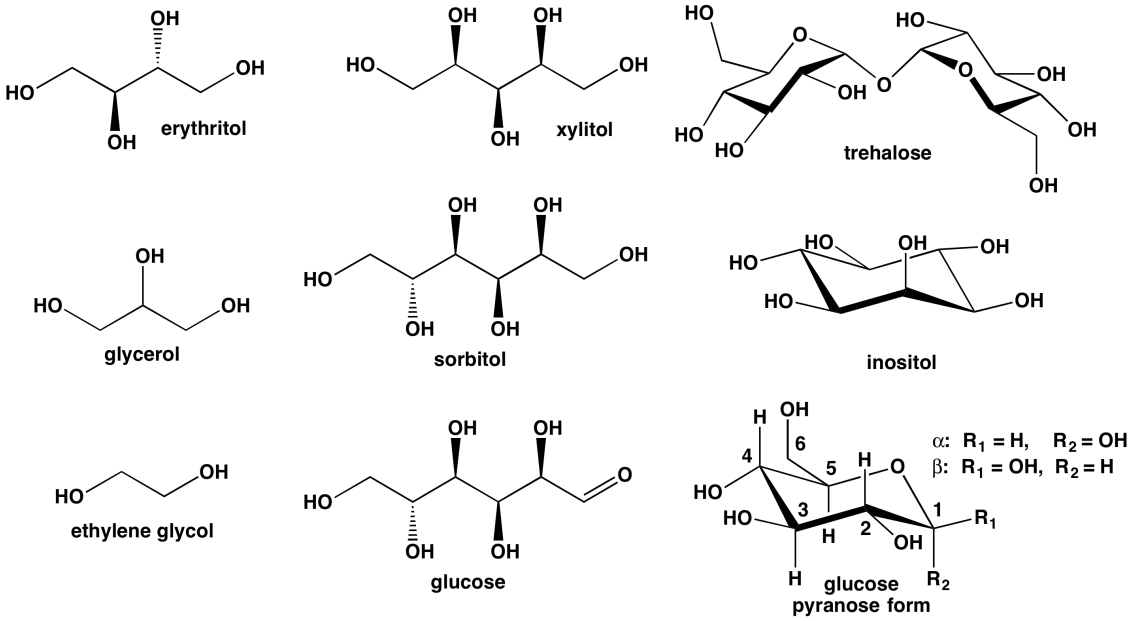

Figure 1.5: The eight carbohydrates studied in this dissertation. Glucose is presented in open-chain aldehyde form to highlihgt its simliarity to sorbitol. 99.5% of the time it is in the α or β pyranose form[53].

the molecules sorbitol and myo-inositol can be thought of as fraternal twins with sorbitol being analogous to glucose in the open chain state, and myo-inositol representing glucose with increased symmetry and no ability to undergo a ring-opening reaction. Ethylene glycol is the most distantly related of the family, being the smallest possible "true" carbohydrate (the only smaller candidate being methanol, a somewhat scandalous suggestion) with glycerol, erythritol, and xylitol being the "missing links" that connect ethylene glycol to the rest of the family tree, one carbon at a time.

Before discussing specific carbohydrates, I define three terms. In this paper, I refer to three types of carbohydrate containing RMs: *Nonaqueous, equivalent,* and *loaded*. The two forms releveant to the work presented in the following chapters are *equivalent* and *loaded* RMs, examples of which are shown in Fig. 1.6

1. *Nonaqueous* RMs: These RMs are prepared with a nonaqueous polar solvent such as ethylene glycol or glycerol in the place of water. Various nonaqueous polar solvents have been demonstrated to facilitate the formation of RMs.[42] Most of the carbohydrates I worked with cannot completely replace water, with only ethylene glycol and glycerol being able to form stable RM emulsions without water present, and even then only at low loading, e.g., $w_{EG} < 2$

or $w_{Glycerol} < 4$. As most of the targets of this study, especially glucose, sorbitol, and trehalose, will not form nonaqueous RMs, this class of carbohydrate RM will only be discussed in passing.

2. w_0 *equivalent* RMs: These RMs are prepared volumetrically, rather than by mass, using an equivalent volume of aqueous solution in place of water. For example, $w_0 = 10$ equivalent RMs containing glucose could be prepared by adding 180 μL of 2 M aqueous glucose in solution in place of 180 μL of millipore water to 10 mL of 0.1 M AOT in isooctane. These solutions are useful for comparison sake between standard RMs and their w_o equivalent of a particular carbohydrate, but they are also relatively time consuming to make compared to the third class of carbohydrate containing RMs.

3. Carbohydrate *loaded* RMs: In these systems, a solution containing RMs prepared with water are added to solid (or liquid) carbohydrate. In these cases the final volume of polar phase has increased compared to the w_o reported for a non-loaded RM. These are the most common carbohydrate RMs I prepared, simply due to the ease of production and the consistency that can be achieved between RM solutions with different carbohydrates. Splitting off multiple aliquots of the same RM solution before loading each one with a different carbohydrate is the most reliable way of ensuring each solution has precisely the same H_2O/AOT ratio with the only change being the character of the carbohydrate added.

Trehalose is related to the other carbohydrates via being a disaccharide of glucose, but also by having a semi-mystical reputation in certain biochemical circles. This stems from the presence of trehalose in certain extremophiles, such as the famously hardy tardigrade which can survive desiccation, freezing, and the vacuum of space thanks, in part at least, to its stores of trehalose[54]. The disaccharide has even been used in commercial applications to preserve blood platelets for treatment of injured soldiers in the field[55]. While it is not the overarching driver of the experiments I performed, I did include trehalose in my experiments specifically because of the reputation that

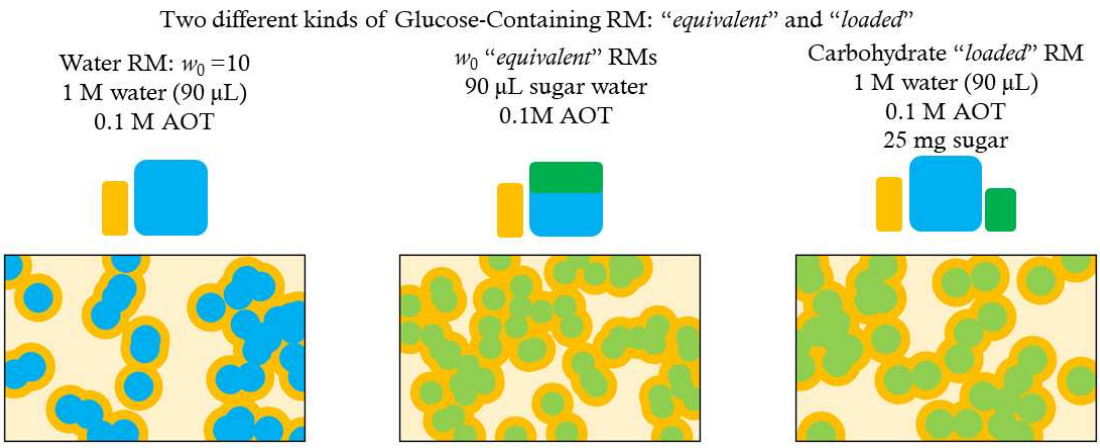

Figure 1.6: Regular RM solutions (left) are made using water and surfactant in oil. w_0 *equivalent* RM solutions (middle) are made with the same volume of polar phase, but as this polar phase is sugar water, the w_0 mole ratio is obviously different. And *loaded* RMs (right) are an RM solution that has had polar phase added to it.

trehalose carries with it, and the hope being that whatever special properties it carries will aid in understanding the role of nanoconfined carbohydrates as a whole.

With these ideas in mind, you can come along with me on a journey of carbohydrate0laden RMs. In which we see strange size reductions when material is added (Ch 2), dramatic changes in viscosity with RM size (Ch 3), discover the location of glucose in an RM (Ch 4), and find that water and carbohydrates have a testy relationship when held in close quarters (Ch. 5).

Bibliography

(1) Rabinovich, G. A.; van Kooyk, Y.; Cobb, B. A. *Annals of the New York Academy of Sciences* **2012**, *1253*, DOI: 10.1111/j.1749-6632.2012.06492.x.

(2) Dimitroff, C. J. *Cancer Res.* **2015**, *75*, 3195–202.

(3) Byrd, J. C.; Bresalier, R. S. *Cancer Metast. Rev.* **2004**, *23*, 77–99.

(4) Bertozzi, C. R.; Kiessling, L. L. *Science* **2001**, *291*, 2357–64.

(5) HubÃ¡lek, Z. *Cryobiology* **2003**, *46*, 205–229.

(6) Talon, U.; Smith, L. J.; Brady, J. W.; Lewis, B. A.; Copley, J. R. D.; Price, D. L.; Saboungi, M. L. *J. Phys. Chem. B* **2004**, *108*, 5120–5126.

(7) Lee, S. L.; Debenedetti, P. G.; Errington, J. R. *J. Chem. Phys.* **2005**, *122*, 204511.

(8) Sidebottom, D. L. *Phys. Rev. E* **2007**, *76*, 011505.

(9) Zhu, L.; Cai, T.; Huang, J.; Stringfellow, T. C.; Wall, M.; Yu, L. *J. Phys. Chem. B* **2011**, *115*, 5849–55.

(10) Shiraga, K.; Suzuki, T.; Kondo, N.; Tajima, T.; Nakamura, M.; Togo, H.; Hirata, A.; Ajito, K.; Ogawa, Y. *J. Chem. Phys.* **2015**, *142*, 234504.

(11) Mason, P. E.; Neilson, G. W.; Barnes, A. C.; Enderby, J. E.; Brady, J. W.; Saboungi, M. L. *Journal of Chemical Physics* **2003**, *119*, 3347–3353.

(12) Harpham, M. R.; Ladanyi, B. M.; Levinger, N. E.; Herwig, K. W. *Journal of Chemical Physics* **2004**, *121*, 7855–68.

(13) Kotlarchyk, M.; Huang, J. S.; Chen, S. H. *Journal of Physical Chemistry* **1985**, *89*, 4382–4386.

(14) De, T. K.; Maitra, A. *Adv. Coll. Interface Sci.* **1995**, *59*, 95–193.

(15) Eskici, G.; Axelsen, P. H. *The Journal of Physical Chemistry B* **2016**, *120*, 11337–11347.

(16) Abel, S.; Sterpone, F.; Bandyopadhyay, S.; Marchi, M. *Journal of Physical Chemistry B* **2004**, *108*, 19458–19466.

(17) Almgren, M.; Johannsson, R.; Eriksson, J. C. *The Journal of Physical Chemistry* **1993**, *97*, 8590–8594.

(18) Balakrishnan, S.; Javid, N.; Weingartner, H.; Winter, R. *Chemphyschem* **2008**, *9*, 2794–801.

(19) Chowdhary, J.; Ladanyi, B. M. *J Phys Chem B* **2009**, *113*, 15029–39.

(20) Eastoe, J.; Robinson, B. H.; Steytler, D. C.; Thornleeson, D. *Adv. Coll. Interface Sci.* **1991**, *36*, 1–31.

(21) Fayer, M. D.; Levinger, N. E. *Annu. Rev. Anal. Chem.* **2010**, *3*, 89–107.

(22) Faeder, J.; Albert, M. V.; Ladanyi, B. M. *Langmuir* **2003**, *19*, 2514–2520.

(23) Nandi, S.; Ghosh, S. K.; Bhattacharya, S. C. *Colloids and Surfaces a-Physicochemical and Engineering Aspects* **2005**, *268*, WOS:000233079200019, 118–123.

(24) Piletic, I. R.; Moilanen, D. E.; Spry, D. B.; Levinger, N. E.; Fayer, M. D. *Journal of Physical Chemistry A* **2006**, *110*, 4985–4999.

(25) Zulauf, M.; Eicke, H. F. *J. Phys. Chem.* **1979**, *83*, 480–486.

(26) Losdorfer Bozic, A.; Siber, A.; Podgornik, R. *J Biol Phys* **2013**, *39*, 215–28.

(27) Frey, T. G.; Mannella, C. A. *Trends in Biochemical Sciences* **2000**, *25*, 319–324.

(28) Jasnin, M.; Moulin, M.; Haertlein, M.; Zaccai, G.; Tehei, M. *Embo Reports* **2008**, *9*, 543–547.

(29) Foglia, F.; Hazael, R.; Simeoni, G. G.; Appavou, M. S.; Moulin, M.; Haertlein, M.; Forsyth, V. T.; Seydel, T.; Daniel, I.; Meersman, F.; McMillan, P. F. *Scientific Reports* **2016**, *6*, 9.

(30) Aslund, I.; Topgaard, D. *Journal of Magnetic Resonance* **2009**, *201*, 250–254.

(31) Natali, F.; Dolce, C.; Peters, J.; Gerelli, Y.; Stelletta, C.; Leduc, G. *Journal of the Physical Society of Japan* **2013**, *82*, 7.

(32) Leterrier, J. F. *Cellular and Molecular Biology* **2001**, *47*, 901–923.

(33) Hensel, J. K.; Carpenter, A. P.; Ciszewski, R. K.; Schabes, B. K.; Kittredge, C. T.; Moore, F. G.; Richmond, G. L. *Proceedings of the National Academy of Sciences* **2017**, 201700099.

(34) Nave, S.; Eastoe, J.; Heenan, R. K.; Steytler, D.; Grillo, I. *Langmuir* **2000**, *16*, 8741–8748.

(35) Levinger, N. E.; Swafford, L. A. *Annu. Rev. Phys. Chem.* **2009**, *60*, 385–406.

(36) Nucci, N. V.; Pometun, M. S.; Wand, A. J. *Nat Struct Mol Biol* **2011**, *18*, 245–9.

(37) Silber, J. J.; Biasutti, A.; Abuin, E.; Lissi, E. *Advances in Colloid and Interface Science* **1999**, *82*, 189–252.

(38) Baruah, B.; Roden, J. M.; Sedgwick, M.; Correa, N. M.; Crans, D. C.; Levinger, N. E. *Journal of the American Chemical Society* **2006**, *128*, 12758–12765.

(39) Burglova, K.; Hlavac, J.; Bartlett, J. R. *Journal of Nanoparticle Research* **2015**, *17*, 17.

(40) Markaryan, S. A.; Sarkisyan, A. R.; Shaginyan, G. A. *Russian Journal of Physical Chemistry A* **2015**, *89*, 1808–1813.

(41) Sargsyan, A. R.; Shahinyan, G. A.; Markarian, S. A. *Russian Journal of Physical Chemistry A* **2014**, *88*, 858–862.

(42) Correa, N. M.; Silber, J. J.; Riter, R. E.; Levinger, N. E. *Chemical Reviews* **2012**, *112*, 4569–4602.

(43) Mathew, J.; Schroeder, D. L.; Zintek, L. B.; Schupp, C. R.; Kosempa, M. G.; Zachary, A. M.; Schupp, G. C.; Wesolowski, D. J. *Journal of Chromatography A* **2012**, *1231*, 46–51.

(44) Ball, P. *Chemical Reviews* **2008**, *108*, 74–108.

(45) Yuan, S.-L.; Cai, Z.-T.; Xu, G.-Y.; Jiang, Y.-S. *Chemical Physics Letters* **2002**, *365*, 347–353.

(46) El Aferni, A.; Guettari, M.; Tajouri, T. *Journal of Solution Chemistry* **2017**, *46*, 89–102.

(47) Kim, D.-W.; Oh, S.-G.; Lee, J.-D. *Langmuir* **1999**, *15*, 1599–1603.

(48) Andrade, S. M.; Costa, S. M. B. *Chemistry â A European Journal* **2006**, *12*, 1046–1057.

(49) Doussin, S.; Birlirakis, N.; Georgin, D.; Taran, F.; Berthault, P. *Chemistry-a European Journal* **2006**, *12*, 4170–4175.

(50) Moilanen, D. E.; Fenn, E. E.; Wong, D.; Fayer, M. D. *Journal of the American Chemical Society* **2009**, *131*, 8318–8328.

(51) Laage, D.; Hynes, J. T. *Science* **2006**, *311*, 832–835.

(52) Crans, D. C.; Levinger, N. E. *Accounts of Chemical Research* **2012**, *45*, 1637–1645.

(53) Roslund, M. U.; TÃ€htinen, P.; Niemitz, M.; SjÃ¶holm, R. *Carbohydrate Research* **2008**, *343*, 101–112.

(54) Hengherr, S.; Heyer, A. G.; KÃ¶hler, H.-R.; Schill, R. O. *FEBS Journal* **2008**, *275*, 281–288.

(55) Wolkers, W. F.; Walker, N. J.; Tablin, F.; Crowe, J. H. *Cryobiology* **2001**, *42*, 79–87.

Chapter 2

Wild Behavior of Captive Carbohydrates

The material presented in this chapter is in preparation for publication. A complete manuscript including topics from this and the next chapter is under final editing and will be submitted to the Journal of Physical Chemistry B with me as first author. Co-authors include Dr. Christopher D. Rithner, Jack B. Washington, Brett Cosgrove, Eduardo Palomares, Derrick Vasquez and Nancy E. Levinger. Jack Washington, Brett Cosgrove, Eduardo Palomares and Derrick Vasquez contributed to solubility and size measurements of the carbohydrate loaded reverse micelles.

2.1 What Happens to a Reverse Micelle when Carbohydrates Are Added to It?

This is the story of carbohydrates in reverse micelles (RMs). Every experiment presented here stems from the intent to put glucose and other carbohydrates in RMs alongside another biomolecule such as proteins, nucleic acids, or even chunks of cellular organelles that need a specific shape to work properly and watch what happens as carbohydrates snuggle up to proteins. Of course, the mere act of putting glucose in RMs turned out to be interesting enough to require research all its own. As I had never worked with glucose or other carbohydrates in RMs I first needed to find out if I could make RMs that contained a significant amount of carbohydrate and what conditions led to stable RM plus carbohydrate solutions. The first thing to try was extremely straightforward: get as much glucose as possible into a RM solution and see if the result is still a solution of reverse micelles. Instantly something became extremely clear: while the solubility of glucose in water is ~3.4 M (0.094 mole fraction)[1] the glucose solutions I could use to make stable RMs had to be 2.5 M or lower to even have a chance of making stable RM particle systems. Additionally when I measured the sizes of the RMs in solutions I made, they consistently showed two strange behaviors: size reduction, and a bimodal distribution including particles much larger

(up to 500x the diameter of the original) than regular RMs when too much glucose was present. This gave me three mysteries: what makes RMs so bad at solvating carbohydrates (a famously water soluble class of molecule), how are the RMs shrinking, and what are these giant particles? In this chapter I describe the preparation of RMs that solubilize glucose, and a range of other carbohydrate molecules as well as the characterization of carbohydrate mixtures that were able to form stable RM emulsions.

2.1.1 Materials and Methods

2.1.1.1 Materials

Aerosol OT (AOT, sodium bis(2-ethylhexyl)sulfosuccinate, also known as sodium docusate, $\geq$99%), isooctane (2,2,4-trimethylpentane, ACS grade and anhydrous), cyclohexane-d_{12} (99.6% isotopic purity), and hexane-d_{14} (98%), as well as the carbohydrates D-trehalose dihydrate, myo-inositol, D-sorbitol, xylitol, meso-erythritol, glycerol, and ethylene glycol (all 99% or $\geq$99% purity) were purchased from Sigma-Aldrich. D-glucose (anhydrous) and toluene (HPLC grade) were purchased from Fisher. All reagents were used as received without further purification. Millipore filtered and deionized water (18.2 MΩ-cm) was used to prepare reverse micelles.

2.1.1.2 Sample Preparation

Unless otherwise stated, all RM solutions were prepared with a surfactant concentration of 0.1 M. I employed two similar methods for producing reverse micelles solutions. The first involved dissolving a measured mass of AOT into approximately half the final volume of nonpolar solvent used for the microemulsion and quantitatively transferring this solution to a volumetric flask. Water was then added by mass to achieve a desired loading, described by $w_0 = {}^{[H_2O]}/_{[AOT]}$. This solution was diluted to the final volume with nonpolar solvent and sonicated for 30-60 minutes. Samples were visually inspected for turbidity; clear samples lacking visible precipitate or phase separation indicated microemulsion formation. For example, 4.446 g AOT, and 1.801 g H_2O diluted with isooctane will make 100 mL of w_0 =10 RM solution with [AOT] = 0.1 M. The second method starts with a 0.500 M AOT stock solution (22.23 g AOT/ 100.0 mL final solution) from which serial

dilutions were used to prepare RM solutions. This method was primarily used for smaller volume solutions. For example, 2 mL AOT stock plus 0.540 g water diluted with isooctane will make 10 mL of $w_0 = 30$ RM solution with [AOT] = 0.1 M.

As discussed in Chapter 1.3, I prepared two separate classes of carbohydrate containing RMs (Fig. 1.6):

1) w_0 *equivalent* RMs: These samples are prepared by adding the equivalent volume of an aqueous solution as water would normally be added. To make w_0 *equivalent* RM solutions, a carbohydrate solution with the desired mole ratio, e.g., 25:1 H_2O:glucose, or 80:1 H_2O:trehalose, was substituted for the Millipore water usually used to prepare samples. As the aqueous carbohydrate solutions have a different density than water (e.g., 1.1g/mL for a 30:1 H_2O:glucose solution vs 1.0 g/mL for pure water at 25°C) they were prepared by volume, rather than mass. So 10 mL of $w_0 = 30$ equivalent glucose RMs would use 540 μL of 30:1 glucose solution, rather than 0.540 g (approximately 0.491 mL of 30:1 solution). This way even though the w_0 of a solution made with 540 μL of glucose solution, it has less water than the 30:1 H_2O:AOT obtained in w_0 =30. The ratio of $\frac{V_{\text{polar phase}}}{A_{\text{surfactant}}}$ is (wait for it...) *equivalent to* a plain water RM with $w_0 = 30$, and therefore it is a w_0 =30 *equivalent* RM solution. This is a standard method used to prepare RMs with probe molecules at low concentration where most of the RMs have only water and the aqueous solution used to prepare the RMs has a density essentially identical to bulk water.

2) Carbohydrate *loaded* RMs: These samples are prepared by adding carbohydrate to RMs that already contain the w_0 defined by water and AOT. Carbohydrate *loaded* RM solutions were produced by first making a large quantity of water-containing RM solution (usually 100 mL). To this solution a desired amount of each carbohydrate was added, by mass, to a 20 mL screw-top scintillation vial followed by an amount of RM solution added via volumetric pipette. For example, 144 mg glucose with 10 mL of w_0 =20 RM solution results in a 25:1 H_2O:glucose loaded RM solution. Solutions of this type are far easier to make, and allow for more consistent comparison between different loading molecules, a majority of DLS experiments were performed with carbohydrate loaded solutions. For carbohydrates other than glucose, I kept the loading to

approximately 20% by mass (approximately 50 mg of carbohydrate for w_0 =10 RMs). The water added sample was produced with the same volume percent as the glucose sample (approximately 15.6 µL of water for 10 mL w_0 =10 RMs) as the density of water is so much lower than that of glucose (1.0 g/mL for water vs 1.6 g/mL for glucose). These solutions were then characterized via dynamic light scattering.

2.1.1.3 Data Collection and Analysis

Dynamic Light Scattering (DLS) experiments were performed on a Malvern Zetasizer Nano (S/N MAL1086566) DLS instrument with Zetasizer software (Ver 7.12). Solutions were prepared as above, with scrupulous care taken to ensure ultraclean, speck-free solutions and glassware, as contaminated (i.e. "dusty") samples are particularly detrimental to the collection of quality DLS data.

NMR experiments were performed on an Inova spectrometer operating at 400MHz for ^{1}H running VNMRJ software (version 4.2). ACD/NMR Processor Academic Edition[2] was used to process all data. Graphing and data processing was performed on custom in-house code written in the Python 2.7 language, using the SciPy toolkit.[3]

2.1.2 The Size of Reverse Micelles Containing Carbohydrates

As combining carbohydrates with RMs was new to me the obvious first experiment was also a simple one: pick a carbohydrate and a reverse micelle solution, add the carbohydrate to it and see if the result is still a reverse micelles. The carbohydrate I chose was glucose, as it is a monosaccharide, readily available from many different suppliers, and an extremely relevant biomolecule. After a few false starts stemming from solubility of glucose in reverse micelles being far lower than expected, I was able to make a series of clear, colorless, homogeneous solutions containing water, AOT, and glucose suspended in isooctane. To determine if these solutions contained reverse micelles, or at least particles with a similar particle size distribution (PSD), DLS is a very powerful technique for the production of any new reverse micelle formulation. Not only is DLS a good way to check for consistency in particle formation, but it is one of the only ways to directly ob-

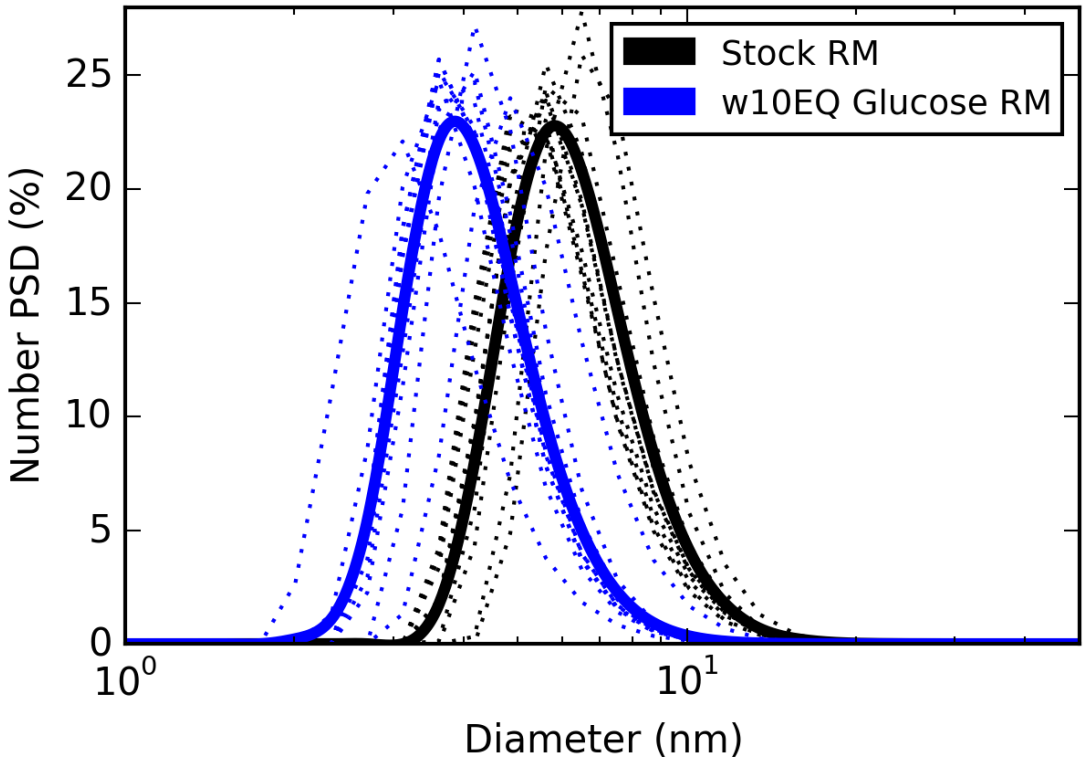

Figure 2.1: Particle size distributions (dots = raw data, solid line = averaged data) of two different stock unloaded w_0 =10 RM solutions (black) and two separate w_0 =10 equivalent solutions made with 30:1 water:glucose solution (blue). Despite having the same theoretical $\frac{\text{Volume}}{\text{Area}}$ ratio, the $w_0 = 10$ equivalent RMs are markedly smaller than the regular $w_0 = 10$ RMs. Averaged data are smoothed with a spline fit for presentation.

serve reverse micelles without resorting to x-ray or neutron scattering. As an example, a w_0 =10 RM solution has an average hydrodynamic diameter of approximately 5 nm and is completely undetectable via the naked eye due to its extremely small scattering cross section. A new RM formulation could swell to ten times the size of a standard w_0 =10 RM solution and still present the same macroscopic appearance. DLS allowed me to see changes occurring at the subwavelength scale. In this case of glucose loaded and equivalent RMs I was extremely glad that I used DLS as a method to detect the reverse micelle particles, as the PSD of w_0 equivalent RMs revealed the surprising trend of always being smaller than the RMs containing only water in AOT despite having the same volume of polar phase. This behavior is extremely obvious in Fig. 2.1. Said more dramatically: glucose appears to make the reverse micelles shrink!

2.2 Dynamic Light Scattering

Dynamic light scattering is a method for measuring particle size based on variations in scattering intensity from particles diffusing through a light source[4]. While particles diffuse past each other sometimes they move between orientations relative to the detector that result in constructive and destructive interference, that is the distances equal to $N\lambda$ vs $\left(N + \frac{1}{2}\right)\lambda$. With a fast enough detector and autocorrelator, these variations can be characterized and related to the diffusion speed of the particles. Then the Stokes-Einstein equation and viscosity of the solvent can be used to discern the average particle diameter of the system. Because the raw data measured is a variation in signal intensity, and because small particles are very weak scattering agents, the ideal light source for DLS is extremely bright, with a very stable intensity profile, i.e., a laser. As DLS measures variations in scattering intensity rather than angle, the laser wavelength can be much longer than the diameter of the particles being measured, because it does not matter if the scattering is in the Rayleigh or Mie regime, only that scattering is occurring. This makes DLS particularly advantageous for characterization of RMs, proteins, polymer nanoparticles, and other small, weakly scattering molecules. The only limitation for DLS is that the particles of interest must be able to form a stable suspension in a solvent. As RMs are defined by being a stable water-in-oil nanoemulsion, it is almost as if DLS was invented specifically to characterize them. In fact the only difficulty in performing DLS of RMs is that the very smallest RMs ($w_0 \leq 2$) are so small that they generate signals near the lower size limits of the instrumentation.

A typical DLS experiment is shown in Fig. 2.2. In this image a scattering trace (bottom left) is transformed into a correlation curve via autocorrelation (top) and finally analysis of this correlation curve via the Stokes-Einstein equation gives the particle size distribution (bottom right). Larger particles will have stronger scattering events, but diffuse through the solution more slowly and therefore have a longer correlation time, while small particles will have short correlation time that rapidly decays. This relationship can be used to discern both the average diameter of the particles, and the polydispersity. In Figure 2.3, the difference in decay time between small w_0 =5 RMs and

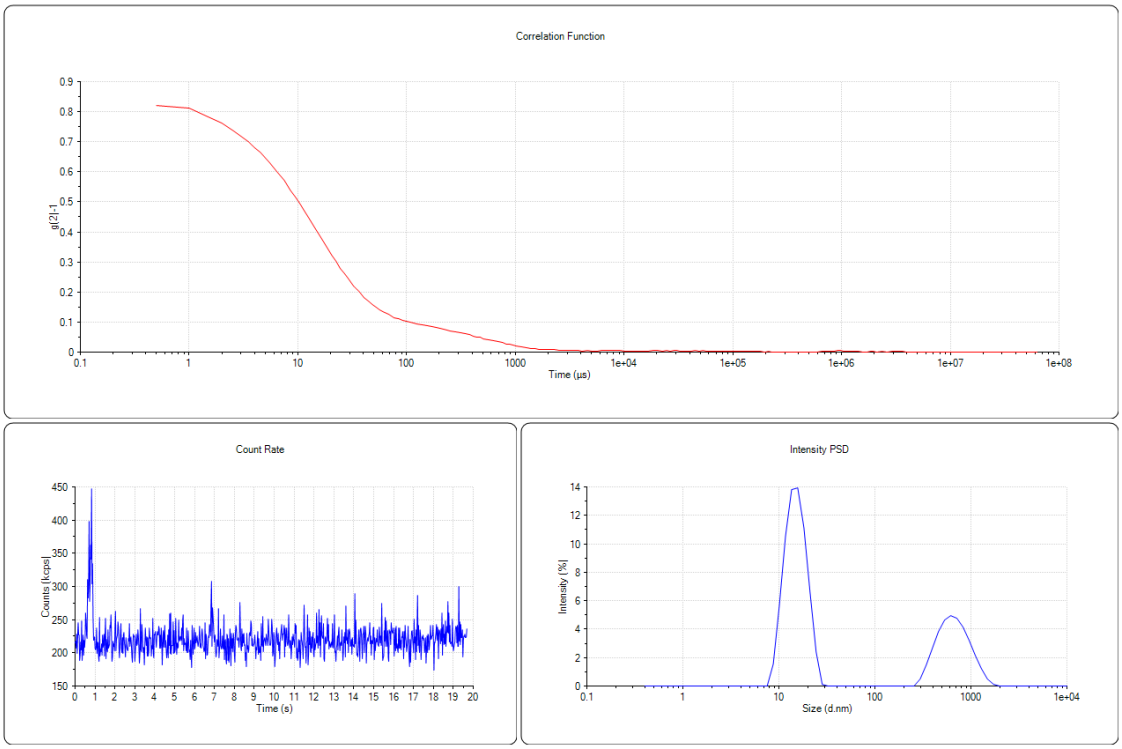

Figure 2.2: A sample with a bimodal particle distribution (in this case w_0=40 RMs with excess glucose loading to produce a precipitate) in the process of data collection. As can be seen, the raw scattering data (bottom left) includes scattering events for both large (large rare peaks) and small particles. This shows up as an autocorrelation curve (top) with two decays, and a particle size distribution (bottom right) with two size populations.

large w_0= 20 is readily apparent. But also apparent is a broader polydispersity, for $w_0 = 20$ RMs shown by the more gradual decay rate of the autocorrelation curve.

2.2.1 Statistical Analysis

Examining Fig. 2.1 it is easy to see that the average diameter of both standard and w_0 *equivalent* RMs containing glucose have different average diameters, but as the PSD of each overlaps, it is *not* clear that the difference in size between the two sets of particles is *statistically significant*, simply through observation. This can be more clearly demonstrated in Fig.2.4 which plots 12 PSD measurements for 4 different RM solutions (dotted lines) along with the average of each individual solution and the combined average of all 24 PSD measurements (gold lines). From these graphs, it is clear that the $w_0 = 40$ RM solutions have distinct sizes even when the data is combined, while

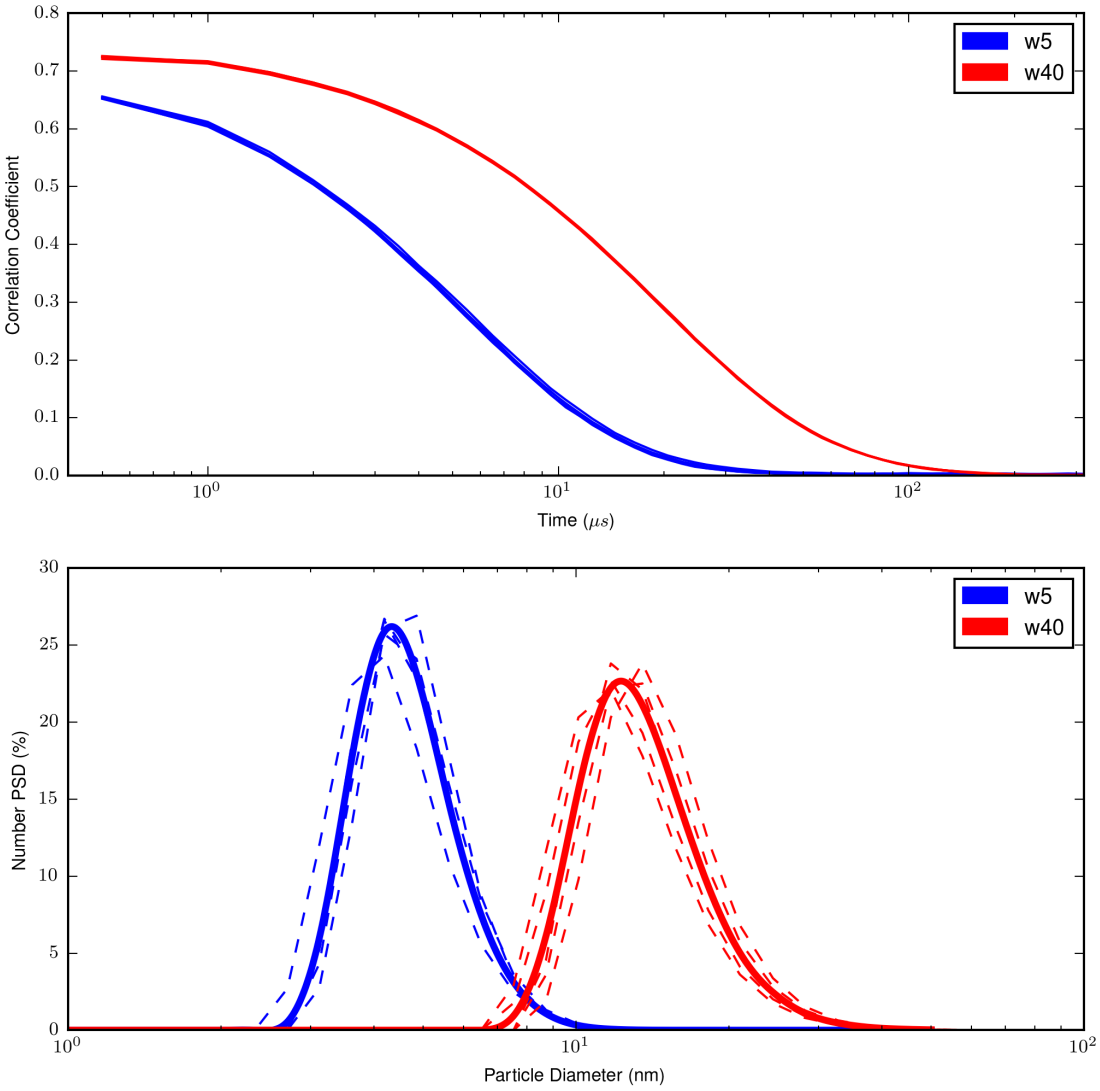

Figure 2.3: Correlelograms for $w_0 = 5$ and 40 AOT RMs (top) and the particle size distribution for these correlelograms (bottom). The top traces include three acquisitions for each size RM, but they are so similar they are overlaid on top of each other. The bottom size distributions include raw data (dashed lines) and average data with a spline smooth (solid lines) for clarity.

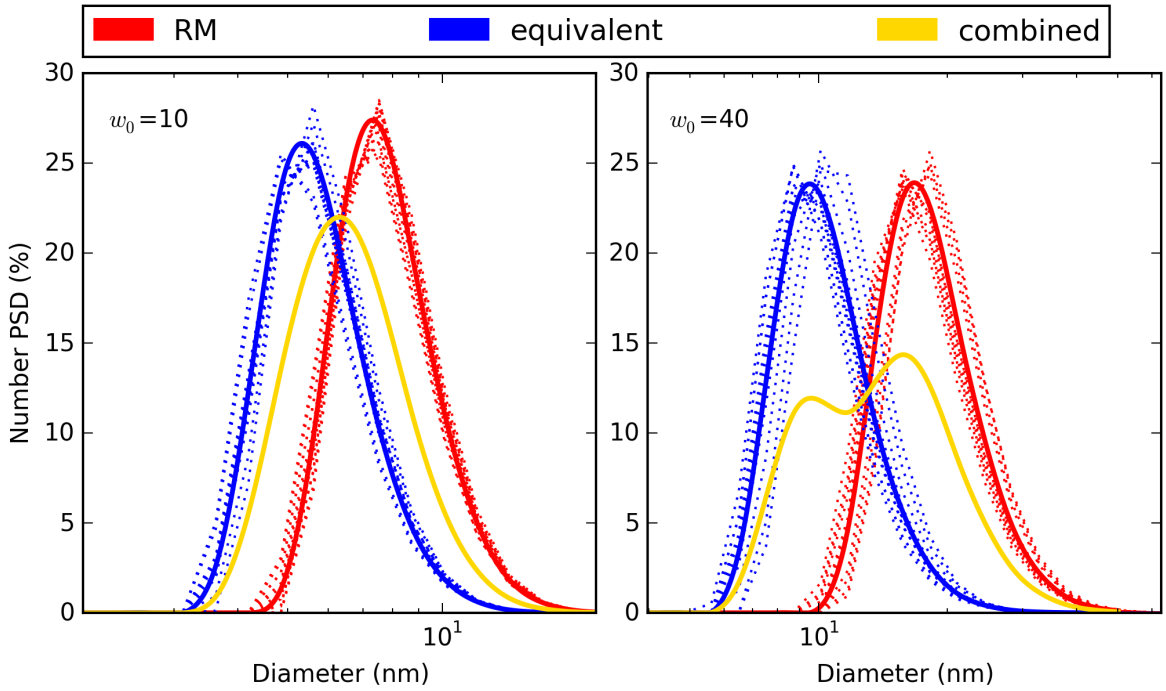

Figure 2.4: The particle size distribution (PSD) of both standard (red dots) and w_0 *equivalent* (blue dots) RMs. Averaging the standard and w_0 *equivalent* PSDs separately gives two distinct average PSDs (solid red and blue lines)

the w_0= 10 solutions simply present a single average size with a broader polydispersity. Therefore, in order to be confident that the $w_0 = 10$ RMs do represent different sizes I have performed a Student's t-test comparing the average diameters of the 12 standard RM solutions to those of the 12 w_0 *equivalent* RM solutions. The null hypothesis of this t-test is $H_0 : \overline{d}_{RM} - \overline{d}_{eq} = 0$ or that there is no statistical difference between the average diameter of the standard RMs and the w_0 *equivalent* RMs. The result of this test is that I can reject the null hypothesis with extreme prejudice (p=1.3×10^{-19}), and state that, indeed, the standard and w_0 *equivalent* RMs are different sizes.

2.2.2 DLS of Soft, Sweet, Particles.

As I have already mentioned when discussing Figure 2.1, the size distributions of w_0 equivalent RM solutions are smaller than their pure water twins. To test this I also performed DLS of carbohydrate loaded RMs, which can be thought of as "swelling" the RM by addition of polar

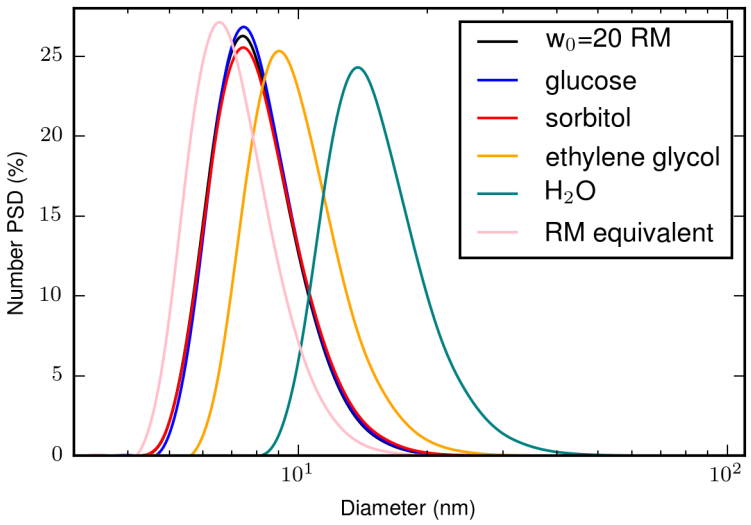

Figure 2.5: Size distributions of w_0 =20 AOT RMs that are loaded with different carbohydrates and water as well as a $w_0 = 20$ equivalent RM made with 30:1 H_2O:glucose solution. The glucose and sorbitol loaded RMs share the same size distribution as the original stock RMs, while both ethylene glycol and water swell the RMs. A RM solution made with an equivalent volume of 30:1 H_2O:glucose solution ($w_0 = 20$ equivalent glucose RMs) have a notably smaller size distribution than the stock or carbohydrate loaded RMs. Data has been smoothed with a spline fit for presentation.

phase. By beginning with a single RM solution and adding extra glucose to one and extra water to another, I was able to see that the exact same RM solution would noticeably swell when extra water was added but remain unchanged when glucose or sorbitol were added. Figure 2.5 presents this data for a series of w_0= 20 RMs loaded with water and three different carbohydrates, as well as a $w_0 = 20$ equivalent RM. As is easily seen, both the glucose and sorbitol loaded RMs have the same average diameter and polydispersity despite the solution containing demonstrably more polar phase than the regular RMs. The $w_0 = 20$ equivalent RMs still show a "shrinking" behavior while both the water and ethylene glycol RMs swell, which I must emphasize is the behavior that should be expected of both glucose and sorbitol loaded RMs!

2.2.3 Sweet But On The Edge

Behavior of the reverse micelle solutions prepared depended on the amount of carbohydrate added. For example, if the solution had an excess of glucose, extra glucose would drop to the bottom of the container, as described below. While measuring the supernatant solution of glucose

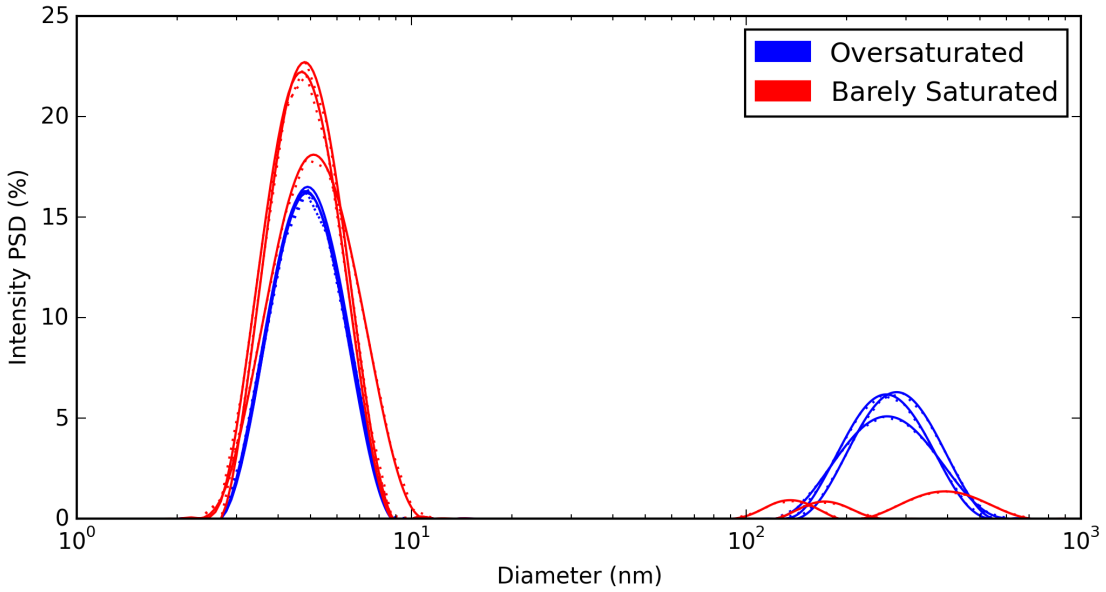

Figure 2.6: $w_0 = 5$ RM solutions with just enough glucose added to promote formation of large particles (red) and with a notable excess of glucose, causing clear loss of intensity in small particles and growth in large ones. Dots are the raw data and lines are a spline fit for presentation.

loaded RMs that had an excess of glucose, I noticed an extremely interesting development in the PSD of the RM solution. As the quantity of excess carbohydrate rose, a new bimodal size distribution grew in consisting of large (>100 nm) particles in addition to more standard RM-sized particles (Fig. 2.6). Particles prepared in this manner (that is, with visible precipitate and large particles observable via DLS) were **not** used elsewhere in the work presented here or in any other chapter. This is because there is no way to separate the large particles, as they are still some aggregation of aot/water/glucose/isooctane, though their exact identity is unknown. While none of the RM solutions presented elsewhere have large particles that are *observable* via DLS, that does not necessarily mean they aren't present and simply too low of a concentration to show up when DLS measurements are taken.

2.2.4 Solubility of Nanoconfined Carbohydrates

As I have already mentioned, the amount of glucose that can be loaded into an RM is far smaller than expected compared to the solubility of glucose in water. This means I needed to determine the solubility of glucose in RMs as a separate value from the solubility of aqueous glucose. Despite the

first monograph on the successful purification and measurement of solubility for D-glucose being printed in 1922[5] the solubility of glucose in water is a surprisingly controversial subject. This is due to glucose being happy to form glucose hydrates and glasses, making the difference between dilute sugar solution and solid hydrate easy to discern, but the difference between a supersaturated solution and a combination of saturated solution with suspended glucose hydrate difficult to distinguish. Considering how difficult solubility measurements are for macroscopic bulk glucose solutions, it is no surprise that measuring the solubility of glucose in nanoscopic RM water pools was both difficult and imprecise.

2.2.4.1 Solubility Methods

The method I used to determine the solubility of a carbohydrate in a RM solution is as follows:

1. Make 250 mL of 0.1M AOT RM solution (prepared as in Sec. 2.1.1.2) without any carbohydrate in it.
   (a) Example for a standard w_0 =10 solution: 11.1g AOT, 4.5g H_2O, dilute to 250 mL with isooctane
2. Measure ~0.6g of carbohydrate into a 250mL screw-cap bottle
3. Add 50.00 mL of RM solution and a magnetic stir bar.
4. Stir vigorously for at least 45 minutes
5. Add 1.00 mL of RM solution, record the total volume
6. Stir vigorously for at least 45 minutes
7. Repeat steps 5 and 6 until there is no carbohydrate precipitate (approximately 90 mL final volume expected for glucose, determined from smaller scale experiments)
8. Double-check the final volume with a graduated cylinder

The reverse micelle systems studied using this procedure were w_0 =5 and 10 H_2O/AOT/isooctane RMs with 0.10 M AOT, and w_0 =10 H_2O/AOT/toluene RMs with 0.10M AOT . This large scale experimental data was in close enough agreement with smaller scale versions (e.g. w_0 =50 RMs studied using 20 mL of total solution, 5 mL initial solution, and 0.05 g of glucose) that further solubility measurements were performed on small scale solutions to save time and money.

2.2.4.2 Solubility of Selected Carbohydrates in AOT RMs

To discuss and measure the solubility of carbohydrates in RMs I need to first define a new term called the "loading limit". In these studies the loading limit is the minimum mole ratio of water to carbohydrate required to have a solution of carbohydrate loaded reverse micelles with no apparent phase separation or precipitate. This term is useful because the composition of a RM solution can change significantly from one laboratory to another, or even from one experiment to another. Precise measurement of the loading limit is quite difficult due to the slow kinetics of dissolution for carbohydrates into RM solution (often requiring stirring/sonicating overnight or gentle heating to fully dissolve the carbohydrate), and the minuscule amount of water in a standard RM solution. Recall from the materials and methods section 2.1.1.2 that a 10 mL RM solution may contain as little as 90 μL of water for a solution of $w_0 = 5$ RMs! Still, I (and four undergraduate researchers) persevered, and we acquired some rough solubility data for carbohydrates in AOT RMs, as seen in table 2.1. These solubility values are expressed as the mole ratio of water to carbohydrate $n_{H_2O} : n_{carb}$ for the sake of comparison across systems of differing w_0, surfactant concentration, or preparation method. A $w_0 = 5$ RM with 0.2 M AOT would contain twice the water per mL of solution as the 0.1 M AOT RM solutions used to collect the data presented and therefore reporting the "solubility" of these two RM preparations as direct g/mL or mol/L concentrations would be misleading.

The loading limits measured and presented are unfortunately difficult to collect and I would prefer a more efficient method. Recent advances in gauging the solubility of oligosaccharides in water[1,7] and ionic liquids[8,9] using HPLC methods have opened up options to measure the loading

Table 2.1: Loading limits for reverse micelles formed from AOT. The loading limit is expressed as the mole ratio of water required to stabilize carbohydrates in reverse micelles at 0.1 M AOT in nonpolar solvent (isooctane or toluene). Lower numbers correspond to higher solubility. All measurements performed at room temperature ($\sim 25^\circ$ C)

	w_0	Glucose	Sorbitol	Xylitol	Myo-inositol	Glycerol	EG
Aqueous solution	-	10					
RM in isooctane	5	19.4	11.4	8.7		0^a	0^a
	10	22.3	11.1	8.1	51	0^a	0^a
	50	16.6				0^a	0^a
RM in toluene	10	102.4	70.5				

[a]Glycerol and ethylene glycol do not require water to form reverse micelles.[6]

limit of carbohydrates in RMs in ways that I hope will be easier, faster, and more accurate, and these methods are in development.

2.2.4.3 Why is the solubility of carbohydrates in RMs so much lower than in bulk aqueous solution?

Despite the data in Table 2.1 not being the most trustworthy, it is still useful as a qualitative measure of loading limit for glucose, sorbitol, and inositol in RM solutions. Particularly interesting is the massive difference in loading capacity between $w_0 = 10$ RMs made in isooctane and those made in toluene. Clearly the AOT/H_2O/Toluene system is much less receptive to carbohydrate loading, despite containing the same amount of water as the AOT/H_2O/Isooctane system.

As discussed in Section 1.2.2 at w_0= 5 and 10, a significant amount of the RM interior is comprised of "shell" water with a high ionic strength and proton gradient.[10,11][10,11] Considering the solubility of glucose in a w_0=10 RM is about 1/2 that of glucose in water, and a w_0=10 RM is about 50:50 core:shell water[11], it would be reasonable to assume the reduction in solubility arises primarily from water interacting with AOT headgroups, or "shell water", being less able to solvate glucose. But if this were the case I should not have observed any change in solubility between $w_0 = 10$ and $w_0 = 50$ RMs, as the AOT concentration (and therefore total amount of surface area) is constant. This means that the reduction in solubility must come from a change in the RM interior

as a whole, and whatever that change is is probably also contributing to the observed oddity in the PSD of carbohydrate containing RMs.

2.3 What Happens to a Carbohydrate When It's Added to a Reverse Micelle?

The change in RM size and reduction in carbohydrate solubility in the RM interior compared to aqueous solution show that glucose and other carbohydrates change the behavior of the RM interior. But it is also true that the RM greatly effects the carbohydrate. Some of these changes can be seen in the ^1HNMR of glucose in an RM. One notable change is an adjustment to the anomeric ratio of glucose in RMs vs aqueous solution. The two common forms glucose takes in aqueous solution are the α and β pyranose forms (Fig. 1.5, Ch. 1). The α enantiomer is stabilized by the intramolecular anomeric interaction between carbon #1 and the adjacent oxygen during the ring opening reaction, while the β form is stabilized by interaction with solvent[12]. This results in crystalline glucose being 100% α, while aqueous glucose solution has a α/β ratio of 0.61[13]. Luckily the 1α and 1β protons have significantly different chemical shifts (refer to Fig. 4.2 in Ch. 4), which allows easy determination of the α/β ratio through integration of the NMR signals. Fig. 2.7 presents precisely such data, specifically of a 40:1 D_2O:glucose solution both in bulk and encapsulated as w_0=10 *equivalent* AOT RMs. Comparing these values shows that the β enantiomer is destabilized in RMs compared to bulk solution ($\alpha/\beta = 0.55$ in bulk and 0.71 in RMs). Norris et. al. have noted the propensity for ions in solution to affect the anomeric ratio of glucose. Specifically, sodium cations have been found to mildly destabilize the β anomer[12] while Takeuchi et. al. note fluoride as a slight stabilizing effect.[14] Considering the nature of the AOT headgroups, with $-SO_3^-$anion and Na^+cation, it is extremely likely that approximately half of the glucose resides at the RM interface alongside the majority of the Na^+ counterions, thus destabilizing a large portion of β glucose.

In addition to changes in the anomeric ratio, another observation is that the ^1H NMR signals associated with glucose hydroxyl peaks are sharp and discernible, in stark contrast to aqueous

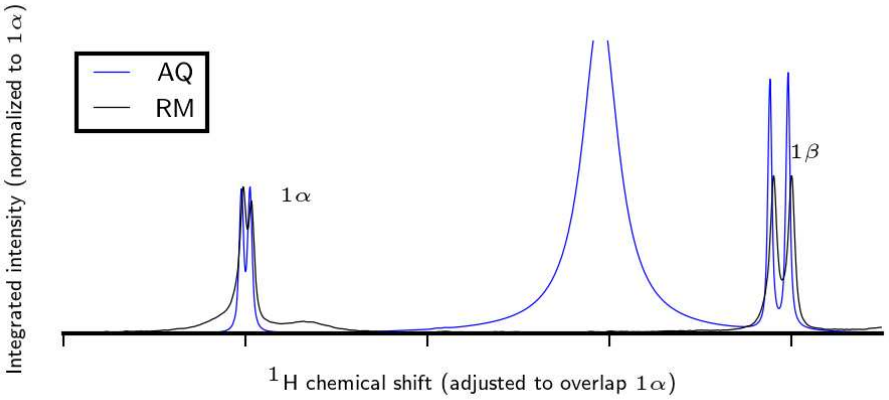

Figure 2.7: ^1H NMR spectra of glucose in 40:1 D_2O:glucose solution in bulk aqueous phase (blue trace) and encapsulated in a w_0 =10 AOT reverse micelle (black trace) showing enantiomeric ratios α/β of 0.55 in AQ and 0.71 in RM. As crystalline glucose is entirely the α enantiomer and it can take as long as 12 hours for glucose in solution to reach α/β equilibrium these samples were aged for over a week before this data was aquired. The chemical shift of glucose anomeric protons is not constant between aqueous and RM solution, therefore the RM data has been shifted downfield by ~0.3 ppm and chemical shift values are not displayed.

solution (see Fig. 2.8). This is due to a significant slowing of proton exchange between water and carbohydrate within the RM, a systematic treatment of which is presented in Chapter 5. With the hydroxyl peaks being visible, it is possible to observe a systematic downfield shift of water and glucose hydroxyl protons as a function of increasing w_0. A possible explanation is increasing acidity of the RM interior as a function of w_0. This explanation would be congruent with the behavior of hydroxyl containing "NMR pH probes" which show a downfield shift with increasing acidity[15,16], though the concept of 'pH' for the interior of a RM is still a difficult concept to discuss for RMs as often the H_3O^+ and OH^- concentrations are not high enough to result in at least one ion per RM[10].

2.4 Why is this all happening?

From the DLS data, we surmise that glucose changes the aggregation behavior of AOT reverse micelles. The real question is the nature of this change. This is an extremely difficult question to answer because most interrogation techniques make assumptions about the very nature of a RM that we believe is changing. The average number of water molecules in a RM can be estimated from

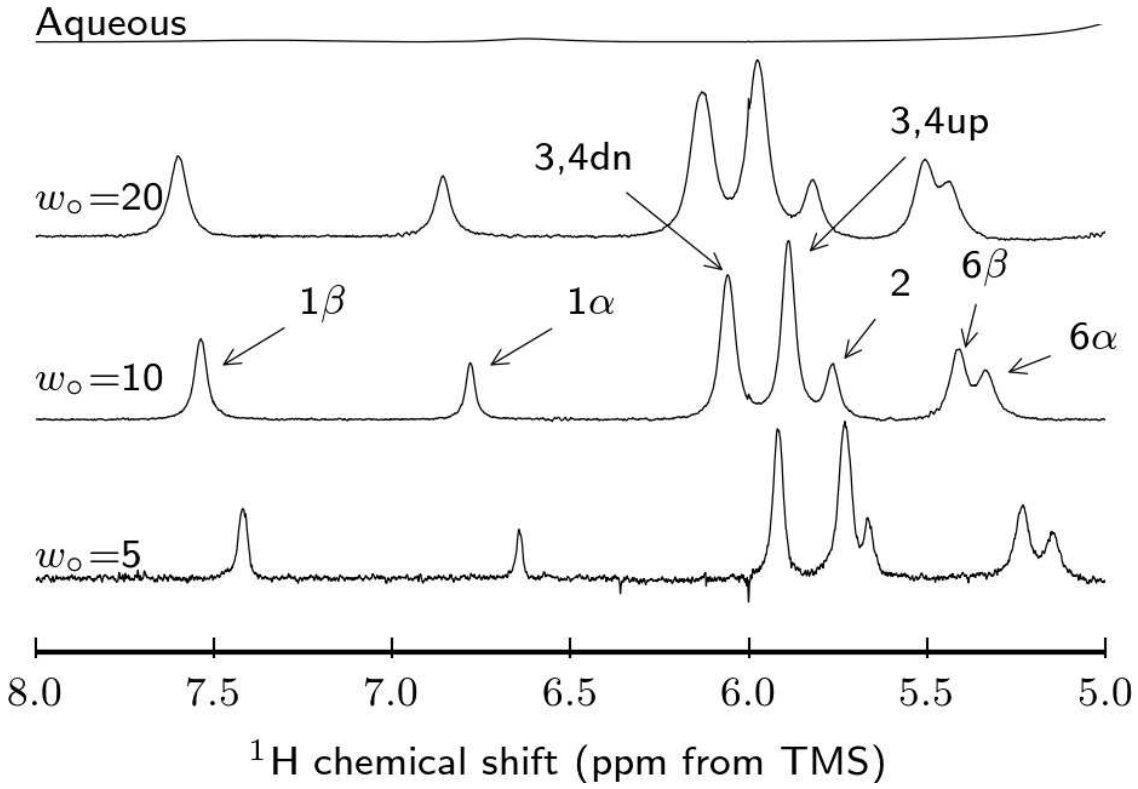

Figure 2.8: Narrowing of glucose hydroxyl peaks due to slowed chemical exchange with water and shifting of the chemical shift of selfsame hydroxyl peaks showing systematic deshielding of the hydroxyl protons as a function of RM size.

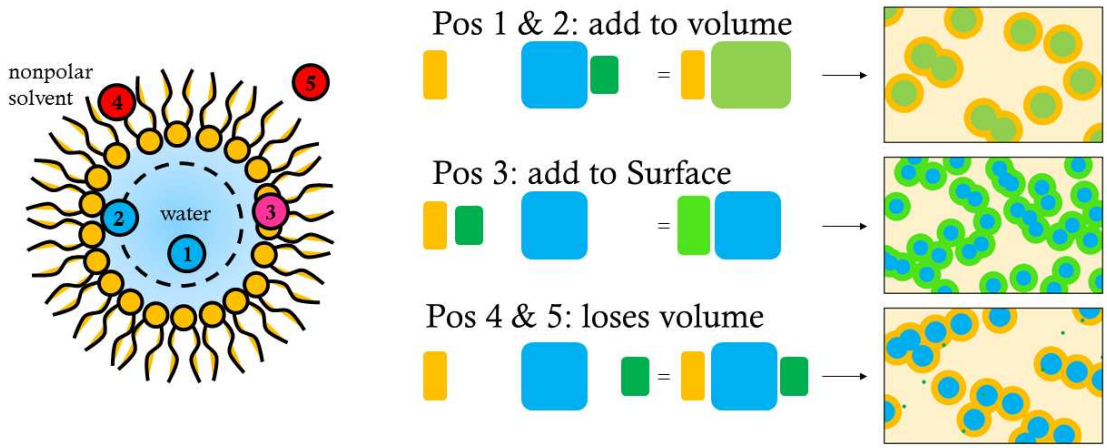

Figure 2.9: When originally preparing glucose RMs, I expected behavior in line with glucose occupying position ① or ②, but instead observed particle shrinking. This could be explained by positions ③, ④, and ⑤, with position ③ being much more likely than the other two.

the hydrodynamic diameter measured via DLS, but this measurement cannot tell us if the diameter of glucose loaded RMs is changing due to insertion of glucose into the interface, compaction of the water pool, or even more exotic changes to the RM system such as glucose suddenly leaving the RM interior entirely. Therefore we must propose many explanations for RM size reduction in order to test them. The ones we have thought of so far are listed in the following subsections.

2.4.1 Surface Addition or Mass Loss

The most straightforward explanation for the RMs getting smaller with addition of glucose is that they are gaining surface area instead of volume, or is simply exiting the RM entirely instead of occupying the water pool. These options are represented by different carbohydrate locations within the RM, as described in Fig. 2.9. In Ch. 4 and 5 I will show that despite position ③ being a reasonable explanation, there is absolutely no evidence for glucose inserting into the interface, while there is significant evidence that it occupies position ② and no reasonable evidence against position ① .

2.4.2 Partial Molar Volume

An explanation for RM size reduction often put forward is the partial molar volume of added carbohydrates. For ideal mixtures, the volume measured upon mixing two aliquots equals the sum of the individual component volumes and excess partial molar volume is zero. Deviation from ideal behavior leads to positive or negative partial molar volume, that is, the volume observed upon mixing is either larger or smaller than the sum of the components, respectively. Rarely, the excess partial molar volume leads to a reduction in the overall solution volume, such as the case when $MgSO_4$ is added to water[17]. However, in most cases, negative excess partial molar volume means that the total volume is less than the sum of the parts, not less than the original volume of one component. The excess partial molar volume for glucose in water has been measured in pure water[18–21], as well as quite a few aqueous solutions[20,22–27], and in ionic liquids[8]. In all cases, its partial molar volume is very small, representing <5% deviation from ideality. No partial molar volumes measured for carbohydrates in aqueous mixtures have a negative partial molar volume that can account for constant RM size with added carbohydrate that we measure. It is possible but unlikely that the thermodynamics governing the partial molar volume in the RMs differs so substantially from bulk aqueous solution as to account for our observation. Thus, we reject the hypothesis that negative excess partial molar volume of the carbohydrates is responsible for the observed constant RM size with added carbohydrate.

2.4.3 RM Eccentricy

It is possible the reduction in the RM size arises from a change in particle eccentricity. Although on average RMs may appear spherical, they are flexible and dynamic, constantly changing aspect ratio, and spending a very small amount of time in an actual spherical configuration. If the AOT RMs are ellipsoidal rather than spherical, as suggested by some computational studies[28–32], then changes to the eccentricity of the particles will affect the apparent particle radius measured. Assuming a spherical form for a RM makes it easy to find the particle size from its diffusion constant[33,34] and the result is that DLS size measurements yield the average radius as estimated

from particle diffusion[35–37] without regard to actually being non spherical. To explore this possibility, we consider a geometric perspective. The volume of an ellipsoid is given by ,

$$V_{ellip} = \frac{4}{3}\pi abc \tag{2.1}$$

where a, b, and c are the primary, secondary, and tertiary radii of the ellipsoid, respectively. Unlike the simple analytical form for the volume of an ellipsoid, the general formula for the surface area of an ellipsoid cannot be expressed as an analytical function that covers both prolate and oblate ellipsoids simultaneously. Instead, I used approximation of the ellipsoid surface area (accurate to within $\pm 1\%$) is given by

$$A_{ellip} = 4\pi \sqrt[1.6]{\frac{ab^{1.6} + ac^{1.6} + bc^{1.6}}{3}} \tag{2.2}$$

When $r = a = b = c$, both expressions for the ellipsoid volume and surface area simplify to the forumlae for a sphere, $V_{sphere} = {}^{4\pi r^3}/_{3}$, and $A_{sphere} = 4\pi r^2$. For given surface area, ellipsoidal RMs should have lower volume and a larger apparent radius than spherical particles. At the same time, we expect DLS measures of spherical particles to have lower polydispersity compared to ellipsoids, because diffusion along any direction for a spherical particle is equivalent. Figure 2.10 shows the deviation in particle radius and volume for a spheroid[†] of constant volume to surface area ratio, that is constant w_0. When $b < a$ the spheroid is prolate; when $b > a$ the particle is oblate. Figure 2.10 shows that for constant volume to surface area ratio (i.e. w_0), a sphere presents the smallest average radius. This indicates that eccentric RMs will have a larger larger average radius compared to spherical RMs of the same w_0.

Results from several simulational studies suggest that AOT RMs are not spherical.[28–32] Among others, Eskici and Axelsen recently reported a detailed analysis of AOT RM size for a given w_0 value. They compared their results from molecular dynamics (MD) simulations with AOT RM sizes that were measured experimentally using DLS, small angle x-ray scattering, fluorescence

[†]an ellipsoid where two of the axes are equal, $b = c$.

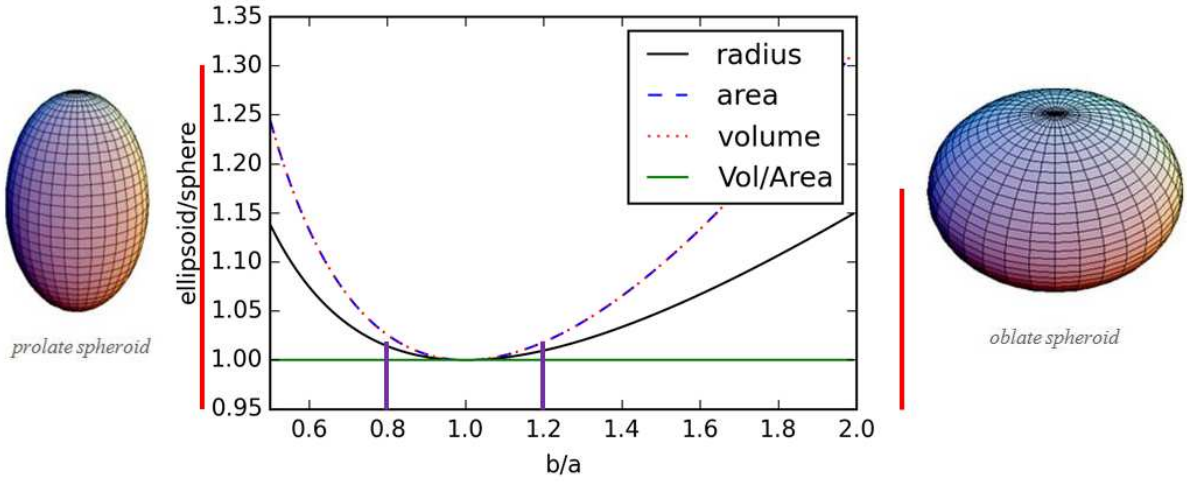

Figure 2.10: A sphere ($b/a = 1$) has the most efficient surface area to volume ratio, and therefore the smallest average radius for any given w_0. Size reduction observed for $w_0 = 40$ and $w_0 = 40$ *equivalent* RMs, could be explained by an eccentricity change from 0.8 or 1.2 (purple lines) to spherical, for $w_0 = 10$ the eccentricity change would have to be from 0.4 or 2.2 (red lines).

recovery after photobleaching, and viscosity. Their results showed that w_0=7.5 RMs were, on average, prolate ellipsoids, with 62 AOT molecules. Our NOESY results indicate that addition of glucose to solutions containing RMs should increase the polar volume. As long as the AOT area/molecule is constant, (we address this assumption below) the total surface area in solution should remain constant. Thus, if addition of glucose to our AOT RM caused the particles to become more spherical, they could accommodate some additional volume without appearing to get larger.

2.4.4 Ionic Screening

Another factor that could impact the RM size upon addition of glucose rests on the surface area per AOT molecule. Various experiments and simulations studies have estimated the area occupied by individual surfactant molecules[28,31,38,39]. Eskici and Axelsen estimate the area per AOT molecule on the basis of its shape and intermolecular interactions[28]. Studies probing aqueous glucose solutions that contain salts show the propensity of glucose to interact with cations, including Na^+[12,40]. If glucose interacting with Na^+ counterion leads it to insert between the AOT anionic

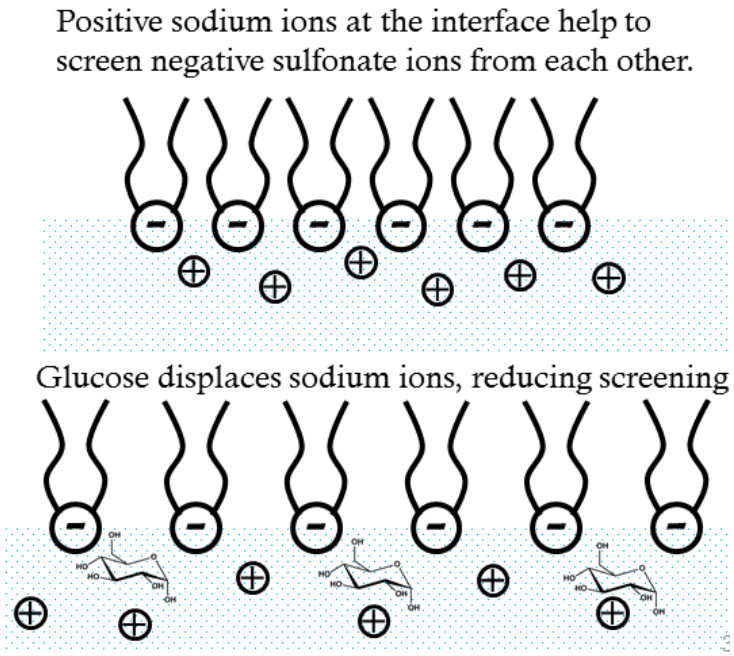

Figure 2.11: Top: a standard AOT RM interface in which electrostatic repulsion of AOT $-SO_3^-$ is mediated by Na^+ ions reducing the net surface charge. Bottom: glucose insertion into the interface displaces Na^+ ions, increasing electrostatic repulsion between AOT headgroups and increasing the average surface area per AOT molecule. A $w_0 = 10$ AOT RM with 30:1 glucose *loading* has approximately 1 glucose for every 2 AOT molecules.

SO_3^- headgroup and the Na^+ counterion, then Coulomb repulsion between neighboring AOT anions could increase the surface area per molecule leading to an effective increase in the overall surface area in the solution. As discussed above, an increase in surface area will yield more particles of smaller size, the effect we observe.

2.4.5 But Why?

In reality, none of these explanations can entirely explain the size reduction observed. The carbohydrates are occupying position ① and ②, ruling out surface addition and mass loss entirely. Partial molar volume requires such a massive volume loss, and deviation of glucose behavior from the norm, that explaining size reduction via this method beggars belief. Instead the size reduction is likely explained by a number of factors working in concert. The particles are a little less eccentric, with slightly larger headgroups, the partial molar volume of glucose in RMs may be slightly

smaller, though this is unlikely. In the next chapters I present experiments that help to determine how glucose is contributing to RM size reduction, and further investigations will not only yield more insights into this behavior but (hopefully) also more information as to the role and behavior of carbohydrates as cryoprotectants, lyoprotectants, and vital biomolecules.

Bibliography

(1) Gray, M. C.; Converse, A. O.; Wyman, C. E. *Applied Biochemistry and Biotechnology* **2003**, *105*, 179–193.

(2) Advanced Chemistry Development, I. **2010**.

(3) Jones, E.; Oliphant, T.; Peterson, P.; others, a. SciPy: Open Source Scientific Tools for Python. http://www.scipy.org.

(4) Berne, B. J.; Pecora, R., *Dynamic Light Scattering: With Applications to Chemistry, Biology, and Physics*, Google-Books-ID: xg3CAgAAQBAJ; Courier Corporation: 2013; 388 pp.

(5) Jackson, R. F.; Silsbee, C. G. *Journal of the Franklin Institute* **1922**, *194*, 95–96.

(6) Correa, N. M.; Silber, J. J.; Riter, R. E.; Levinger, N. E. *Chemical Reviews* **2012**, *112*, 4569–4602.

(7) Taylor, J. B. *Transactions of the Faraday Society* **1957**, *53*, 1198–1203.

(8) Singh, V.; Chhotaray, P. K.; Islam, N.; Gardas, R. L. *Journal of Chemical Thermodynamics* **2016**, *103*, 7–16.

(9) Singh, V.; Panda, S.; Kaur, H.; Banipal, P. K.; Gardas, R. L.; Banipal, T. S. *Fluid Phase Equilibria* **2016**, *421*, 24–32.

(10) Crans, D. C.; Levinger, N. E. *Accounts of Chemical Research* **2012**, *45*, 1637–1645.

(11) Piletic, I. R.; Moilanen, D. E.; Spry, D. B.; Levinger, N. E.; Fayer, M. D. *Journal of Physical Chemistry A* **2006**, *110*, 4985–4999.

(12) Franks, F.; Hall, J. R.; Irish, D. E.; Norris, K. *Carbohydrate Research* **1986**, *157*, 53–64.

(13) Roslund, M. U.; TÃ€htinen, P.; Niemitz, M.; SjÃ¶holm, R. *Carbohydrate Research* **2008**, *343*, 101–112.

(14) Maebayashi, M.; Ohba, M.; Takeuchi, T. *Journal of Molecular Liquids* **2017**, *232*, 408–415.

(15) De Marco, A. *Journal of Magnetic Resonance (1969)* **1977**, *26*, 527–528.

(16) SzakÃ¡cs, Z.; HÃ€gele, G.; Tyka, R. *Analytica Chimica Acta* **2004**, *522*, 247–258.

(17) Dill, K.; Bromberg, S., *Molecular Driving Forces: Statistical Thermodynamics in Biology, Chemistry, Physics, and Nanoscience*, 2nd ed.; Garland Science, Taylor Francis Group, LLC: New York, 2010.

(18) Banipal, P. K.; Banipal, T. S.; Lark, B. S.; Ahluwalia, J. C. *Journal of the Chemical Society-Faraday Transactions* **1997**, *93*, 81–87.

(19) Fucaloro, A. F.; Pu, Y.; Cha, K.; Williams, A.; Conrad, K. *Journal of Solution Chemistry* **2006**, *36*, 61–80.

(20) Banipal, T. S.; Sharma, S.; Banipal, P. K. *Indian Journal of Chemistry Section a-Inorganic Bio-Inorganic Physical Theoretical & Analytical Chemistry* **1999**, *38*, WOS:000084927400004, 1106–1115.

(21) Kishore, N.; Goldberg, R. N.; Tewari, Y. B. *Journal of Chemical Thermodynamics* **1993**, *25*, 847–859.

(22) Kumar, H.; Sheetal *Journal of Chemical and Engineering Data* **2016**, *61*, 2244–2259.

(23) Gheorghe, I.; Stoicescu, C.; Sirbu, F. *Journal of Molecular Liquids* **2016**, *218*, 515–524.

(24) Banipal, P. K.; Dhanjun, H. S.; Sharma, S.; Hundal, H.; Banipal, T. S. *Zeitschrift fÃŒr Physikalische Chemie* **2008**, *222*, 177–204.

(25) Banipal, P. K.; Banipal, T. S.; Ahluwalia, J. C. *Journal of Chemical Thermodynamics* **2002**, *34*, 1825–1846.

(26) Zhuo, K. L.; Wang, J. J.; Yue, Y. K.; Wang, H. Q. *Carbohydrate Research* **2000**, *328*, 383–391.

(27) Zhao, Q.; Sun, Z. J.; Zhang, Q.; Xing, S. K.; Liu, M.; Sun, D. Z.; Li, L. W. *Thermochimica Acta* **2009**, *487*, 1–7.

(28) Eskici, G.; Axelsen, P. H. *The Journal of Physical Chemistry B* **2016**, *120*, 11337–11347.

(29) Hande, V. R.; Chakrabarty, S. *Phys Chem Chem Phys* **2016**, *18*, 21767–79.

(30) Marchi, M.; Abel, S. *J Phys Chem Lett* **2015**, *6*, 170–4.

(31) Abel, S.; Sterpone, F.; Bandyopadhyay, S.; Marchi, M. *Journal of Physical Chemistry B* **2004**, *108*, 19458–19466.

(32) Martinez, A. V.; Dominguez, L.; Malolepsza, E.; Moser, A.; Ziegler, Z.; Straub, J. E. *Journal of Physical Chemistry B* **2013**, *117*, 7345–7351.

(33) Bohidar, H. B.; Behboudnia, M. *Colloids and Surfaces a-Physicochemical and Engineering Aspects* **2001**, *178*, 313–323.

(34) Tovstun, S. A.; Razumov, V. F. *Colloid and Polymer Science* **2015**, *293*, 165–176.

(35) Khan, M. F.; Singh, M. K.; Sen, S. *Journal of Physical Chemistry B* **2016**, *120*, 1008–1020.

(36) Vasquez, V. R.; Williams, B. C.; Graeve, O. A. *Journal of Physical Chemistry B* **2011**, *115*, 2979–2987.

(37) Zulauf, M.; Eicke, H. F. *J. Phys. Chem.* **1979**, *83*, 480–486.

(38) Kotlarchyk, M.; Huang, J. S.; Chen, S. H. *Journal of Physical Chemistry* **1985**, *89*, 4382–4386.

(39) Eastoe, J.; Robinson, B. H.; Steytler, D. C.; Thornleeson, D. *Adv. Coll. Interface Sci.* **1991**, *36*, 1–31.

(40) Mayes, H. B.; Tian, J. H.; Nolte, M. W.; Shanks, B. H.; Beckham, G. T.; Gnanakaran, S.; Broadbelt, L. J. *Journal of Physical Chemistry B* **2014**, *118*, 1990–2000.

Chapter 3

Static Fluorescence Studies

The data presented in this chapter included efforts from undergraduate students Eddie Palomeres, Tania Wyss, Daniel Lenskold, and Trevor Skaar, all of whom I trained and advised to prepare samples, and measure using UV/vis and fluorescence spectroscopy techniques. None of their collected data are presented here, but the results of their experiments aided and informed the methodologies that confirmed the results of this chapter.

3.1 Static But Not Staid.

Static fluoresence studies are some of the most robust techniques available for investigation of nanoconfined systems. By selecting probe molecules with strong absorption cross sections (dyes) and emission intensities (i.e., fluorescent dyes) I can make solutions in which the fluorescent dye is at a low enough concentration that there is only one probe molecule for every 100-100,000 reverse micelles[‡] but still have a strong enough signal to probe the RM interior. In this way, interactions between individual molecules molecules can be explored without resorting to actual single-molecule techniques. An example is the study of a cyanine dye in AOT RMs by McPhee et. al.[1] in which changes in the steady state fluorescence spectroscopy provided evidence for aggregation of a cyanine dye in RMs despite the maximum dye concentration being approximately one dye molecule per 20,000 RMs.

In the first experiment presented here, I take advantage of changes in the viscosity of the aqueous interior as glucose is added to the RMs. In the second experiment reported, I directly take advantage of the distribution of dilute probe molecules in RMs to measure the aggregation num-

[‡] example: w_0 = 10 RMs average to ~100 AOT molecules per RM, if the solution has 0.1 M AOT and a dye molecule has an overall concentration of 5 μM, there are 200 RMs for every dye in the solution

ber (eq 3.1) of the surfactant molecules that comprise the RMs. These experiments increased my understanding of the nature of the RM interior, especially as it pertains to glucose.

3.2 Viscosity in a Nanocavity

A commonly-known property of aqueous carbohydrate solutions is that their resistance to shear stress greatly increases as carbohydrate concentration rises. In other words, sugar water solutions are more viscous than pure water. Alternatively, syrups are syrupy. I took advantage of this behavior to probe changes in the RM interior by measuring the response of a fluorescent dye molecule whose fluorescence quantum yield depends on the viscosity of the environment. My dye of choice was crystal violet (CV, Fig. 3.1), a trimethylphenyl (TMP) derivative dye, displays increases in fluorescence efficiency as the solution viscosity increases, or the environment limits the dye's mobility. Due to its ionic nature, CV is expeted, and indeed does, partition entirely into the aqueous RM interiorg however, as a cation it also partitions specifically into the interfacial layer (the "shell") of an AOT RM interior due to electroscatic attraction to the sulfonate moiety on the AOT headgroup[2]. Using CV to measure the local environment, I can gauge if the glucose is, in fact, in the water pool of the RMs, as well as any effect the RM interior has on glucose's ability to increase the viscosity of water.

3.2.1 Materials and Methods

Materials for "viscosity" measurements: AOT, isooctane, and crystal violet were purchased from Sigma and used used as received with no further purification. Millipore 18 $M\Omega$ water, and tech grade methanol were also used. The structure and fluorescence spectroscopy of crystal violet in sugar solutions is shown in Fig. 3.1.

Sample preparation for viscosity measurements: To introduce CV into the RM samples, I first made a 250 μM stock solution of crystal violet (CV) in methanol that I used to prepare all the samples. For variations $w_0$studies, I added 1 mL of the CV stock solution to two separate 50 mL volumetric flasks and evaporated the methanol, using compressed air to speed up evaporation, until only a thin film of solid CV was left in each flask. I prepared a 0.500 M solution of AOT in

isooctane and added 10 mL of the AOT stock solution to each flask, followed by 0.450 g water to one flask and 4.50 g water to the other. The result is two RM solutions, both with 0.100 M AOT and 5 μM CV, but one is $w_0 = 5$, and the other is $w_0 = 50$.

Samples prepared to study the effect of varying the water:glucose ratio, were made in a similar manner. I prepared four 10 mL flasks by adding 0.200 mL of stock CV to each and evaporating all the methanol. To each flask, I added 2.00 mL of 0.500 M stock AOT solution. To two flasks, I added 90 mg of water ($w_0 = 5$) while the other two got 180 mg of water ($w_0 = 10$) . Finally, glucose was added to one each of the w_0 =5 (10 mg) and w_0 =10 (50 mg) flasks. Finally, each of the four flasks were filled the rest of the way with isooctane and sonicated for ~45 minutes or until all glucose was integrated into the RM solution, whichever came last. This generated two flasks of w_0 =5 RMs, one plain and the other with 93:1 H_2O:glucose as well as two flasks of w_0 =10 RMs, one plain and the other with 36:1 H_2O:glucose, all with constant CV concentration of 5 μM.

For bulk aqueous solutions, I added 0.200 mL of CV stock solution to two separate 10 mL volumetric flasks and evaporated the methanol completely. To one flask I added 4.68 g of glucose along with ~8 mL of water, agitated by shaking until the glucose was completely dissolved, then added enough water to make 10 mL. The other flask I filled to 10 mL with water, agitated with shaking. Then both solutions were sonicated for ~45 minutes. This generated one aqueous glucose solution and one aqueous solution with identical 5 μM CV concentrations.

Following preparation of these standard solutions, I systematically mixed pairs of samples to create a wide range of sample conditions including varying w_0 values, varying glucose concentrations in bulk solution, and varying water:glucose ratios in the RMs. For example 1mL of unloaded $w_0 = 10$ RM solution with 0.5 mL of 30:1 H2O:glucose RM solution yeilds a 90:1 H2O:glucose solution. And mixing 0.5 mL of $w_0 = 10$ RM with 1 mL of $w_0 = 50$ solution results in a $w_0 = 36.7$ solution. The range of samples prepared is presented in Table 3.1.

Materials for aggregation number measurements: AOT, isooctane,1,3,6,8-pyrene tetrasulfonic acid (PTSA), methyl viologen dichloride (MV), 4-phenylbutyric acid (PBA)and cetylpyridinium chloride (CPyC) were purchased from Sigma and used without further purification. Solid NaCl

Table 3.1: Samples prepared for crystal violet fluorescence measurements. Note: all samples have the identical xxx M CV concentration as ensured by preparation with

Sample	variable	variable values					
bulk solution	[glucose] M	0	0.57	1.03	1.54	2.06	2.6
RM size	w_0	5	9.5	14	18.5	23	27...
w_0 =5	$H_2O : G$	93:1	117:1	156:1	234:1	468:1	
w_0 =10	$H_2O : G$	36:1	45:1	60:1	90:1	180:1	

and NaI were purchased from Fisher and 18 $M\Omega$ millipore water was also used. PTSA and MV structures are shown in Fig. 3.5.

For aggregation number studies, ,

Sample preparation for aggregation number measurements:

The goal for SFQ sample preparation is to end up with two RM solutions that are the same w_0 and have the same dye concentration, but one has quencher in it and the other does not. As dye concentrations will usually be between 1-50 μM the primary limitation on how high their concentration can be in the RM solution is the dynamic range of the fluorimiter: if the concentration is too high the detector will saturate. PTSA is, as it turns out, an incredibly strong fluorophore, and so only needs a final concentration of 0.1-0.5 μM in the RM solution before risking detector saturation (and even then an excitation and detection slit with of 1 nm will be required). This is somewhat troublesome because even 1 mg of PTSA dye in 10 mL of water is a 164 μM solution! So make that 164 μM solution, and then make 5 mL of 25 μM solution by diluting 0.762 mL of that solution into a 5 mL volumetric flask. (I chose 25 μM because the I have a 20 μL autopipette and 20 μL of 25 μM solution diluted into a 5 mL total volume gives 0.1 μM final solution, no other reason). For the quencher concentration I made a 0.777 M stock solution of MV (because that the result of dissolving 1g bottle of MV dissolved into 5 mL of water), and then made a 44 mM MV solution by diluting 0.283 mL of the 0.777 M stock to a 5 mL final volume. 44 mM was chosen

Table 3.2: The volume of 25 μM PTSA, 44 mM MV, and plain water required to make RM solutions with final concentrations of 0.1 μM PTSA and 220 μM MV. To make unquenched solution add $V_q + V_{H_2O}$ volume in regular water.

w_0	$V_{dye}(\mu L)$	$V_q(\mu L)$	$V_{H_2O}(\mu L)$	$V_{total}(\mu L)$
5	20.0	25.0	0.0	45.0
10	20.0	25.0	45.0	90.1
20	20.0	25.0	135.1	180.2

because 25 mL (the minimum volume I need to add to the solutions in Table 3.2) will diluted into 5 mL will give ~90% occupancy in a $w_0 = 20$ RM solution (the largest RMs I planned on making).

PBA and CPyC solutions were prepared in approximately the same way as PTSA and MV, only using using 0.01 M NaOH solution rather than water, as PBA is only fully deprotonated at high (>10) pH.

This method, and others I have tried, all involve juggling a large number of different solutions. I believe this is a possible source of failure for SFQ, as missing the addtion of even one solution can completely wreck an entire data series.

Data collection and analysis: Fluorescence data were collected in 10 mm glass and quartz cuvettes (FireflySci), and collected on a fluorometer (Horiba JY Fluorolog, Model FL3-11, S/N 17226-2414-FL), with excitation at 335 nm, and emission collection from 340-550 nm, a 1 nm slit width, and 0.1 s integration time. The fluoresence data was integrated, graphed, and fit to eq. 3.6 using in-house written custom Python 2.7 code and the SciPy toolkit.

3.2.2 What Can Be Learned From Trimethylphenyl Dyes

Trimethylphenyl dyes are a class of dyes that share the behavior of their quantum efficiency being proportional to the viscosity of the solvent in which they are dissolved. For instance, at constant temperature a trimethylphenyl dye will have brighter fluorescence in glycerol than the same dye in methanol because the viscosity of glycerol is higher than methanol. This is due to the difference between the rigid structure of the trimethylphenyl ground state and relative internal rotational freedom present in the in the first excited state[3]. In trimethylphenyl dye, hybridization of the central carbon atom changes from sp^2 to sp^3 during excitation, which permits rotation of

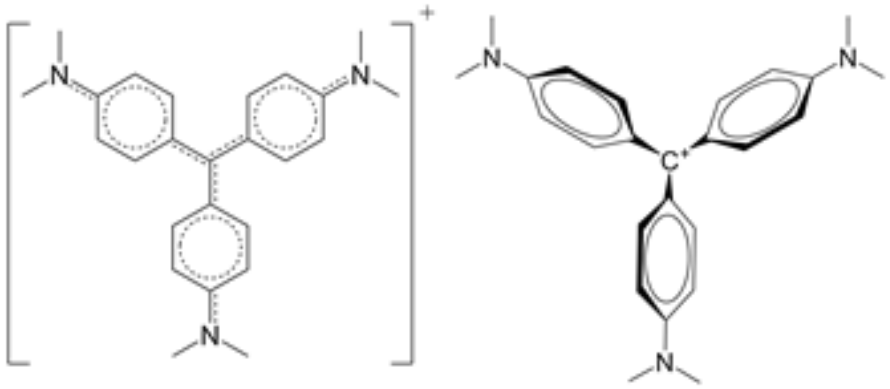

Figure 3.1: Structures adopted by the crystal violet molecule in the ground (left) and first excited (right) electronic states.

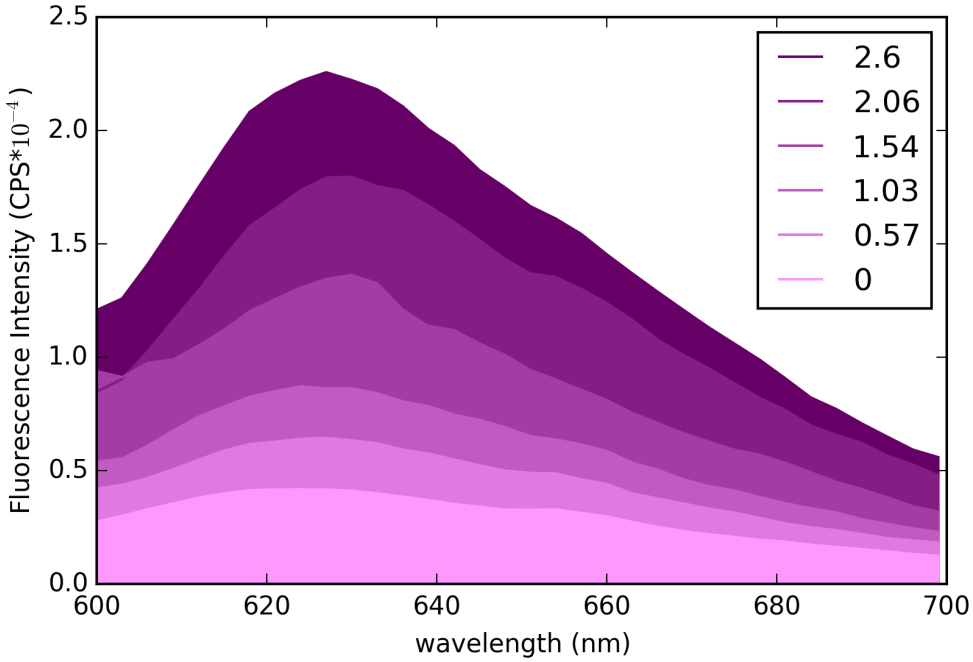

Figure 3.2: Fluorescence spectra of CV in aqueous solution with increasing glucose concentration, showing the increase in CV fluoresence intensity as the solution becomes more viscous.

the three phenyl groups and promotes torsion of the central carbon from a planar to tetrahedral geometry. In the ground state, trimethylphenyl dyes are rigid planar molecules due to the resonance structure between the three phenyl groups and the sp^2 hybridized central carbon atom. In the excited state the central carbon becomes sp^3 hybridized and each phenyl is free to rotate. The less restriction the trimethylphenyl dye is subject to, the more likely it will relax back to the ground state by nonradiative internal conversion, while the more restricted it is the more the geometry of the excited state resembles that of the ground state, and the more likely the trimethylphenyl dye is to fluoresce. Thus, CV fluorescence efficiency rises as the viscosity of the surrounding solvent increases, such as the case of solutions of increasingly high glucose concentration, as shown in Fig. 3.1. Integrating the fluorescence signal allows numeric comparison of the restriction CV experiences in different environments.

3.2.3 Response of CV to RM Environment

I used CV to explore the interior of the RMs as a function of particle size, and glucose loading. Fig. 3.3 shows the CV integrated fluorescence intensity as a function of w_0 (points) compared to its fluorescence intensity in bulk aqueous solution at the same water:glucose value. Two things are readily apparent from these data. The first is an extremely high intensity for CV in any RM compared to CV in bulk water. Even at its lowest intensity, nanoconfined CV is still nearly 10x more fluorescent, and therefore significantly more restricted, than in bulk water. Second, at first the fluorescence intensity decreases with increasing w_0 value, but then it eventually begins to increase again at a w_0 of approximately $w_0 = 30$. Interestingly, I have been able to find a paper that looks at *dynamic* fluorescence as a function of ${w_0}^3$, and they observe a similar behavior for RMs under $w_0 = 30$, but then then their data (in)conveniently cuts off at this point. The increase in fluoresence intensity of CV for RMs with a $w_0 > 30$ could be due to extreme particle eccentricity behaviors. Essentially the RMs could have "pockets" with a small radius of curvature and convinement similar to that of a much smaller RM. If this is the case, then it would mean RM eccentricity strongly deviates from spherical after $w_0 = 30$. Indeed, thinking about this as a possible explanation for the CV behavior is the reason for the calculations I performed in subsection 2.4.3.

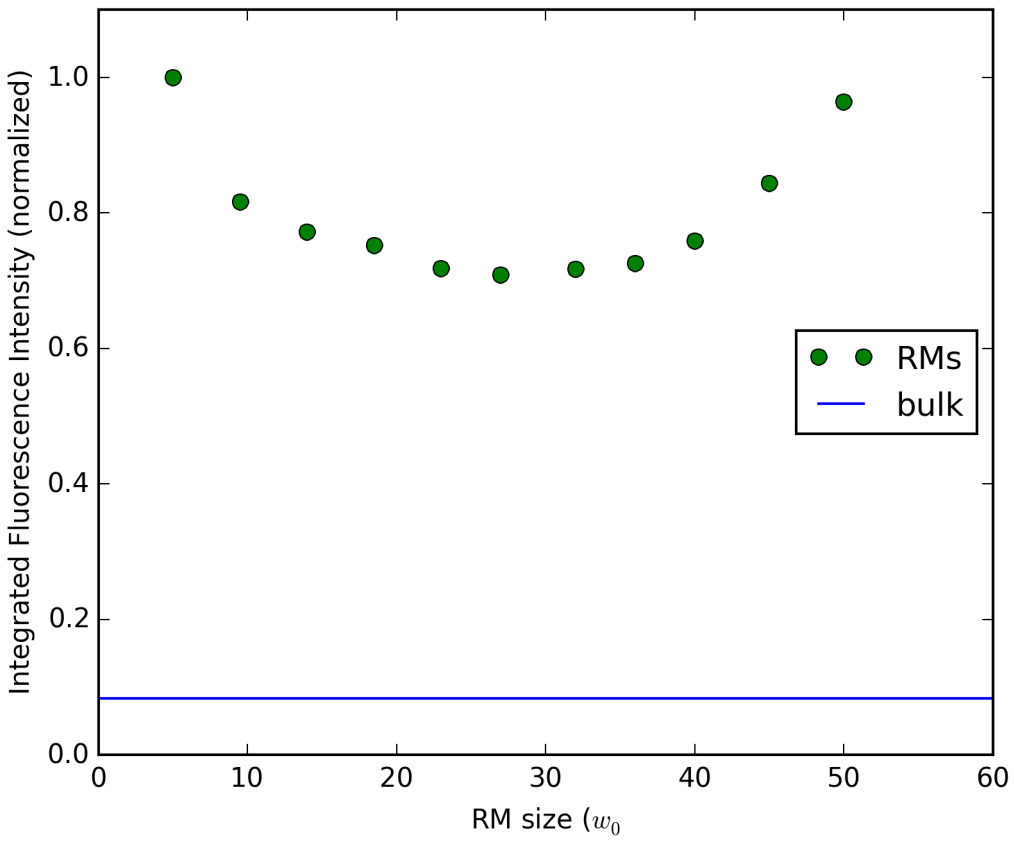

Figure 3.3: Relative integrated fluorescence intensity as a function of reverse micelle size, as a function of w_0 (green points). The blue line is the relative intensity of CV in plain bulk aqueous solution.

3.2.4 Effect of glucose on CV response in bulk solution and RMs

Beyond reproducing the response of CV in a RM environment, we were interested to learn how glucose affects mobility in the RMs. Fig. 3.4 shows CV intensity as a function of glucose loading in bulk water solution and in two AOT/H_2O/isooctane systems with differing w_0 values. These results indicate that glucose causes an increase in local "viscosity" for the CV molecule, that is, CV fluorescence intensity is significantly higher in RMs, and increases with added glucose as expected. Note that a molar ratio of glucose/H_2O = 0.07 corresponds approximately to a 2.6 M aqueous glucose solution. The increasing slope of the data from aqueous solution to $w_0 = 5$ that not only does the fluorescence intensity increase with confinement, but the intensity increase per glucose incorporated into the RM interior also increases. It is also interesting to consider that at the lowest glucose loading in $w_0 = 5$, we estimate that there are fewer than one glucose per RM (but also far fewer than one CV per RM).This indicates the dramatic impact of glucose on the mobility of each CV molecule. It is clear that the glucose causes a significant change in the local environment for the CV even though we expect glucose to have relatively free rotational motion based on our 2D NMR results (see Ch. 4, section 4.4). As noted in Ch. 1, section 2.3, there is likely a large amount of glucose at the RM interface, which is also where the CV is expected to reside (due to electrostatics), the enhanced effect of glucose on CV fluoresence as RM size decreases may be a result of this.

3.2.5 Discussion

The results from CV fluorescence spectroscopy experiments demonstrates a few interesting things. First, the CV fluorescence trends for water/AOT/isooctane RMs suggests that at a certain size, above w_0=30 or so, the RMs change so that the CV senses a more confined environment. This could be due to changes in the RM shape. Second, RMs definitely increase the confinement ability of glucose toward crystal violet. This could be due to confinement effects, or by glucose and CV both preferentially partitioning to the AOT-water interface. Combined with others, these

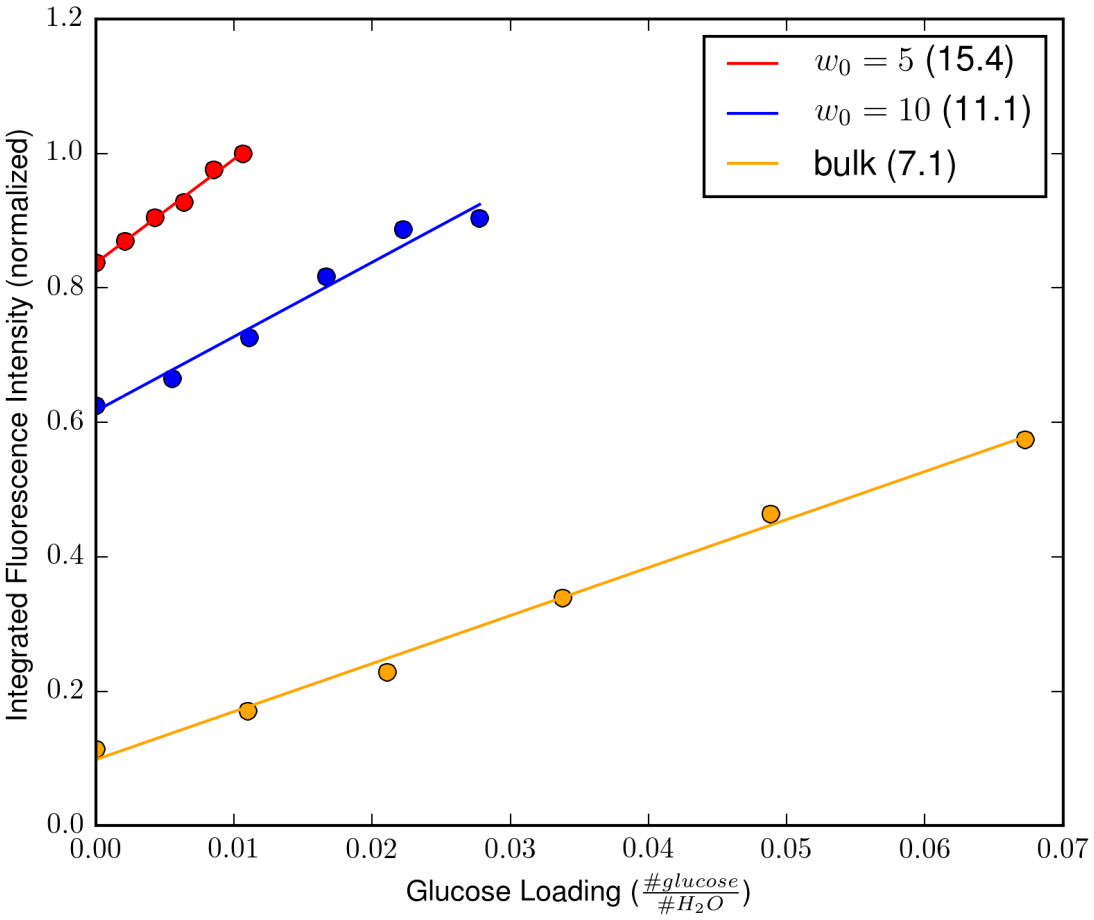

Figure 3.4: Integrated crystal violet fluorescence as a function of increasing glucose concentration, and linear fit to the data, for bulk aqueous glucose (yellow), water/glucose/AOT/isooctane RMs with w_0=10 (blue) and 5 (red). Numbers in parentheses in the legend refer to the slope of each line.

results encouraged us to try to measure the size of RMs with and without glucose through as direct a process as possible, as described in the next section.

3.3 Determination of Aggregation Number via Static Fluorescence Quenching

Details about the molecular nature of the RM aggregates remains a recurring question for the results of these systems. For example, we would love to know just how many AOT, water and glucose molecules comprise the RMs we have prepared. Following the lead of many published studies, we set out to measure the aggregation number for our RMs. This section chronicles our forays into measuring particle sizes and aggregation numbers for those particles. We have been successful in measuring the sizes of the particles but aggregation numbers continue to challenge us.

Given the unexpected results that I found from DLS studies of our sample, I really wanted to get more information telling me *why* they are changing size. A smaller RM *should* contain fewer water molecules simply because it has a smaller volume, but exactly how many water molecules there are and what they are doing I can only guess when just using size measurements. I would really like to know the aggregation number (eq 3.1) of the RMs, that is, the average number of surfactant molecules in an average RM in the solution. Comparing aggregation number to measured size yields lots of information about the behavior of both the RM and any carbohydrate contained in the RM. For example, if a $w_0 = 10$ RM and $w_0 = 10$ equivalent RM made with 30:1 H_2O:glucose have the same aggregation number, but the w_0= 10 equivalent RMs are smaller, then the size reduction must be due to some form of compaction for water, glucose, and AOT in a RM vs. in bulk. In contrast, if the aggregation number for the equivalent RM is smaller than the regular RM, then we could surmise that the sugar-water interior is causing the AOT headgroup to increase in area. Thus makes aggregation number is an extremely useful property of RMs that I would dearly like to know.

$$n_{agg} = \frac{[Surfactant]}{[RM]} \tag{3.1}$$

In theory, it should be surprisingly easy to measure n_{agg} using a clever implementation of Static Fluorescence Quenching (SFQ).[4,5] The idea behind it is nicely straightforward: pick a fluorophore and quencher pair that both selectively partition into the RM and then measure how many RMs have both a fluorophore and quencher in them. A good analogy for thinking about this is the carnival game in which you throw balls into cups. Imagine you don't know how many cups there are, but you get to know that after throwing 20 red balls and 40 blue balls there are four cups with both a red and blue ball. Assuming that the balls are evenly distributed and no cup can contain more than one ball of each color while still having room for a ball of the other color (meaning we have firmly entered the realm of magical theoretical cups), the probability of both balls being in the same cup, P_{rb}, can be expressed as the product of the independent probabilities of the red ball, P_r, and blue ball, P_b, being in a cup, equation 3.2. Solving this equation for N_{cup} easily gives the solution of 200 cups (equation 3.3).

$$P_{rb} = P_r P_b \tag{3.2}$$

$$\frac{N_{rb}}{N_{cup}} = \frac{N_r}{N_{cup}} \frac{N_b}{N_{cup}}$$

$$\frac{N_{cup}^2}{N_{cup}} = \frac{N_r N_b}{N_{rb}}$$

$$N_{cup} = \frac{20 \times 40}{4} = 200 \tag{3.3}$$

The important part of this solution is that you can't get the answer just by knowing that 20 red balls went into 20 different cups. The answer can only be achieved by having two different colored balls and knowing how many times both colors end up in the same cup. Applying this idea to a RM solution the red balls are fluorophores and the blue are quenchers. Each time both a fluorophore and quencher end up in the same RM, the fluorescence intensity decreases, giving me a way to "count" the number of fluorophore-quencher pairs in the system. This method only works if the quencher

interaction with the fluorophore causes complete quenching of the fluorophore fluorescence. If the fluorophore emission is only somewhat reduced, the SFQ method will not yield the correct results.

Many reports of normal (not reverse) micelle aggregation number have been published. Indeed, of the 923 citations to Turro and Yekta's original method,[4] a very large fraction report aggregation numbers for self-assembled systems using SFQ. Although many fluorophore-quencher pairs can be used to measure the aggregation numbers, most applications measuring normal (not reverse) micelles utilize pyrene as the fluorophore. For reverse micelles, pyrene won't work because it reside largely, if not exclusively, in the continuous nonpolar phase and will not be associated with the RMs. Thus, other fluorophore quencher pairs have been used to determine aggregation numbers for RMs.

The measurement of aggregation number is significantly less routine for RMs compared to micelles. Far fewer reports exist in the literature and many report numbers that make no sense, such as aggregation numbers of 20 for $w_0 = 10$ RMs (which should have closer to 100 AOT molecules per RM)[6–9] RMs containing carbohydrates present an even bigger challenge because of the interaction between carbohydrates and iodide preclude using I^-, which is a common fluorescence quencher. I tried several different fluorophore/quencher pairs for my experiments. The system that appeared best suited for the determination used pyrene tetrasulfonic acid (PTSA) as my fluorophore and methyl viologen (MV) as my quencher; PTSA and MV structures are shown in Fig. 3.5. In solution the PTSA carries a 4- negative charge while the MV quencher is positively charged. Net charge on the fluorophore and quencher should lead them both to reside in the RM water pool and Coulomb attraction between negative and positive ions should increase the chance that the two molecules come together in the RM and effecting quenching.

Having to distribute the fluorophore and quencher among RMs (instead of balls in magical cups) means using statistics. In fluorescence quenching studies, there is a chance that more than one dye or quencher can be in a RM. Assuming a Poisonian distribution for the probability of finding *N* quenchers in a RM can be shown by the following equation,

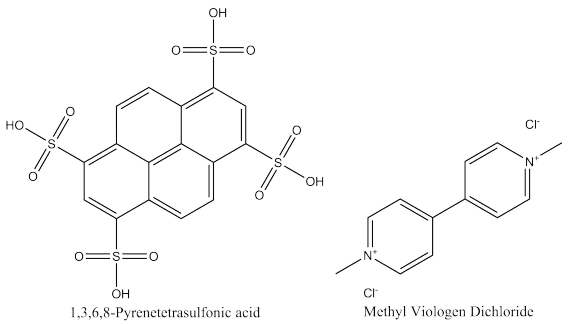

Figure 3.5: PTSA dye and MV quencher.

$$P_N = \left(\frac{[Q]}{[RM]}\right)^N \frac{1}{N!} \exp\left(-\frac{[Q]}{[RM]}\right) \tag{3.4}$$

Here [Q] and [RM] are the concentration of quencher and RM, respectively. Combining equation 3.4 with equation 3.1 and with the following three assumptions[4] should allow me to find the aggregation number of a RM solution. The assumptions are:

1. The distribution of fluorophore and quencher among particles follows Poisonnian statistics;
2. The fluorophore concentration is low enough that the probability of finding more than one fluorophore in any RM approaches zero and can be neglected;
3. Every particle that contains a fluorophore-quencher pair is dark, that is, the quencher has 100% quenching efficiency of the fluorophore.

Assumption 1 is assumed to be true as there is no evidence to the contrary. Assumption 2 can be made to be true by keeping the fluorophore:RM ratio low. It is possible that 1:10 is a low enough concentration, but this ratio is often 1:1000 or even 1:100,000, making the assumption extremely valid (as long as there is no aggregation of the fluorophore through other means such as in McPhee et. al.[1]). Assumption 3 can be tested in two ways. The first is to measure the fluoresence lifetime of the florophore in a system that is significantly (~50%) quenched[4,5], if the fluororophre-quencher pair is not completely dark the system will have two fluoresence lifetimes: the regular one, and

a much shorter one coinciding with the fluorophore:quencher pair. The second method of testing assumption 3 is to make a system with fluorophore and slightly more than one quencher per RM, if quenching is complete there will be no fluorescence.

After demonstrating that the assumptions are reasonable, we can return to the equations. The Poisonnian probability distribution, Eq. 3.4 and definition of aggregation number, Eq. 3.1, can be combined to form an expression of the fluorescence intensity of the solution, I, as a function of the unquenched fluoresence intensity, I^0, and the probability that a RM *does not contain a quencher*, P_0, since these are the only RMs that will *not* be dark.

$$I = I^0 P_0$$

This simplifies the situation because now we only have to evaluate P_N for $N = 0$. Evaluating eq. 3.4 for $N = 0$ and substituting equation 3.4 into equation 3.1 gives:

$$I = I^0 \exp\left(-\frac{[Q]\, n_{agg}}{[Surfactant]}\right) \tag{3.5}$$

But of course I'd prefer to evaluate this equation via linear regression, so after shifting things around and taking the natural log of both sides, behold equation 3.6, a linear equation that uses fluorescence quenching to determine aggregation number[5]:

$$[Surfactant] \ln \frac{I^0}{I} = [Q]\, n_{agg} \tag{3.6}$$

Using equation 3.6 to interpret fluorescence intensity as a function of quencher concentration should yield a relatively straightforward experiment to determine aggregation number, that is, measure the fluorescence intensity of a series of RM solutions with constant concentrations of fluorophore, surfactant, and water, but varying quencher concentration, integrate the fluorescence signals, plot the data, and fit it to 3.6. The slope of the resulting line should be the aggregation number.

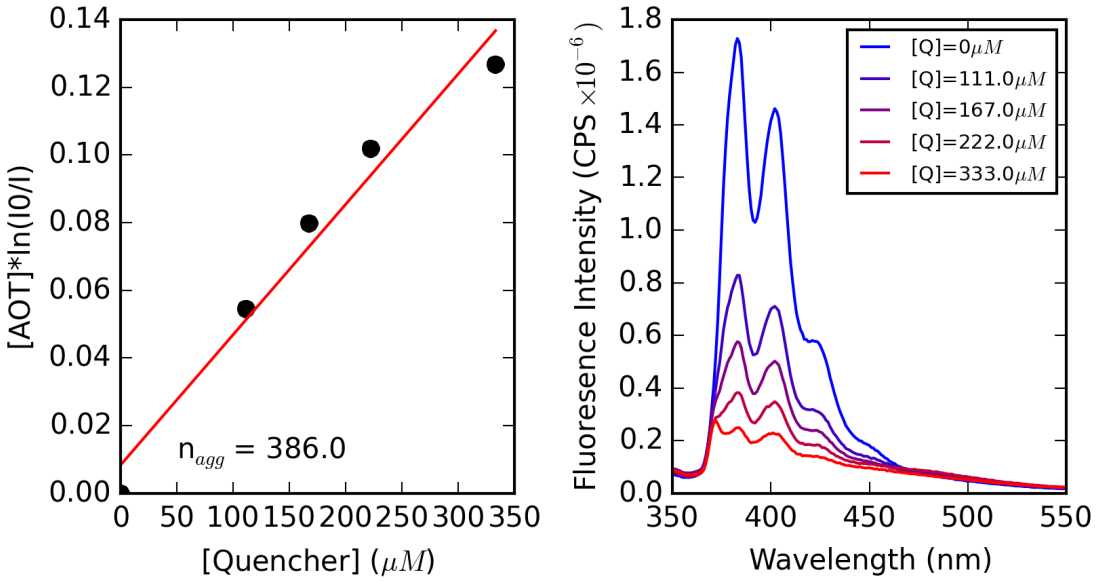

Figure 3.6: Aggregation number determination of a w_0= 25 AOT/isooctane RM using 0.5μM PTSA and MV quencher.

Armed with a method and a system to find n_{agg}, I set out to find the aggregation numbers for my AOT RMs as a test of the method. Fig. 3.6 shows the result of an experiment I performed using PTSA and MV to determine n_{agg} for a w_0 =25 AOT RM. The slope of the line, 386, gives the aggregation number directly. This value agrees reasonably well with values presented in the literature[10,11].

Being able to measure the AOT $n_{agg}$is nice but my real goal is to measure the carbohydrate containing RMs. However, I ran into problems with this idea. Figure 3.7 shows a problem with the SFQ method for measuring AOT and glucose-loaded AOT RMs. Both the RM solutions shown in Fig. 3.7 contain 0.1 μM PTSA dye. Thus, the fluorescence intensity should be the same for each. Instead, the fluorescence intensity is slightly lower in the glucose containing RMs. Although this provides yet another piece of evidence that glucose is in the water pool of the RMs, it also makes it impossible to compare the results from SFQ experiments on water-containing and glucose-loaded RMs precluding my ability to determine the aggregation number of glucose containing RMs.

Although the data in Fig. 3.6 are quite reasonable, the method is not repeatable. Sometimes I get nice data like that in Fig. 3.6, but often I get data like that shown in Fig. 3.8 in which the num-

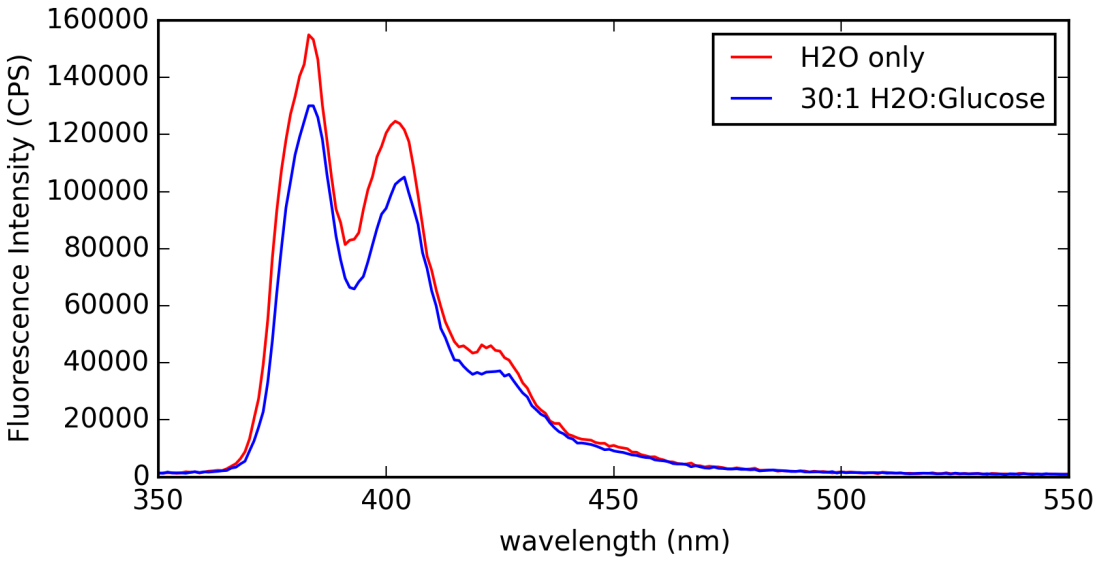

Figure 3.7: Fluorescence spectra of 0.1 μM PTSA in $w_0 = 10$ AOT RMs (red) and $w_0 = 10$ *equivalent* RMs with a 30:1 water:glucose solution (blue) showing slight quenching of the PTSA from glucose (size shrinking should increase PTSA fluroesence, not reduce it)

bers make no sense. In this set of solutions the $w_0 = 20$ RMs are smaller than the $w_0 = 10$ glucose equivalent RM while the $w_0 = 10$ plain RM did not undergo any quenching whatsoever. In addition to me, four different undergraduate students also performed SFQ measurements over a dozen times using two entirely different methodologies. We were never able to get good reproducibility or sensible results.

To test if the difficulty is due to the mild quenching of PTSA by glucose demonstrated in Fig. 3.7 I attempted to use a PBA+CPyC fluorophore quencher pair (Fig. 3.9). This surfactant-like fluorophore-quencher pair has been used successfully for SFQ in micelles.[12] However, I was unable to successfully apply it to AOT RMs, most likely because the surface area was too large to guarantee contact between the two molecules when they occupied the same RM. However, the PBA/CPyC fluorophore/quencher pair has been reported to be effective for n_{agg} determination via *dynamic* fluorescence quenching studies in AOT reverse micelles.[13] The PBA and CPyC pair is ineffective for SFQ because it violates assumption 3 in the above list. That is, CPyC does not completely quench PBA fluorescence. The data acquisition and analysis for dynamic fluorescence quenching is significantly more complex than the SFQ method. Unfortunately, even the dynamic

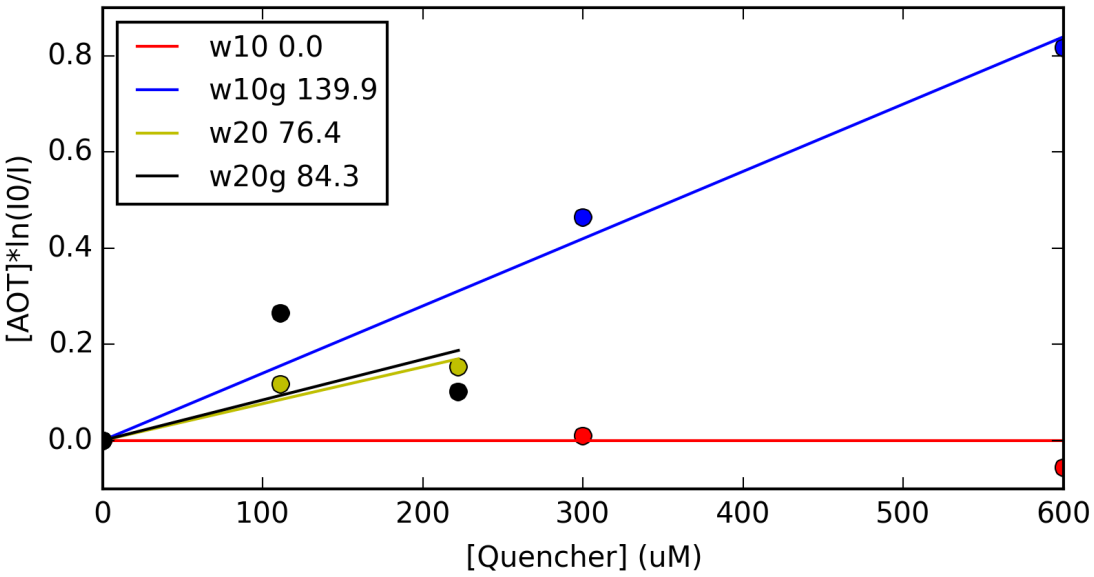

Figure 3.8: Typical SFQ results from RMs and glucose loaded RMs. The flat red line and extreme deviation from linearity for the gold and black lines show how difficult it is to aquire quality data using this method on RMs.

Table 3.3: Dye and Quencher pairs and the problems with them

Dye	Quencher	Difficulty
PTSA	methyl viologen	Inconsistent results, dye quenched by glucose
	iodide	Inconsistent results, iodide reacts with glucose
	chloride	Quencher is not efficient enough
PBA	CPyC	Does not efficiently quench in RMs
$Ru(bpy)_3^{2+}$	9-methylanthracene	Quencher is not sufficiently water soluble

fluorescence quenching method did not yield reproducible results that made sense. Particle sizes generated were either too small or too large by at least a factor of 10 and often more.

As part of an ongoing quest to find n_{agg} of AOT reverse micelles with and without glucose I explored a number of fluorophore/quencher pairs, presented in Table 3.3. The lack of repeatability and reproducibility has plagued me.

3.3.1 Conclusion

Unfortunately, AOT RMs are not particularly conducive to static fluorescence quenching experiments, and are even more poorly suited to the experiments when loaded with glucose. It is

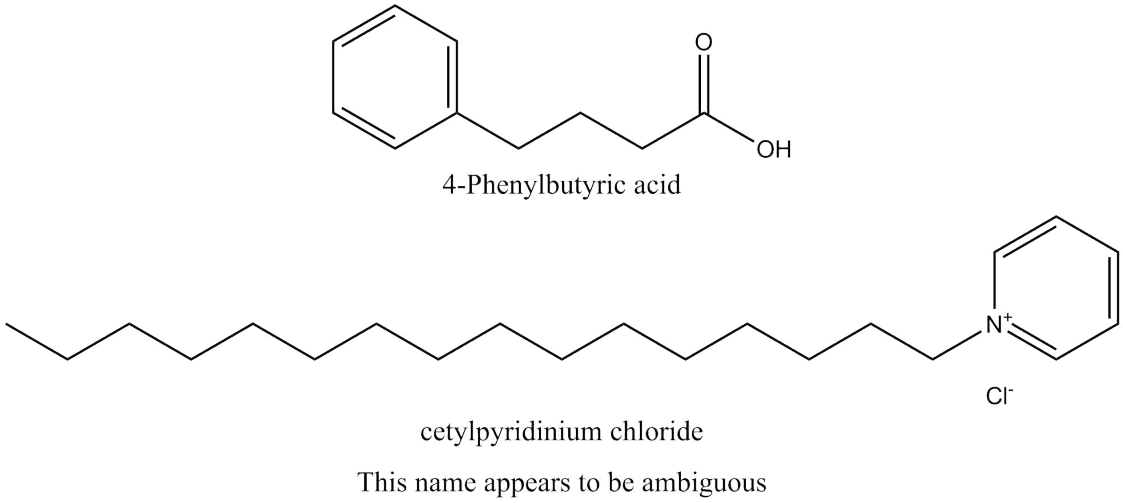

Figure 3.9: 4-Phenylbutyric acid (PBA) and cetylpyridinium chloride (CPyC) fluorophore-quencher pair.

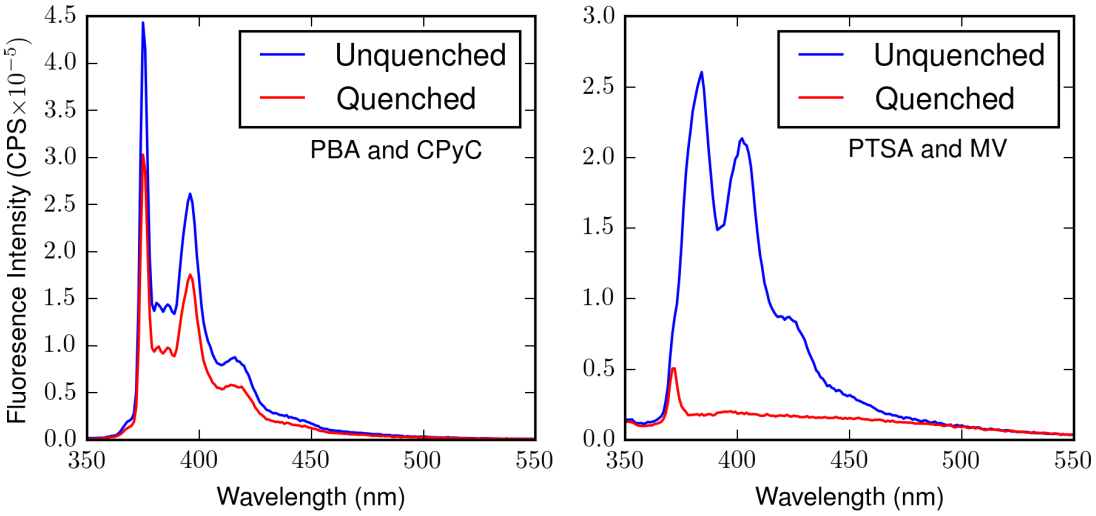

Figure 3.10: Quenching test of two different fluorophore-quencher pairs in $w_0 = 5$ AOT RMs. (left) 4-phenylbutyric acid (PBA) and cetylpyridinium chloride (CPyC); (right) pyrene tetrasulfonic acid (PTSA) and methyl viologen (MV). In both cases the quencher concentration is approximately 1.6 quencher/RM, and should lead to complete quenching (no fluorescence), but only the PTSA+MV system is fully quenched.

unclear if this is inherent to the size and structure of AOT/H_2O/Isooctane RMs, or if it is due to the fluorophore-quencher pairs. Additional systematic studies must be undertaken to figure out the source of these difficulties. One thing is clear, which is that the PBA/CPyC fluorophore quencher pair is unsuited to SFQ in RMs, this is likely due to the two molecules having little to no reason to be in contant when distributed along the RM surface.

Bibliography

(1) McPhee, J. T.; Scott, E.; Levinger, N. E.; Van Orden, A. *The Journal of Physical Chemistry B* **2011**, *115*, 9576–9584.

(2) Oliveira, C. S.; Bastos, E. L.; Duarte, E. L.; Itri, R.; Baptista, M. S. *Langmuir* **2006**, *22*, 8718–8726.

(3) Maruyama, Y.; Ishikawa, M.; Satozono, H. *Journal of the American Chemical Society* **1996**, *118*, 6257–6263.

(4) Turro, N. J.; Yekta, A. *Journal of the American Chemical Society* **1978**, *100*, 5951–5952.

(5) Infelta, P. *Chemical Physics Letters* **1979**, *61*, WOS:A1979GJ43100022, 88–91.

(6) Nandi, S.; Ghosh, S. K.; Bhattacharya, S. C. *Colloids and Surfaces a-Physicochemical and Engineering Aspects* **2005**, *268*, WOS:000233079200019, 118–123.

(7) Nandi, S.; Bhattacharya, S. C. *Journal of Molecular Liquids* **2000**, *89*, 223–231.

(8) Shen, Y.; Duhamel, J. *Langmuir* **2008**, *24*, 10665–10673.

(9) Manoj, K. M.; Jayakumar, R.; Rakshit, S. K. *Langmuir* **1996**, *12*, 4068–4072.

(10) Piletic, I. R.; Moilanen, D. E.; Spry, D. B.; Levinger, N. E.; Fayer, M. D. *Journal of Physical Chemistry A* **2006**, *110*, 4985–4999.

(11) Maitra, A. *J. Phys. Chem.* **1984**, *88*, 5122–5125.

(12) Gallego, M. J. P.; Bravo-Diaz, C.; Gonzalez-Romero, E. *Colloids and Surfaces a-Physicochemical and Engineering Aspects* **2004**, *249*, WOS:000225815700006, 25–28.

(13) Hasegawa, M.; Sugimura, T.; Shindo, Y.; Kitahara, A. *Colloids and Surfaces A: Physicochemical and Engineering Aspects* **1996**, *109*, 305–318.

Chapter 4

2D NMR Studies of Nanoconfined Carbohydrates

(Or "How I learned to stop worrying and love the radio frequency spectrum)

Material presented in this chapter comprises part of a manuscript in preparation entitled, "Sweet Confinement: Glucose and Other Carbohydrates in Reverse Micelles" by Benjamin P. Wiebenga-Sanford, Christopher D. Rithner, Jack B. Washington, Brett Cosgrove, Eduardo Palomares, Derrick Vasquez and Nancy E. Levinger, to be submitted to the Journal of Physical Chemistry B. I have made all the measurements and data analysis reported in this chapter.

4.1 Why 2D NOESY?

In Chapter 2 I demonstrated that glucose resides in the RMs and is insoluble in isooctane without the presence of both surfactant and water. This was the basic requirement to be able to study the interaction of glucose with other biomolecules by adding both to RMs at the same time. The observation of an apparent size reduction for glucose-containing RMs put plans to introduce biological macromolecules in to our confined, sugary environments on hold. Something as exotic as particle size reduction requires that I understand it before moving forward. The most readily available explanation for the RMs shrinking is glucose acting as a surfactant and inserting into position ③ of Fig. 4.1, which would increase the surface area of the system and reduce average particle size via the definition of w_0 and its relation to particle size (see Sec. 1.2). The cartoon depiction of an AOT RM in Fig. 4.1 designates five potential locations fork glucose or other carbohydrates to reside. Occupying positions ① or ② results in glucose adding to volume, increasing particle size. For glucose to occupy positions ④ or ⑤ it would need to leave the water pool, reducing the available volume, and lead to size reduction. While positions ④ and ⑤ could explain RM size reduction there is no theoretical basis for glucose partitioning into either position. Glucose is 60 times less soluble in ethanol than water[1], making the idea that it would suddenly become soluble in isooctane a ludicrous proposition.

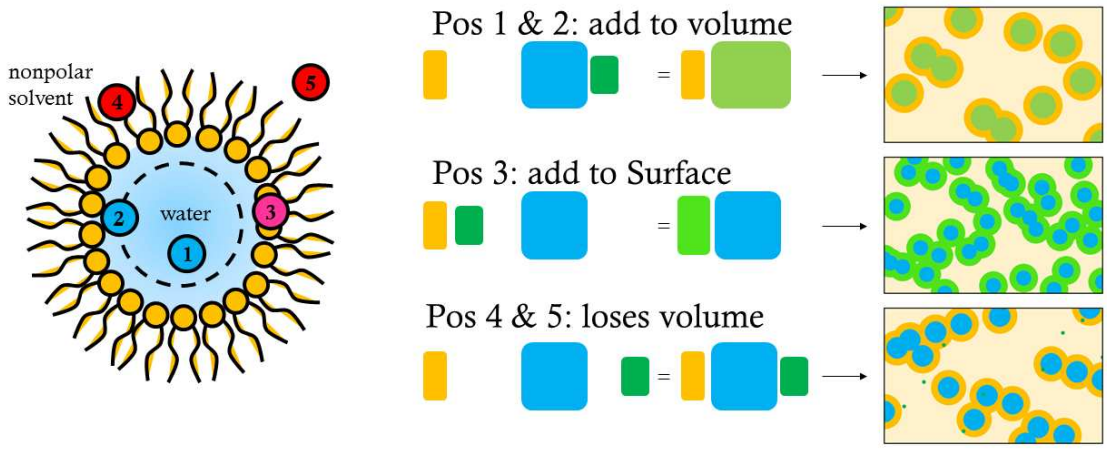

Figure 4.1: Possible locations for glucose to reside within the reverse micelle. ① Fully solvated by water, an environment that shares many qualities of bulk water[2], ② adsorbed to the interface in contact with Na^+ and SO_3^- ions, a highly polar, high ionic strength aqueous environment, ③ inserted into the surface in contact with AOT, a polar and highly restricted environment that would also involve contact with AOT headgroup protons and esters, ④ hanging out in the AOT tails, ⑤ dissolved in the nonpolar solvent (isooctane in this case). As glucose is completely insoluble in nonpolar solvent positions ④ and ⑤ are essentially impossible. The experiments performed in chit chapter give strong evidence against positions ③, ④, and ⑤, leaving only ① and ② as locations for glucose or the other carbohydrates studied, neither of which explain the observed size reduction for carbohydrate-loaded RMs.

The difference between locations ① through ⑤ can be defined through their proximity to other species in the system. This makes ^{1}H-^{1}H NOESY (Nuclear Overhauser Effect [NOE] SpectroscopY) a natural choice to find out which positions the glucose is occupying. Because the NOESY signal is proportional to $1/r^6$ where r is the distance between the interacting nuclei, this technique is well suited to measuring the location of species with respect to each other. Each location pictured in Fig. 4.1 have predicted diagnostic NOESY signals to differentiate them from the others. For position ①, deep in the water pool at the interior of the RM, glucose is only near water; position ② will include water and the possibility of contact between glucose and AOT headgroup protons 1,1'-3,3' as defined in Fig. 4.2; position ③ will involve significant interactions between glucose and AOT headgroup protons 1,1'-3,3', reduced or no interaction with water, and a possibility of interaction with other AOT tail protons; position ④ is buried in the aliphatic surfactant tails and will have only the rarest chance of interaction with anything but those tails and the nonpolar solvent; finally position ⑤ is solvated by the nonpolar phase and will show no AOT-glucose

or water-glucose interactions. In principle, the carbohydrate molecules could reside in any of these environments, ①-⑤, however the high solubility of the carbohydrates in water, glucose loading capacity of RMs being proportional to the w_0 of the RMs (i.e., larger RMs don't just dissolve more glucose, but a larger amount of glucose per water molecule) and the insolubility of glucose and other carbohydrates in nonpolar solvents makes positions ④ and ⑤ functionally impossible. So really I'm looking to distinguish between positions ①, ②, and ③, and expecting that positions ① and ② will be most likely but position ③ doing the best job of explaining the RM size change due to glucose (spoiler: nothing about the following data shows glucose to be in position ③, ④, or ⑤, which makes the size reduction that much more mysterious).

Glucose was chosen to be the primary carbohydrate of study entirely due to its cost, availability, and biological relevance but a serendipitous benefit to using glucose for the experiments presented here is that it has rich ^{1}H-NMR spectroscopy and almost no signal overlap with AOT. As shown in Fig. 4.2, a number of glucose aliphatic protons are baseline separated from each other, and only protons 6 and 5α overlap with AOT proton signals at all. Another enormous benefit to the experiments done here is that as I was particularly concerned with the behavior of glucose in an aqueous environment. Thus, I opted against using D_2O for my polar phase to avoid isotope effects. This decision directly led to the glucose hydroxyl protons having an NMR response, instead of being exchanged for deuterium, and directly led to the observation and subsequent measurement, of slowed proton exchange between water and glucose in reverse micelles (a topic discussed in depth in Chapter 5). Again, the particulars of glucose ^{1}H-NMR spectroscopy were a benefit as, by complete chance, glucose hydroxyl protons in a reverse micelle have a dramatically different and readily apparent visual appearance compared to bulk aqueous glucose. By comparison sorbitol, xylitol, and even trehalose (Figs. 4.17, 4.18, and 4.16, respectively) show far less dramatic changes to their hydroxyl proton ^{1}H-NMR spectra, and this observation (not to mention the publication resulting from it[3]) would have been missed entirely!

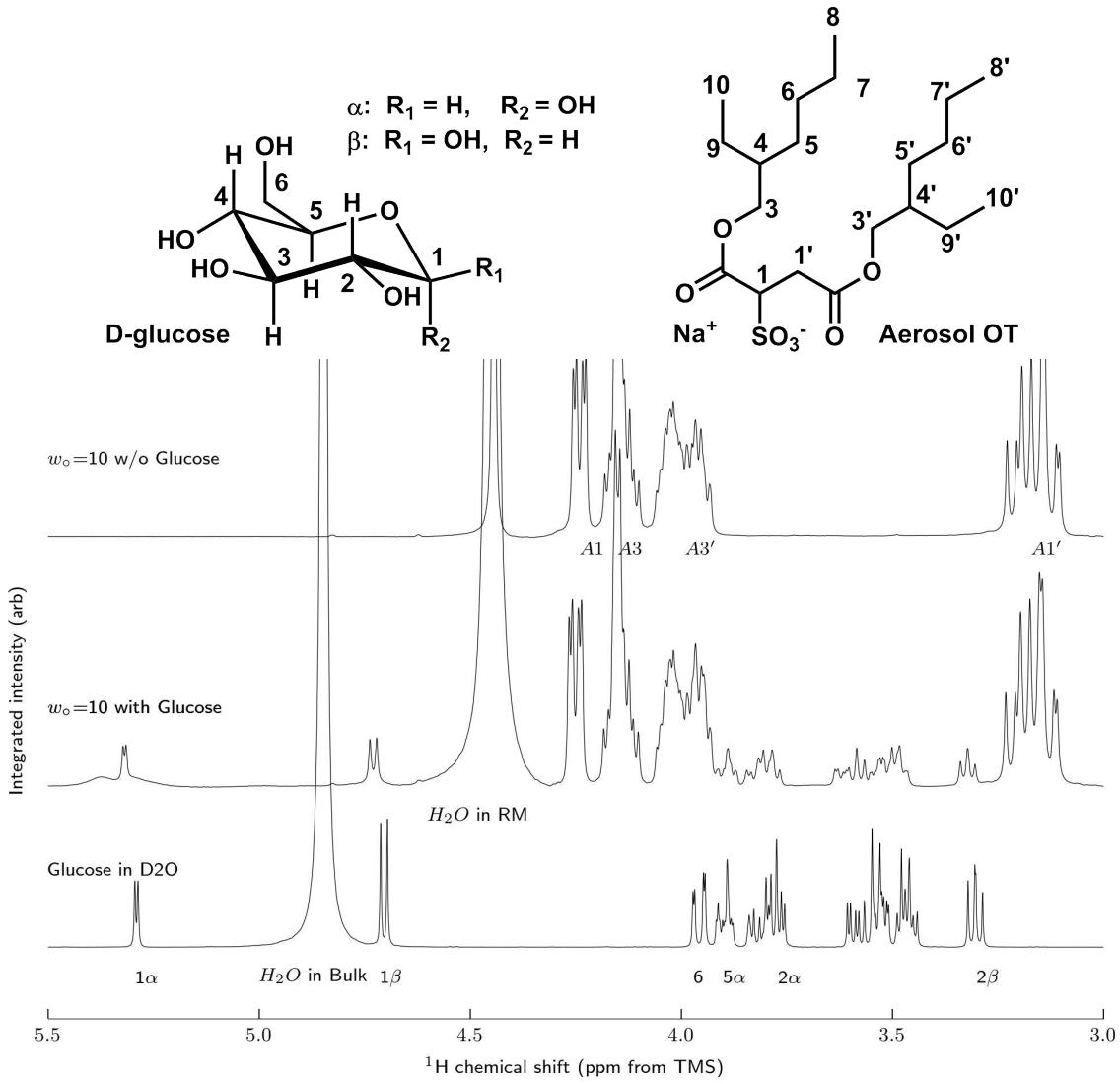

Figure 4.2: AOT and glucose spectra with all resonances for glucose, water, and AOT headgroups (1-3, and 1'-3') identified. Resonances beyond 3 ppm are entirely due to nonpolar solvent and AOT 4,4'+ protons which are not expected to interact with glucose and mostly overlap each other, so their assignments are omitted.

4.2 Introduction to 2D NOESY

NOESY is one of the most important kinds of 2D NMR spectroscopy, as it elucidates the distance between nuclei. The NOESY process is represented in Fig. 4.3. First a standard NMR spectrum is taken with the entire system taken at equilibrium (Fig. 4.3 reference spectrum). Then one spin is targeted and moved 180° out of phase. We wait some mixing time, as this non-equilibrium spin affects those around it, and knocks them out of equilibrium as well; then another NMR spectrum is collected (Fig. 4.3 irradiated spectrum) and the reference spectrum is subtracted. The result is the targeted peak, B, is now doubly negative: once from being knocked 180° out of phase, and again from having a standard positive NMR subtracted from it. Any proton unaffected by this process will show a flat baseline after subtraction, while the affected peaks will show a positive or negative residual, depending on whether the out-of-phase peak was a positive or negative influence on it, as shown in Fig. 4.3 Irr-Ref (NOESY). There is a second possible reason for a NOESY signal to be zero, which is related to relaxation dynamics as demonstrated in Fig. 4.6.

NMR signal intensity in general, and the strength of the NOE interaction in specific, depends on the population difference between nuclear spins aligned α (against, or anti-parallel to, the B field, high energy) and β (with, or parallel to, the B field, low energy), which in a 500 MHz NMR spectrometer is only ~80 ppb. This minuscule population difference is why NMR signals are so weak, why NOESY signals are weaker still, and why quality NOESY spectroscopy is so dependent on access to high field magnets. Modern NMR spectroscopy is performed by measuring the radio frequency signals given off by excited nuclei as they return to equilibrium (the free induction decay, or FID). This means modern NMR is intimately connected to nuclear relaxation, and in NMR spectroscopy all relaxation is stimulated relaxation. Spontaneous relaxation has such a long timescale in NMR that it can be safely ignored. The primary relaxation mechanism for all nuclei is chemical shift anisotropy [§]and while it is the most prominent relaxation mechanism (being the

[§]This entirely jargon term can be unpacked as follows: each nucleus has an electron cloud surrounding it, which produces a localized magnetic field that opposes the applied magnetic field. This changes that proton's Larmor frequency (chemical shift) slightly. The orbitals in a molecule are anisotropic, which results in an oscillating magnetic field as the molecule tumbles. Some of these oscillations are close enough to the Larmor frequency to stimulate the surrounded nucleus, which results in relaxation due to "chemical shift anisotropy".

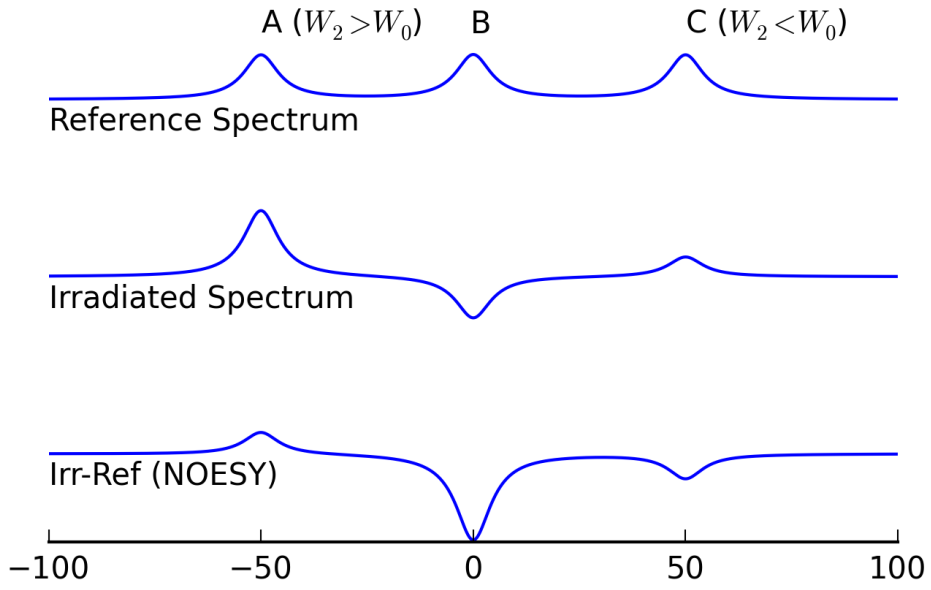

Figure 4.3: A cartoon representation of the NOE process for three spins A, B, and C. In this case spin A is in the fast motion regime while spins B and C are both in the slow motion regime. In the reference spectrum there is no NOE enhancement. The irradiated spectrum involves applying a $180°$pulse to spin B and waiting a set time, τ, for NOE enhancement to evolve. The result is a (greatly exaggerated) increase in the intensity of spin A, and (again exaggerated) reduction in the spin B intensity. Subtracting the reference spectrum from the irradiated spectrum reveals the amount and phase of NOE enhancement that A and C feel from B (A and C don't influence each other in this example).

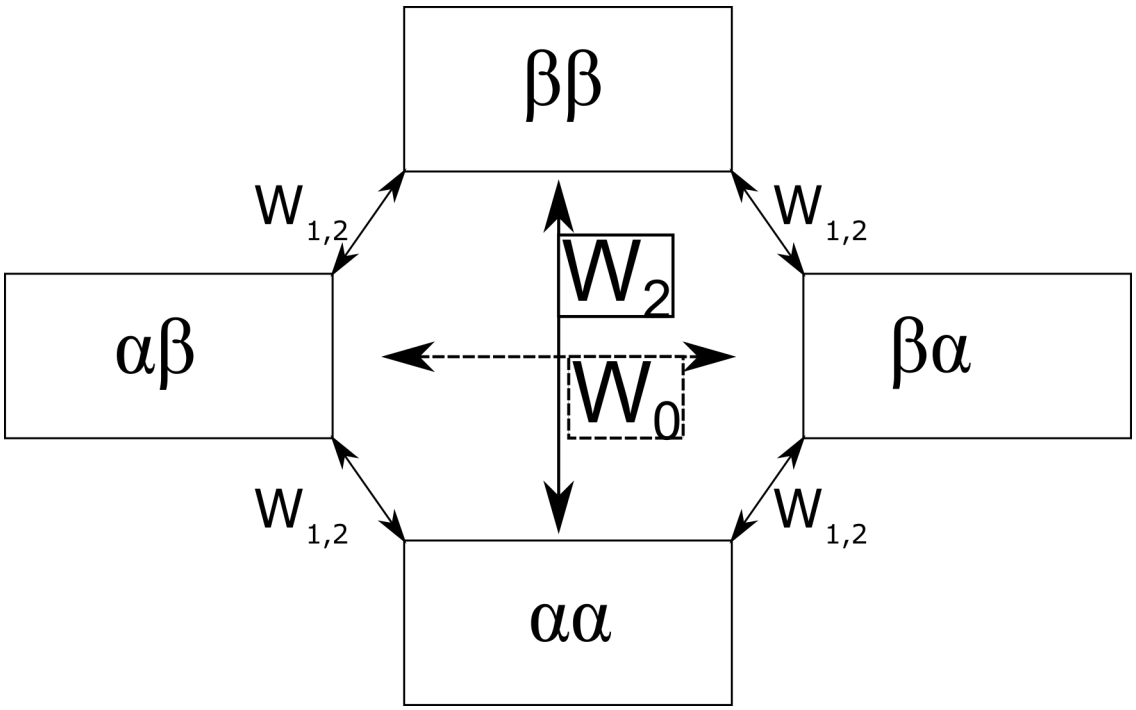

Figure 4.4: The possible transitions in a two spin system. $W_{1,X}$ means a W_1 transition in which spin X is changing. W_0 and W_2 are two-quantum transitions, in W_0 there is no energy change while in W_2 both spins change from high to low energy or from low to high.

source of anywhere from 90-100% of the relaxation observed), there is also relaxation due to the interaction of two nuclei in close proximity. This is, quite literally, the defining method of relaxation for NOESY, as it is called the nuclear Overhauser effect (NOE), or sometimes cross-relaxation. This interaction between two nuclei is represented by transitions W_0 and W_2 in Fig. 4.4.

The nature of the W_0 and W_2 transitions is of great importance to NOESY spectroscopy, as the W_2 transition slightly increases the population difference between α and β spins (positive enhancement) while the W_0 transition reduces the population difference (negative enhancement). The combination of these rate constants is called the cross relaxation constant, ${\sigma_{12}}^4$, and is shown in equation 4.1. Here the $b = \mu_0 \hbar \frac{\gamma_1 \gamma_2}{4\pi} \frac{1}{r^3}$, meaning that $\sigma_{12} \propto \frac{1}{r^6}$, the source of NOESY's distance dependence. The $j(\omega)$ terms are referred to as the reduced spectral density function $j(\omega) = \frac{2\tau_c}{1+\omega_0^2 \tau_2^2}$ and is the source of NOESY's dependence on molecular motion via its relation to angular correlation time (Fig. 4.5) and the Larmor frequency.

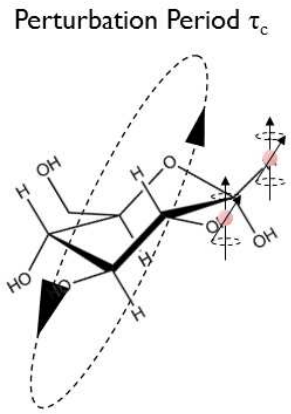

Figure 4.5: Angular correlation time of a single molecule is defined as the average time it takes that molecule to spin 1 radian away from its starting position.

$$\sigma_{12} = \mathrm{W}_2 - \mathrm{W}_2 = b^2 \left[\frac{3}{10} j\left(2\omega_0\right) - \frac{1}{20} j\left(0\right) \right] \tag{4.1}$$

In NOESY spectroscopy fast motion gives rise to a positive phase signal, while slow motion is a negative phase. The terms "fast" and "slow" are usually of little use because they are relative terms, but in the case of NOESY they can be reasonably well defined, as there is something to relate them to, specifically the Larmor frequency (500 MHz for the 11 T magnet used in my experiments). In this way, fast motion is anything with correlation time substantially faster than the Larmor frequency$\left(\frac{1}{\tau_c} \gg \omega_\circ\right)$ while slow motion is the reverse case $\left(\frac{1}{\tau_c} \ll \omega_\circ\right)$. When motion is fast, the W_2 term dominates σ_{12} because there is lots of energy available to stimulate a transition with a large energy difference between the two states. In the slow motion regime there isn't much energy to promote *any* transition. Thus, W_0, with no energy difference between the two states, dominates by default. This motional dependence is nice, because it lets us know if *either* spin is moving fast, or if *both* spins are moving slowly, but it also brings a danger. Specifically the crossing point in Fig. 4.6 that occurs when $\tau_c\omega_\circ = \sqrt{\frac{5}{4}}$. This is the point at which the positive and negative enhancement effects cancel each other out and no NOESY signal is present in the spectrum despite there being a NOE interaction between spins.

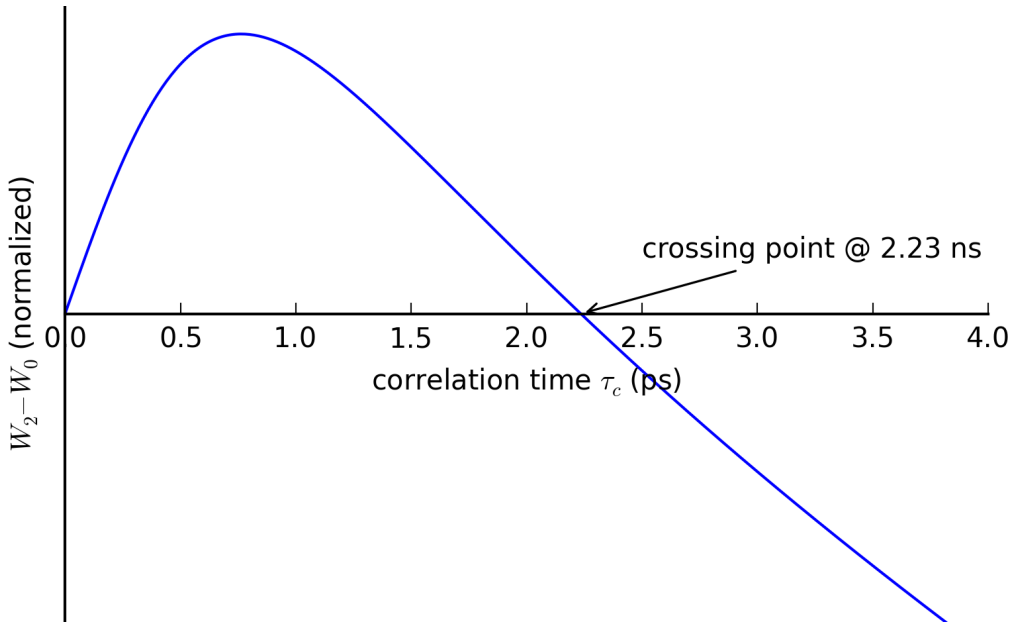

Figure 4.6: NOESY phase dependence on molecular motion. For molecules that tumble quickly in solution $\left(\frac{1}{\tau_c} \gg \omega_\circ\right)$ the NOE enhancement factor is positive, while for slow tumbling $\left(\frac{1}{\tau_c} \ll \omega_\circ\right)$ it is negative. If the tumbling time is close to the Larmor frequency (specifically if $\tau_c\omega_\circ = \sqrt{\frac{5}{4}}$) then the NOESY enhancement will be zero. To identify if the NOE exists requires ROESY spectroscopy to be visible.

4.2.1 2D ROESY Spectroscopy

To protect against the danger of missing NOE interactions due to the crossing point in Fig. 4.6 I also performed Rotational Overhauser Effect SpectroscopY (ROESY) which is extremely similar to NOESY except it is in a rotational reference frame spinning at the Larmor frequency. This is achieved by rotating the spin population into the x-axis and then applying a strong RF field for the duration of the experiment. This RF field is strong enough to "lock" the spins into the x-axis, and therefore a rotational frame. The advantage of this is that now the cross relaxation term is now equation 4.2 which, unlike NOESY, cannot be negative and has no crossing points. Meaning unlike NOESY, all NOE interactions are visible in ROESY spectroscopy. The reason ROESY is not the dominant form of 2D-NMR over NOESY comes from two deficiencies in ROESY: bombarding the sample with a strong RF field heats the sample, limiting the duration of a ROESY experiment and (more importantly) any molecular motion information for species with correlation times *not* near the crossing point is lost!

$$\sigma_{12} = b^2 \left[\frac{3}{20} j\left(2\omega_0\right) + \frac{1}{10} j\left(0\right) \right] \tag{4.2}$$

4.3 Proton Exchange as Applied to NOESY/ROESY

Nearly every treatment of NOESY will mention that it detects "through-space interactions (and exchange)". That "(and exchange)" term is important because Fig. 4.4 only represents possible *relaxation pathways*. Spin populations can also change by physically moving a proton from spin 1 to spin 2. Because of this, NOESY will register a cross-peak for keto-enol tautomerism, cis-trans isomerism, physically adsorbing to a surface and re-solubilizing, or chemical exchange from one molecule to another[5]. It is this last behavior that concerns the experiments in this chapter and Chapter 5 because glucose hydroxyls are labile and readily exchange with water. Therefore if the glucose is able to exchange with water, it will always show a cross peak in the NOESY. This is something of a problem, as glucose-water exchange is common and its signal drowns out any possible NOESY, but in our case it is not really a big problem. Proton exchange requires the two species to be within hydrogen bonding distance (~2.5 Å)[6] for exchange to occur. This means that the significant evidence of chemical exchange in these spectra is a reasonable replacement for NOESY as a measure of the proximity of water to glucose hydroxyl groups. We can discern the difference between signals arising from exchange and NOE by using ROESY spectroscopy. Cross peaks due to chemical exchange are always negative because the exchanging proton has already been flipped 180° but NOE in ROESY is always positive. Therefore a negative peak in ROESY is definitely due to exchange.

4.4 Glucose NOESY Data and Discussion

Having become an "expert" at NOESY spectroscopy, it's time to look at the NOESY spectrum of a glucose-loaded RM and see what interactions there are. Fig. 4.7 presents the entire spectrum of a glucose loaded RM in hexane-d_{14}. This way the nonpolar solvent does not have an NMR trace and only AOT, glucose and water interactions will show up. By using a deuterated alkane,

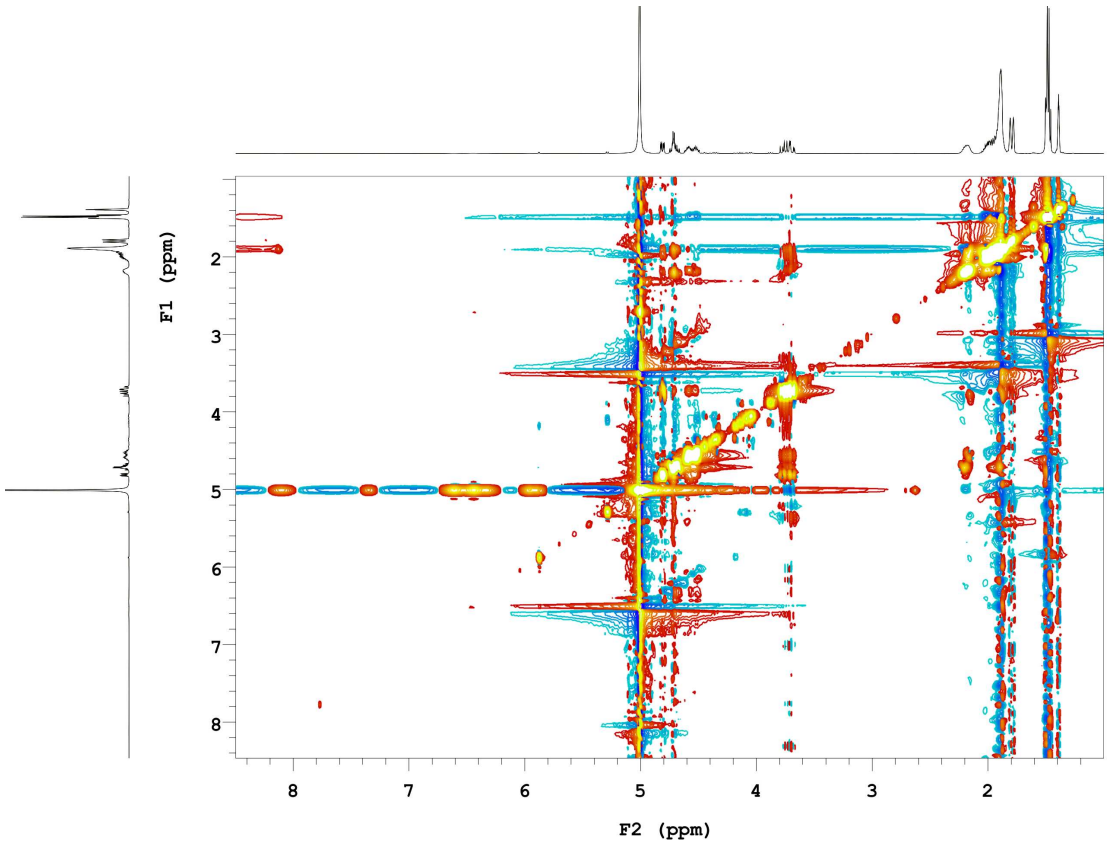

Figure 4.7: NOESY of $w_0 = 10$ glucose loaded RM with [AOT]=0.1M, glucose:H_2O = 1:25 with hexane-d_{14} as the nonpolar solvent. This spectrum is messy, but also necessary as it shows no cross peaks between the AOT tail groups (all of which have a chemical shift of 2 ppm or less) and glucose. For this reason I was free to use the standard isooctane solvent to prepare the rest of my NMR samples, despite it being laden with protons that occupy the same chemical shift region as the AOT tail groups.

we eliminate signals that arise from the nonpolar continuous phase. We used hexane-d_{14} instead of the standard isooctane because the cost of perdeuterated isooctane is prohibitive (at least 10 times more expensive than the hexane-d_{14}, which is already pretty expensive). AOT RMs form readily in a range of alkanes[7] so knowledge aquired in these hexane RMs can be transferred to the isooctane RMs used in the rest of the experiments.

At chemical shifts greater than 6 ppm, the cross peaks arise exclusively from chemical exchange between water and glucose hydroxyl groups. This stuff is super interesting, but not NOESY and so gets its own chapter (Chapter 5). As I already said when first discussing Fig. 4.2, everything upfield of 3 ppm arises only from AOT-AOT, or AOT-nonpolar solvent interactions and gives no insight into the location of the glucose. So the portion of the NOESY spectrum I will focus on for

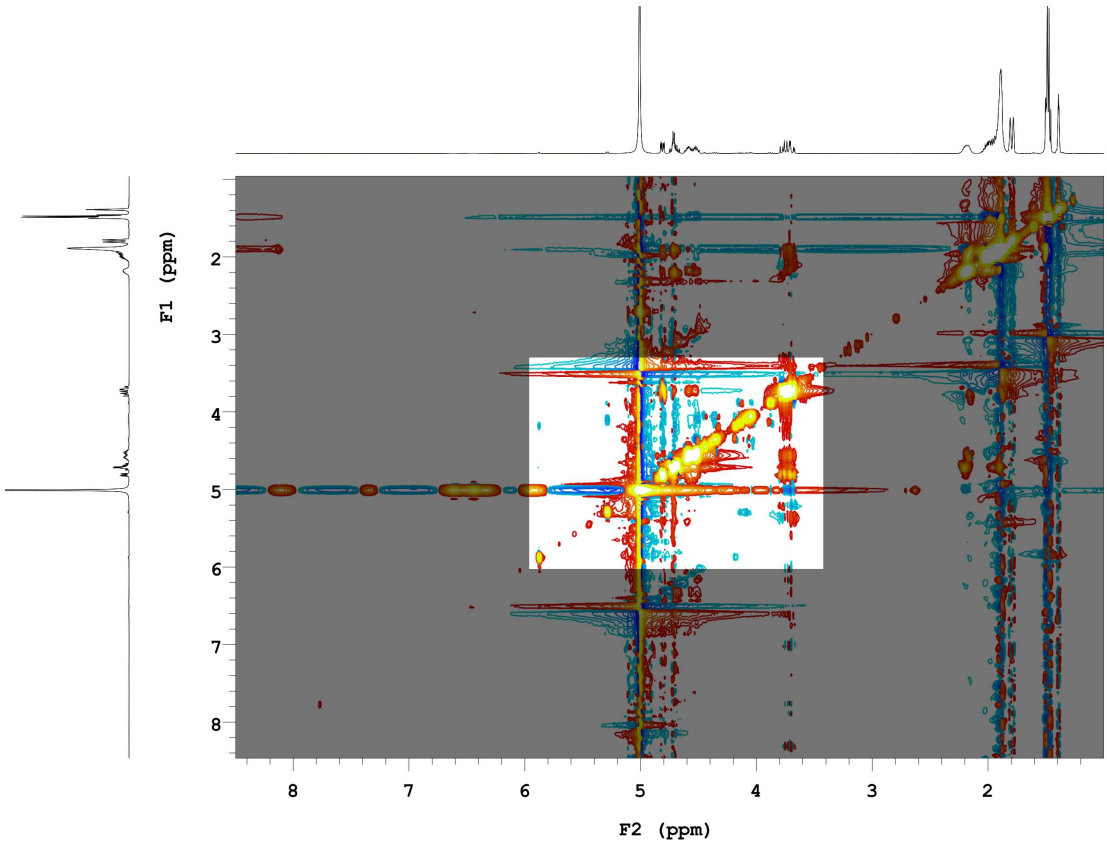

Figure 4.8: A NOESY spectrum of glucose loaded RM with d14 hexane instead of isooctane. Everything outside of the highlighted box is irrelevant to this chapter. Everything upfield is purely AOT-isooctane or isooctane-isooctane interactions, and everything downfield is chemical exchange, which is discussed in the next chapter.

the rest of this chapter is the one containing glucose alkyl and AOT headgroup protons between 3 and 6 ppm. This is the unshaded portion of Fig. 4.8. This lets me use a zoomed-in spectrum that makes further analysis easier to describe (Fig. 4.9).

I will first simply describe all the remaining peaks present. Please refer back to Fig. 4.2 at the beginning of this chapter for a reminder of proton labels and locations of species present in Fig. 4.9. The first peak to discuss is water at 4.25 ppm. It is enormous compared to the rest of the peaks because water is the highest concentration species in the sample aside from nonpolar solvent. Because of this, and because water is the smallest molecule and most likely to change environments due to simple translational movement during the experiment, inconsistencies in the water peak result in imperfect subtraction of reference water signal from the irradiated signal. This

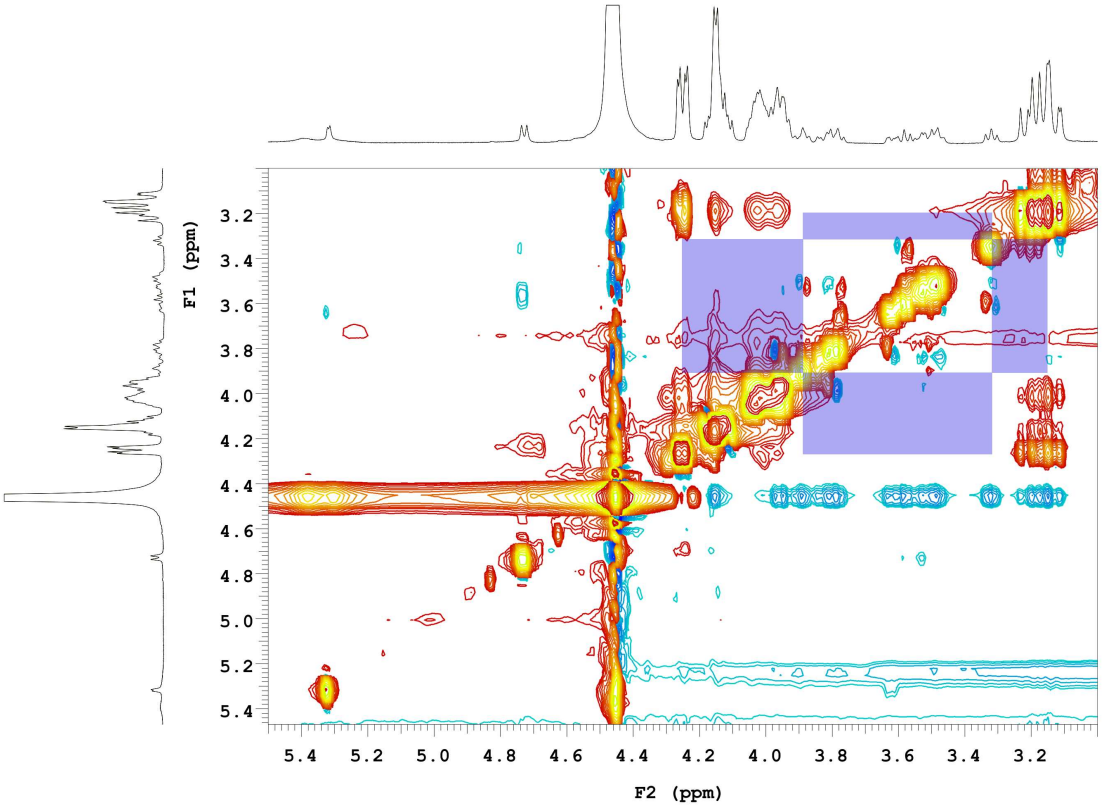

Figure 4.9: The NOESY spectrum, highlighting the parts of the spectrum in which glucose-AOT NOE should be. As can be seen, there is no NOE cross peak in these purple boxes, greatly reducing the plausibility that glucose is occupying position ③.

results in the large vertical artifact at the same chemical shift as water. Next are the two anomeric protons 1α and 1β, which are downfield (larger chemical shift value) of water near 4.7 and 5.3 ppm, respectively. These two protons have NOE interactions with water that are somewhat overwhelmed due to overlap with alcohol exchange peaks. The ratio of α/β is also different in a RM than in bulk water, as discussed in Chapter 2. Finally, there is the most complicated section of the spectrum: the non-anomeric glucose alkyl and AOT headgroup protons, 3 to ~4.3 ppm. Certain protons (such as AOT $1'$ and glucose 2β) are easily differentiated from each other but there is a significant overlap of the AOT $3'$ and glucose 6 protons at ~3.6 ppm; this overlap is the only significant complication to the rest of the analysis of this NOESY spectrum.

Before talking about signals that are present, I want to discuss that which is not present. Specifically, the purple boxes drawn on Fig. 4.9 highlight where major interactions between glucose and AOT *would be* if glucose was inserted into the AOT interface. It's absence of evidence, but also

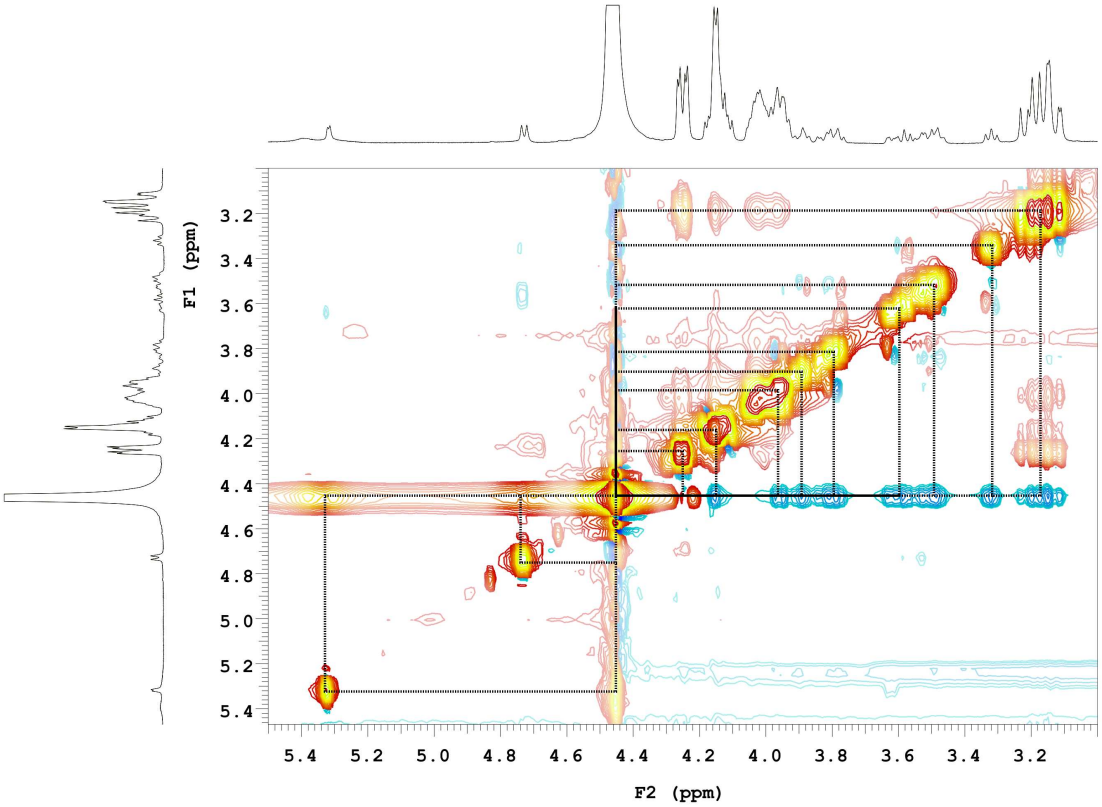

Figure 4.10: Dotted lines indicate all the interactions that water has with the rest of the system. Water interacts with nearly everything and is tumbling rapidly, both unsurprising results, unfortunately.

evidence of absence. Next are all of the interactions that water has with the AOT and glucose as highlighted in Fig. 4.10. Put simply: water gets with everything except for the AOT tail protons (referring back to Fig. 4.7 for the lack of cross peak between water and these groups) These peaks are also positive phase; evidence that at least one of the species involved is tumbling rapidly. Of course, one of the species involved is water, and if anything in this system were to tumble rapidly it would be water. Therefore no insights into the motional regime of AOT or glucose can be found from cross peaks with water. Ideally, this free movement and lack of interaction with any AOT proton would allow me to confidently state that glucose is occupying position (1). However, the AOT sulfonate group, with a $\sim 5\,\mathring{A}$ diameter[8], is large enough that it could hold the glucose molecule beyond the 4-5 $\mathring{A}$ maximum effective range within which the NOE effect is considered to be observable[4].

Next up are the AOT-AOT cross peaks, highlighted in Fig. 4.11. The AOT 1' proton has interactions with all of the other three AOT peaks, while the rest appear not to interact with each other. This is somewhat troubling as there should be strong (equivalent to the AOT 1') interactions between at least AOT 1 and 3, and probably between 3 and 3'. The most likely explanation is that these cross peaks are present, but subsumed by their proximity to the diagonal and its effect on the NOESY baseline. It is important to note that the lack of AOT-glucose interactions cannot be explained via the same argument. Much more exciting than the cross peaks is the *sign* of these peaks which make it clear that AOT is tumbling slowly. Despite AOT being the largest molecule in the system, a free-floating AOT molecule would still be expected to have a short correlation time. This is strong evidence that the AOT molecules are bound to the interface of the RM aggregate and rotating on the timescale of the entire RM, a tumbling period significantly longer than 2 nanoseconds.

Now come the final hardest to see, but possibly most important cross peaks. Highlighted in Fig. 4.12 are the NOE cross peaks between the glucose 1α and 2α protons, as well as 1β and 2β. These are certainly intramolecular NOEs as $\alpha - \beta$ interactions are not present. The population of α and β glucose in solution is near enough to 50:50 that if intermolecular interactions were present, I would expect to see three sets of peaks, with relative intensities of 50:25:25 for $\alpha - \beta : \alpha - \alpha : \beta - \beta$ (a Punnet square of NOE!) but they are simply not present. Additionally, the cross peaks that are present are positive, indicating fast-moving glucose. This shows that each glucose molecule has enough space between it that there is no NOE between two different molecules, and that the molecules are rotating freely and not bound to a surface. This is our first positive evidence that the glucose is not inserted into the AOT interface; if glucose were inserted among the AOT molecules, it too would be a part of the RM aggregate and tumbling slowly. The fact that it is not means it is well in the water pool and free to tumble independent of the AOT surface aggregate. This limits the possible locations for glucose in the RM only to positions ① or ② in Fig. 4.1.

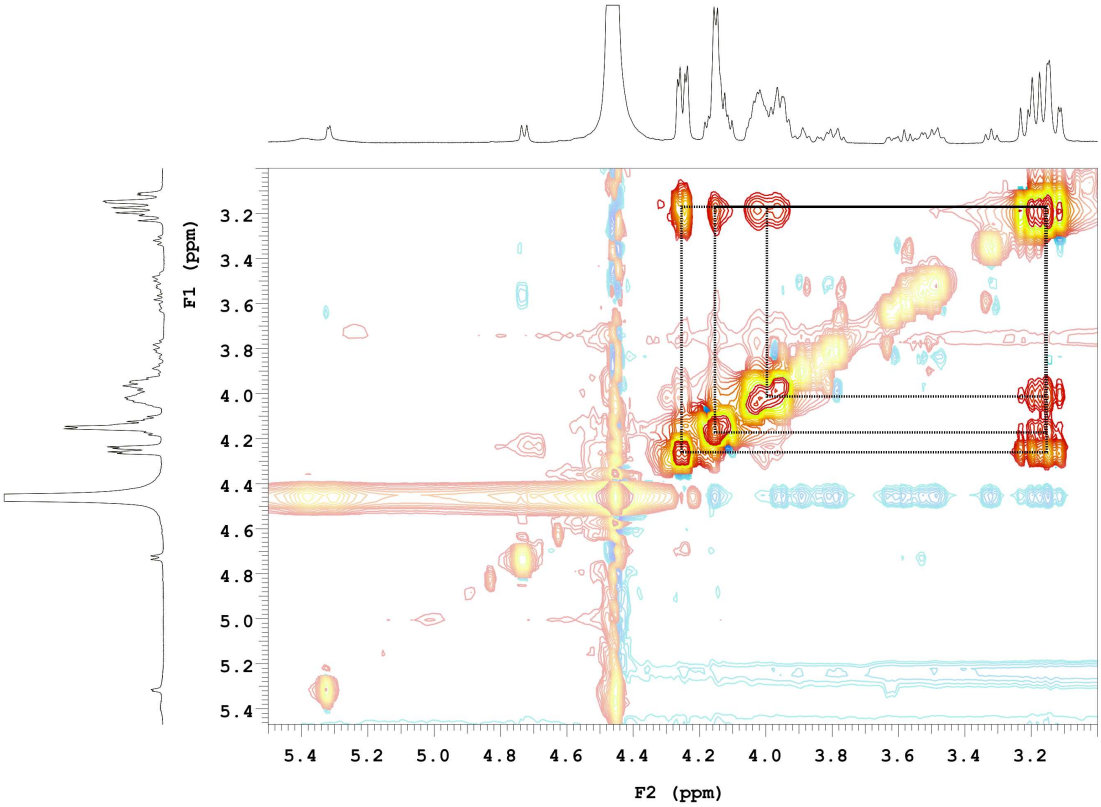

Figure 4.11: Here we see AOT-AOT interactions. The only lacking interaction is between AOT 1 and 3, though it may be present and overwhelmed by baseline errors stemming from proximity to the diagonal. The sign of all AOT-AOT cross peaks shows that the AOT is tumbling slowly. This is perfectly in line with the interpretation of nearly all AOT molecules forming the surface of the RM and tumbling at the rate of the entire RM aggregate, instead of as single molecules.

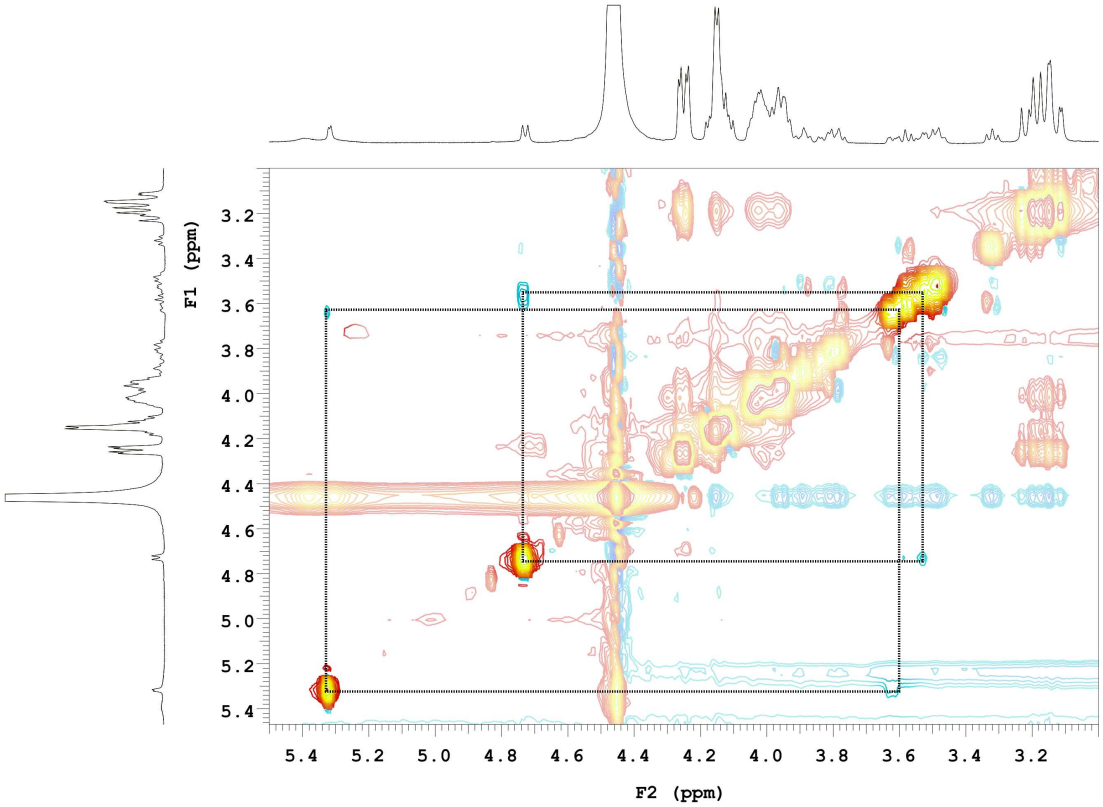

Figure 4.12: Anomeric interactions. These are exclusively intramolecular cross peaks, as the interactions are restricted to protons of the same anomer. That is, the 1α proton only talks to 2α, and the same for exclusive crosstalk between 1β and 2β. These peaks are also positive, indicating glucose is rotating quickly w.r.t. the Larmor frequency.

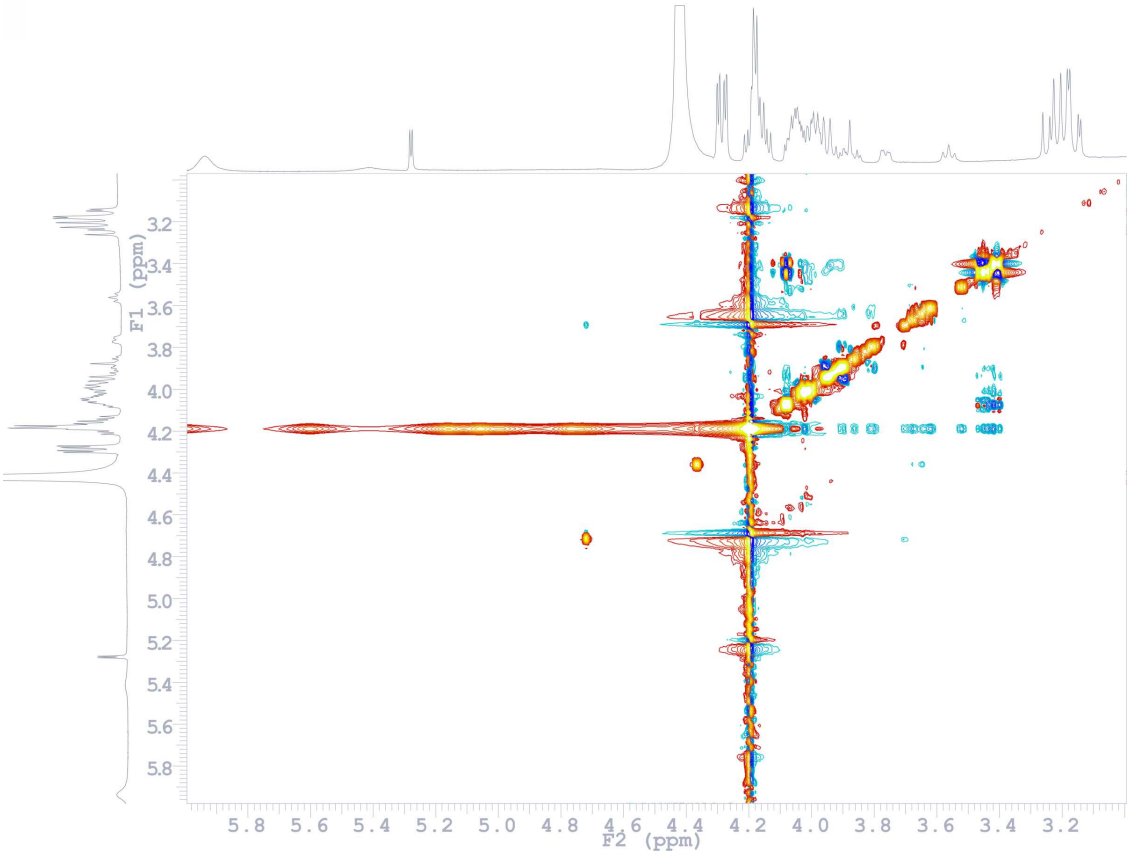

Figure 4.13: ROESY spectrum of glucose in AOT/isooctane RM. This spectrum demonstrates that the NOESY spectra presented elsewhere in this chapter are not missing any NOE cross peaks due to $\sigma_{12} \approx 0$, and confirms that the water-hydroxyl cross peaks are due to chemical exchange.

4.4.1 ROESY Data

As discussed in section 4.2.1, 2D ROESY spectroscopy can "catch" interactions between species that are rotating at or near the Larmor frequency of the spectrometer and also all NOE peaks are positive (blue) in ROESY spectroscopy. In the spectrum presented in Fig. 4.13, there are no new cross-peaks, indicating that everything is either rotating quickly or slowly w.r.t. the Larmor frequency. The only other important piece of informtion provided by the ROESY spectrum is that the AOT-AOT cross peaks change phase from negative to positive, while the water-hydroxyl cross peaks remain negative. This indicates that AOT-AOT interactions are NOE and further confirms that the water-hydroxyl interactions are chemical exchange.

4.5 NOESY of Non-Glucose Carbohydrates

Other than glucose, I also performed NOESY and ROESY spectroscopy on trehalose, sorbitol, xylitol, meso-erythritol, glycerol, and ethylene glycol. An attempt was made at collecting a NOESY of myo-inositol, but it proved to not be soluble enough in RM solutions to provide a intelligible spectrum. Other than chemical shifts, each non-glucose carbohydrate studied shares the majority of behaviors with glucose:

1. None of the NOESY spectra show AOT-carbohydrate interactions. This was even true for ethylene glycol, which has been reported to insert into the surface of AOT RMs, when it comprised the entire polar phase.[9], In the case presented here, the major polar constituent is still water.

2. All the spectra show that water interacts with all AOT and carbohydrate protons, with a positive phase showing that water is tumbling quickly.

3. All the spectra show the same AOT-AOT as in the glucose spectrum, with a phase showing AOT is tumbling at the same rate as the RM aggregate.

4. All the spectra show chemical exchange between water and the carbohydrate hydroxyl groups.

Fig. 4.15 presents the region of an ethylene glycol NOESY containing AOT 1-3 and 1'-3' protons as well as glucose aliphatic and hydroxyl protons. This spectrum most highlights the one behavior that other carbohydrates don't share with glucose: the structure of their NMR spectra are universally boring compared to glucose. Ethylene glycol shows the simplest spectrum with one each of the aliphatic and hydroxyl protons due to NMR equivalence. But examining the spectra presented in the appendix for this chapter will show similar simplicity for the other non-glucose carbohydrates studied. Even more unfortunately, they do not have α and β protons with a chemical shift much different from the rest of the aliphatic protons that can give evidence of the tumbling rates for these molecules. Despite this, all carbohydrates studied (other than trehalose) are the same size as glucose or smaller, and therefore there is no reason to believe they would be tumbling slowly.

These spectra do help to solve one major question still remaining from the glucose spectra. As I mentioned in a previous discussion of Fig. 4.2, the signals for the glucose 5α and 6 protons overlap with AOT 3', which has a prominent NOE cross peak with AOT 1'. Because of this any NOE between glucose 5α or 6 could be subsumed beneath this cross peak and would not be observed. I have performed preliminary studies using HSQC-NOESY (heteronuclear single quantum coherence) and ^{13}C labeled glucose to filter out any NOE that does not involve a proton directly bonded to carbon 13, which would remove the AOT-AOT cross peak and leave only NOE between the ^{13}C-labeled glucose and AOT but these experiments have yet to provide conclusive data. Happily, the 2D-NOESY spectra of ethylene glycol, glycerol, and meso-eryritol all present well defined carbohydrate spectra that have no overlap with AOT protons and there is no AOT-AOT cross peak under which they could be subsumed. Two of these three molecules (ethylene glycol and glycerol) have a history of inserting into the surface as the sole polar phase in RMs, but none of these three carbohydrates show interaction with AOT protons here, giving yet another piece of evidence toward throwing out position ③ as a possible location for glucose.

4.6 Conclusions

The 2D-NOESY and ROESY spectra I have presented and analyzed in this chapter show evidence that glucose and other carbohydrates partition exclusively into the water pool of AOT / water / isooctane reverse micelles. It also shows that the AOT surfactant in the RMs are bound to the surface and tumbling slowly, while glucose is unbound and tumbling quickly. This puts to rest the idea that glucose and other carbohydrates are reducing the size of w_0 equivalent reverse micelles by having "surfactant like" behavior and inserting into the surface of the reverse micelles. This also opens up the most dangerous and exciting question in science: why? It is my hope that this work has laid the foundation for further investigation into nanoconfined carbohydrates, and that pursuit of the answer to this question will elucidate insights into the interactions of carbohydrates and other biomolecules as yet unimagined.

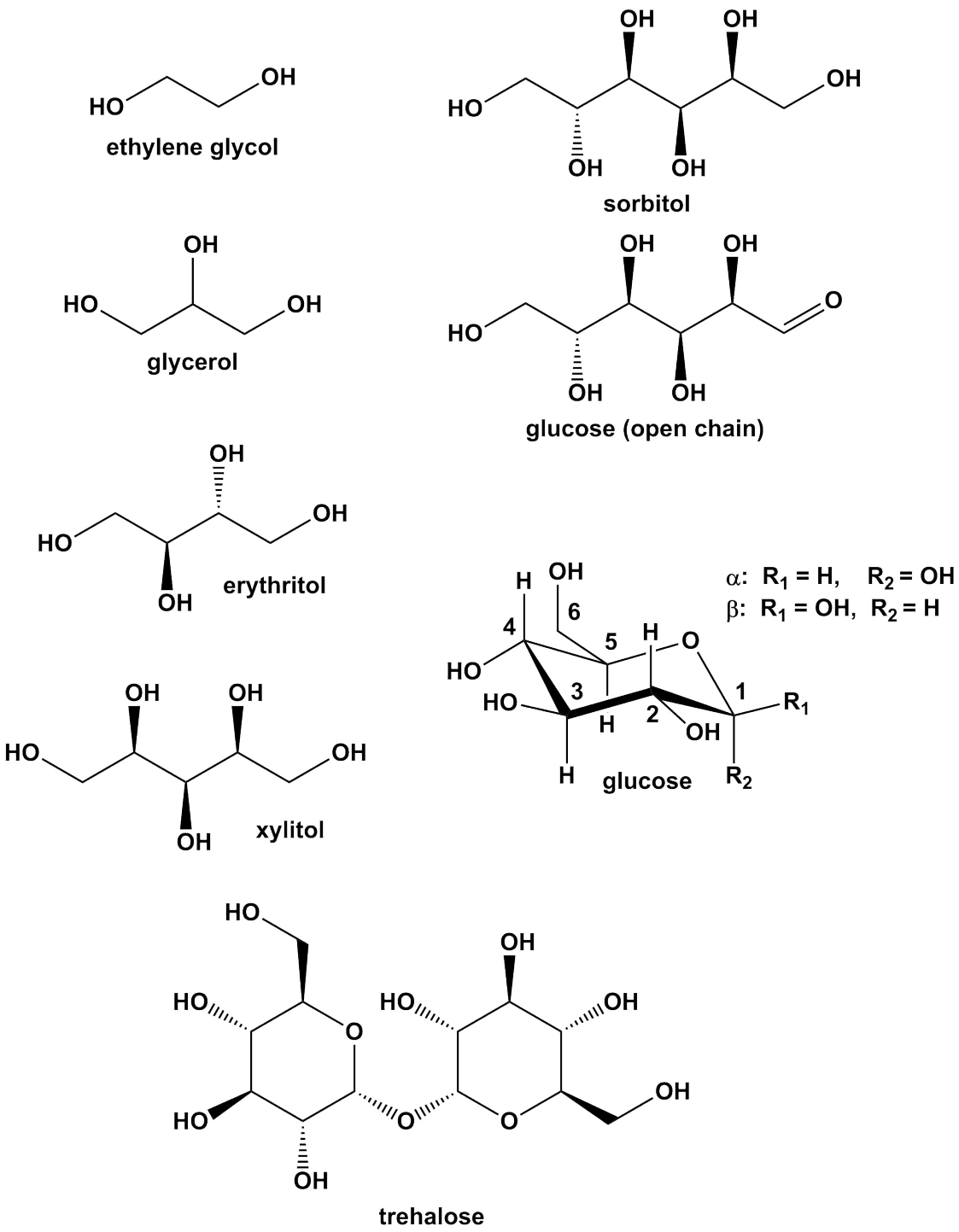

Figure 4.14: Molecular structures of glucose, sorbitol, xylitol, erythritol, glycerol,ethylene glycol, myo-inositol, and trehalose. This is the family of carbohydrates that I studied using NOESY and ROESY NMR.

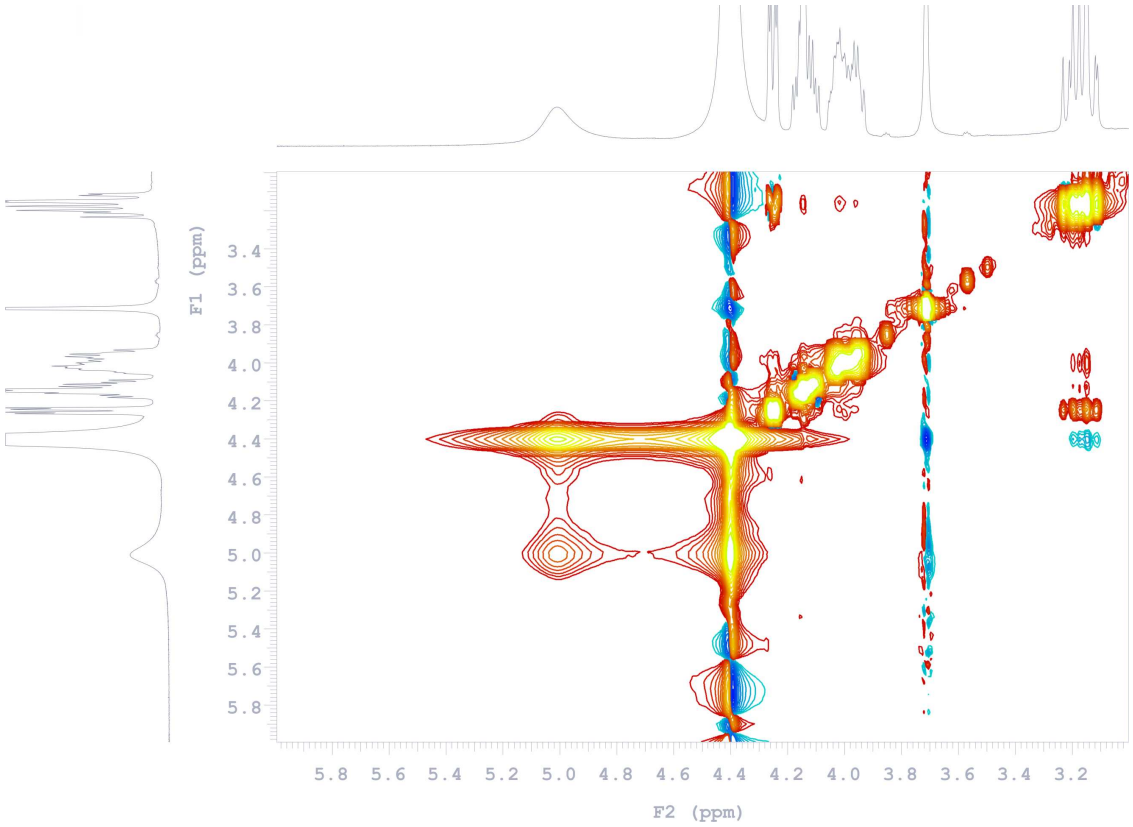

Figure 4.15: Ethylene Glycol NOESY

Bibliography

(1) Bouchard, A.; Hofland, G. W.; Witkamp, G. J. *Journal of Chemical and Engineering Data* **2007**, *52*, 1838–1842.

(2) Piletic, I. R.; Moilanen, D. E.; Spry, D. B.; Levinger, N. E.; Fayer, M. D. *Journal of Physical Chemistry A* **2006**, *110*, 4985–4999.

(3) Wiebenga-Sanford, B. P.; DiVerdi, J.; Rithner, C. D.; Levinger, N. E. *The Journal of Physical Chemistry Letters* **2016**, *7*, 4597–4601.

(4) Keeler, J., *Understanding NMR Spectroscopy*; John Wiley Sons: New York, 2011.

(5) Neuhaus, D.; Williamson, M. The Nuclear Overhauser Effect in Structural and Conformational Analysis. http://www.wiley.com/WileyCDA/WileyTitle/productCd-0471246751.html (accessed 10/12/2017).

(6) Hassanali, A.; Giberti, F.; Cuny, J.; KÃŒhne, T. D.; Parrinello, M. *Proceedings of the National Academy of Sciences* **2013**, *110*, 13723–13728.

(7) De, T. K.; Maitra, A. *Adv. Coll. Interface Sci.* **1995**, *59*, 95–193.

(8) Chowdhary, J.; Ladanyi, B. M. *J Phys Chem B* **2009**, *113*, 15029–39.

(9) Correa, N. M.; Silber, J. J.; Riter, R. E.; Levinger, N. E. *Chemical Reviews* **2012**, *112*, 4569–4602.

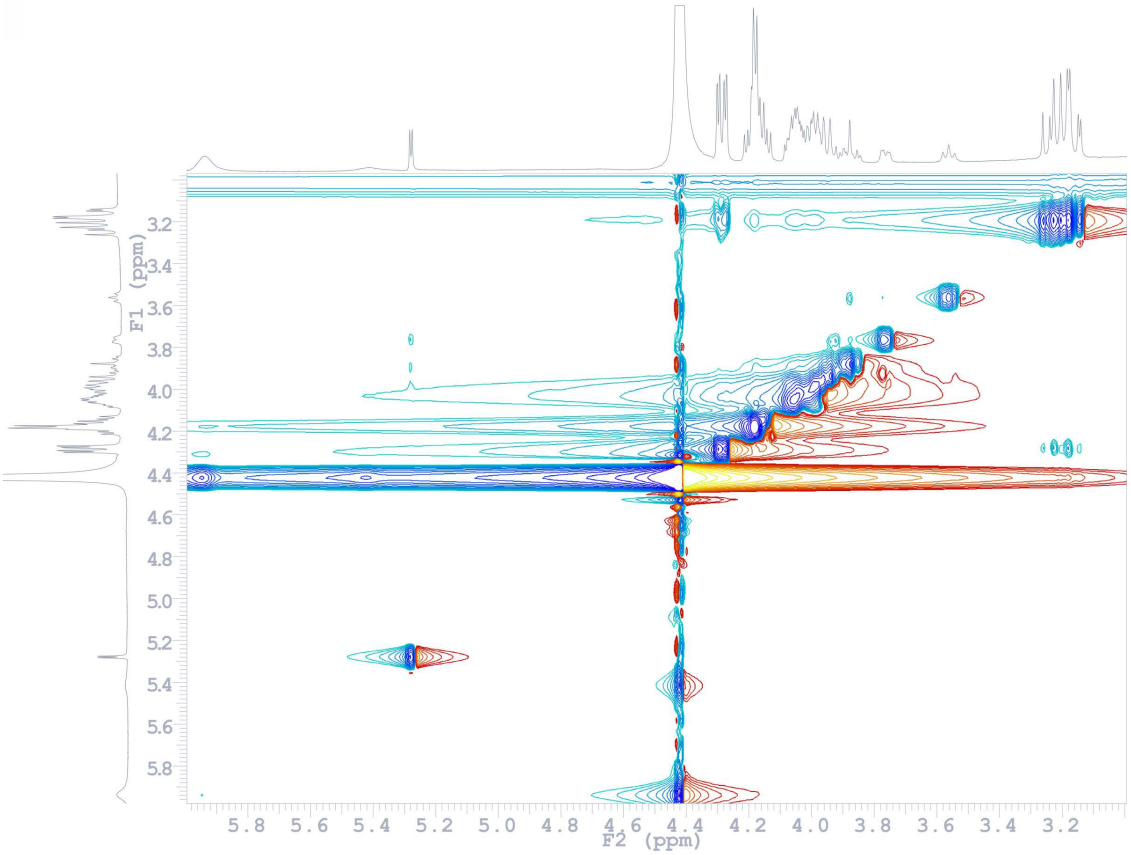

Figure 4.16: NOESY for $w_0 = 10$ trehalose loaded AOT/isooctane RM showing the same behaviors as glucose NOESY: strong water-glucose and water-AOT interactions, strong interactions between AOT 1' and the other three AOT headgroup protons that are the correct phase for AOT tumbling at the rate of the RM aggregate. Trehalose is the carbohydrate closest to having interesting NMR spectroscopy, as the two hydroxyl peaks present are sharp and well defined. If trehalose were the first carbohydrate studied, it may have been the impetus for the exchange studies in the next chapter.

4.A Appendix

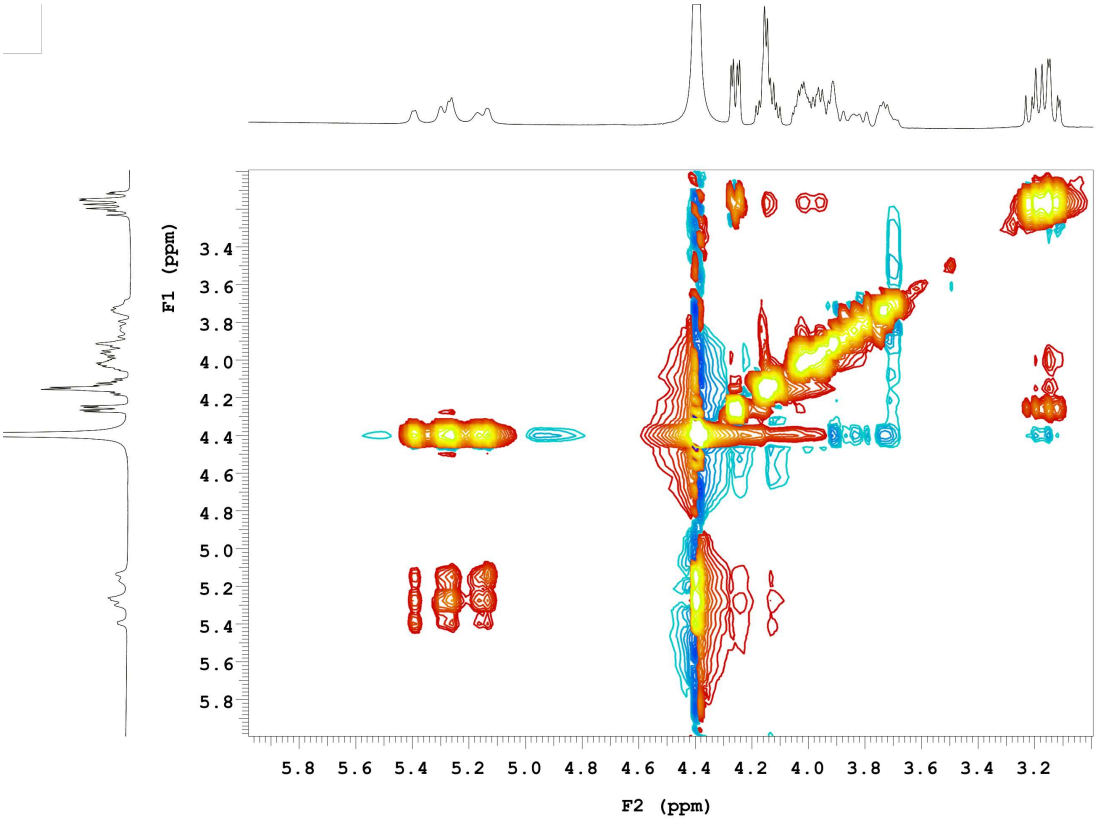

Figure 4.17: NOESY for $w_0 = 10$ sorbitol loaded AOT/isooctane RM showing the same behaviors as glucose NOESY: strong water-glucose and water-AOT interactions, strong interactions between AOT 1' and the other three AOT headgroup protons that are the correct phase for AOT tumbling at the rate of the RM aggregate.

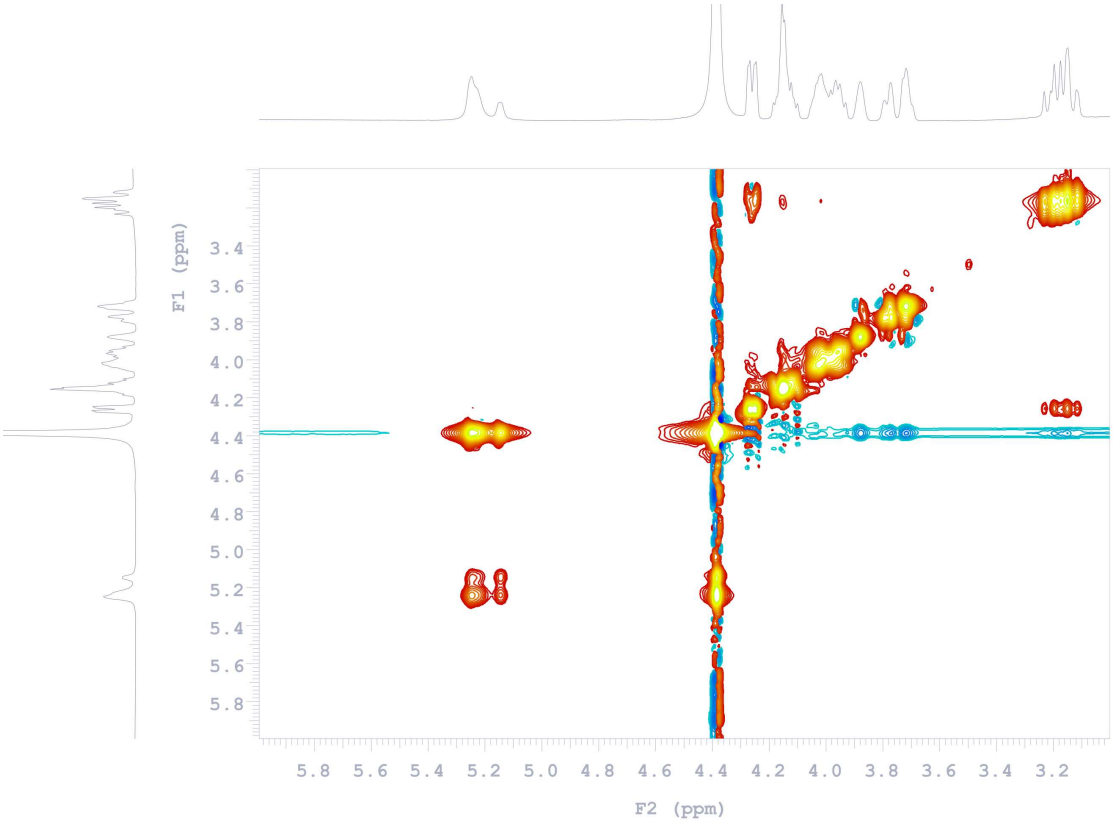

Figure 4.18: NOESY for $w_0 = 10$ xylitol loaded AOT/isooctane RMs showing the same behaviors as glucose NOESY: strong water-glucose and water-AOT interactions, strong interactions between AOT 1' and the other three AOT headgroup protons that are the correct phase for AOT tumbling at the rate of the RM aggregate.

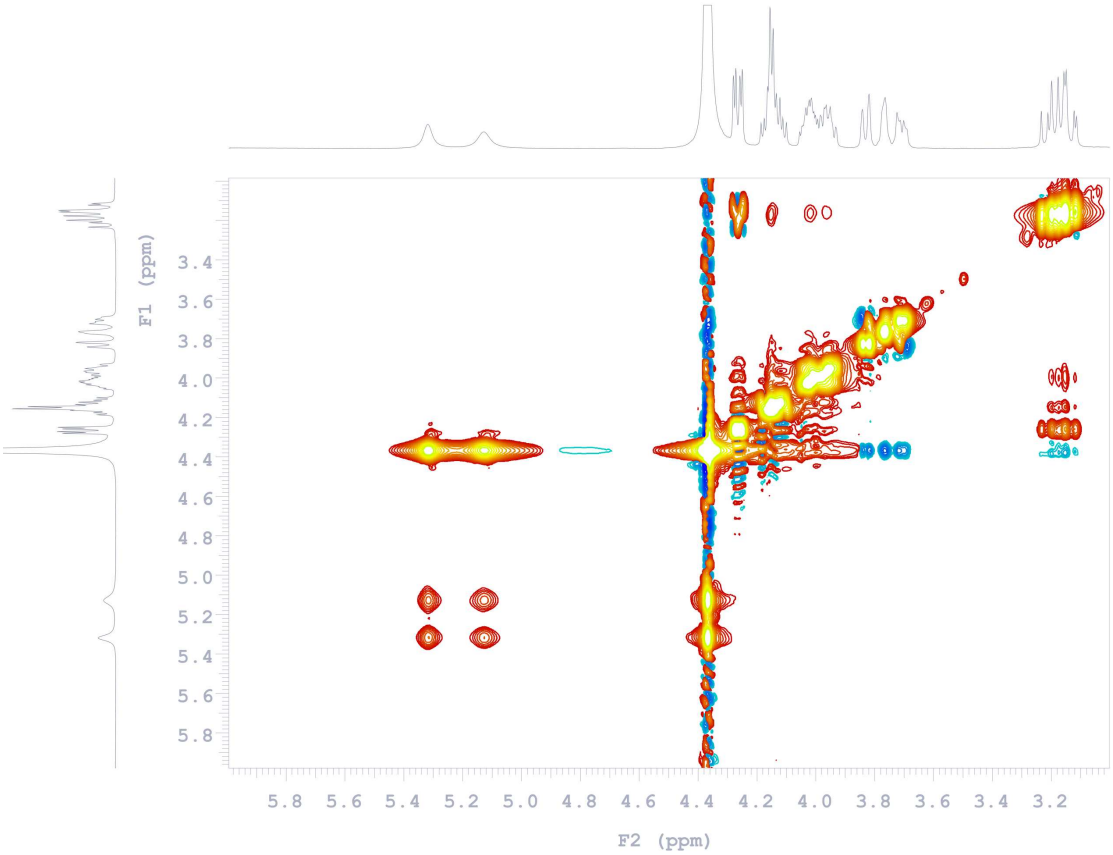

Figure 4.19: NOESY for $w_0 = 10$ erythritol loaded AOT/isooctane RM showing the same behaviors as glucose NOESY: strong water-glucose and water-AOT interactions, strong interactions between AOT 1' and the other three AOT headgroup protons that are the correct phase for AOT tumbling at the rate of the RM aggregate.

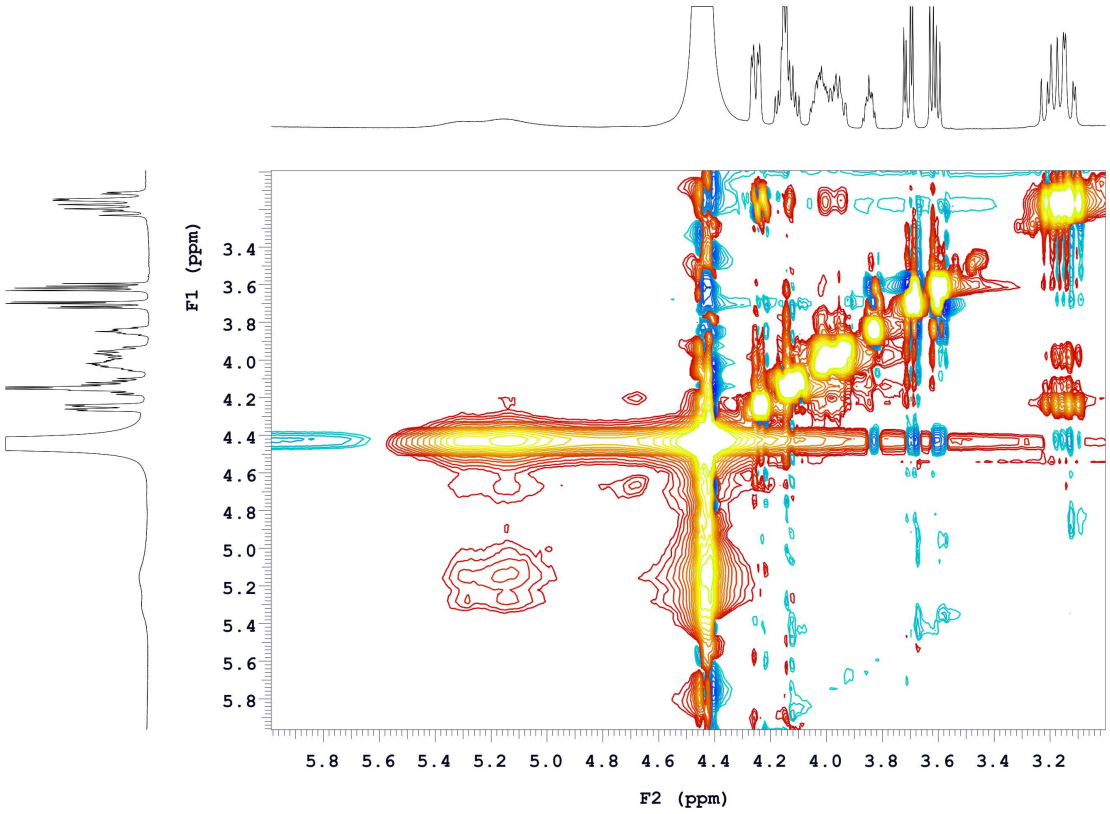

Figure 4.20: NOESY for $w_0 = 10$ glycerol loaded AOT/isooctane RM showing the same behaviors as glucose NOESY: strong water-glucose and water-AOT interactions, strong interactions between AOT 1' and the other three AOT headgroup protons that are the correct phase for AOT tumbling at the rate of the RM aggregate.

Chapter 5

The Case of Carbohydrate Hydroxyl Exchange in Reverse Micelles

5.1 Introduction

Parts of this chapter have been published in the Journal of Physical Chemistry Letters under the title "Nanoconfinement's Dramatic Impact on Proton Exchange between Glucose and Water"[1]. Coauthors on the paper contributed to discussions and text but all experiments and analysis were performed by me.

This series of experiments were sparked by the extremely surprising response in NMR spectra we observed from the hydroxyl protons on glucose encapsulated in AOT RMs (structures in fig 5.1). While glucose hydroxyl groups in aqueous glucose solution are essentially undiscernable in ^{1}H NMR due to proton exchange with water, glucose hydroxyls become clear and distinct when glucose is encapsulated in AOT RMs (fig 5.2). This effect arises due to slow down in proton exchange between water and glucose, a behavior usually only observed with changes in temperature[2], pH[3], or solvent[4]. Chemical exchange represents one of the earliest processes studied using magnetization transfer NMR methods[5], and the opportunity to measure chemical exchange in a previously unexplored environment is exciting. Here, exchange is tracked via experimentally induced perturbation of a particular spin magnetization which propagates through the network of various couplings present in a chemical system, resulting in disturbance of distant yet coupled spins. Application of this method has elucidated structures and structural fluctuations in biochemical systems and is often termed ZZ-exchange, ZZ-spectroscopy, or EXSY (EXchange SpectroscopY.[6] In the case of glucose and water exchange, proton coupling arises through the mass exchange of protons from the water reservoir to the far smaller reservoir of glucose hydroxyl protons. The systems' spins are prepared so that only the water protons are polarized and aligned parallel or anti-parallel

to the magnetic Z-axis; these spin polarized water hydroxyl protons exchange with glucose hydroxyl protons transferring polarization that is observed in the resultant NMR spectra. Analysis of the glucose signal amplitude reveals chemical exchange rates for water hydroxyl with individual glucose hydroxyl groups.

In the study reported here, I have encapsulated aqueous D-glucose, sorbitol, and trehalose in AOT RMs (fig 5.1), which allows exploration of the effect of a confined environment on carbohydrate-water exchange. Additionally, I have encapsulated aqueous glucose in benzyl-hexadecyl-dimethylammonium chloride (BHDC) RMs. In contrast to AOT, the BHDC polar headgroup is cationic and unable to form hydrogen bonds with carbohydrates, allowing comparison of the effects of confinement and confinement plus hydrogen bond formation that is possible with the AOT headgroup. I present results from a series of 1D-EXSY NMR experiments that measure the rate of chemical exchange between water molecules and carbohydrate hydroxyl groups in the water pool of AOT and BHDC RMs. Results from these experiments demonstrate that the exchange rate between water and carbohydrate hydroxyl groups is substantially slower than it is in bulk aqueous solution and that it does not depend on hydrogen bonding between the carbohydrate and surfactant headgroup.

5.2 Experimental Methods

5.2.1 Materials

Aerosol OT (AOT, sodium bis(2-ethylhexyl)sulfosuccinate, sodium docusate, $\geq$99%), isooctane (2,2,4-trimethylpentane, ACS grade), cyclohexane-d_{12} (99.6 atom % D), benzene , BHDC and the carbohydrates, that is, D-glucose, sorbitol, and trehalose, were all obtained from Sigma-Aldrich and were used as received. Millipore filtered and deionized water (18.2 MΩ-cm resistivity) was used throughout. All glassware was rinsed with 5 M HNO_3 solution. DMSO and DMSO-$d_6$were from Aldrich.

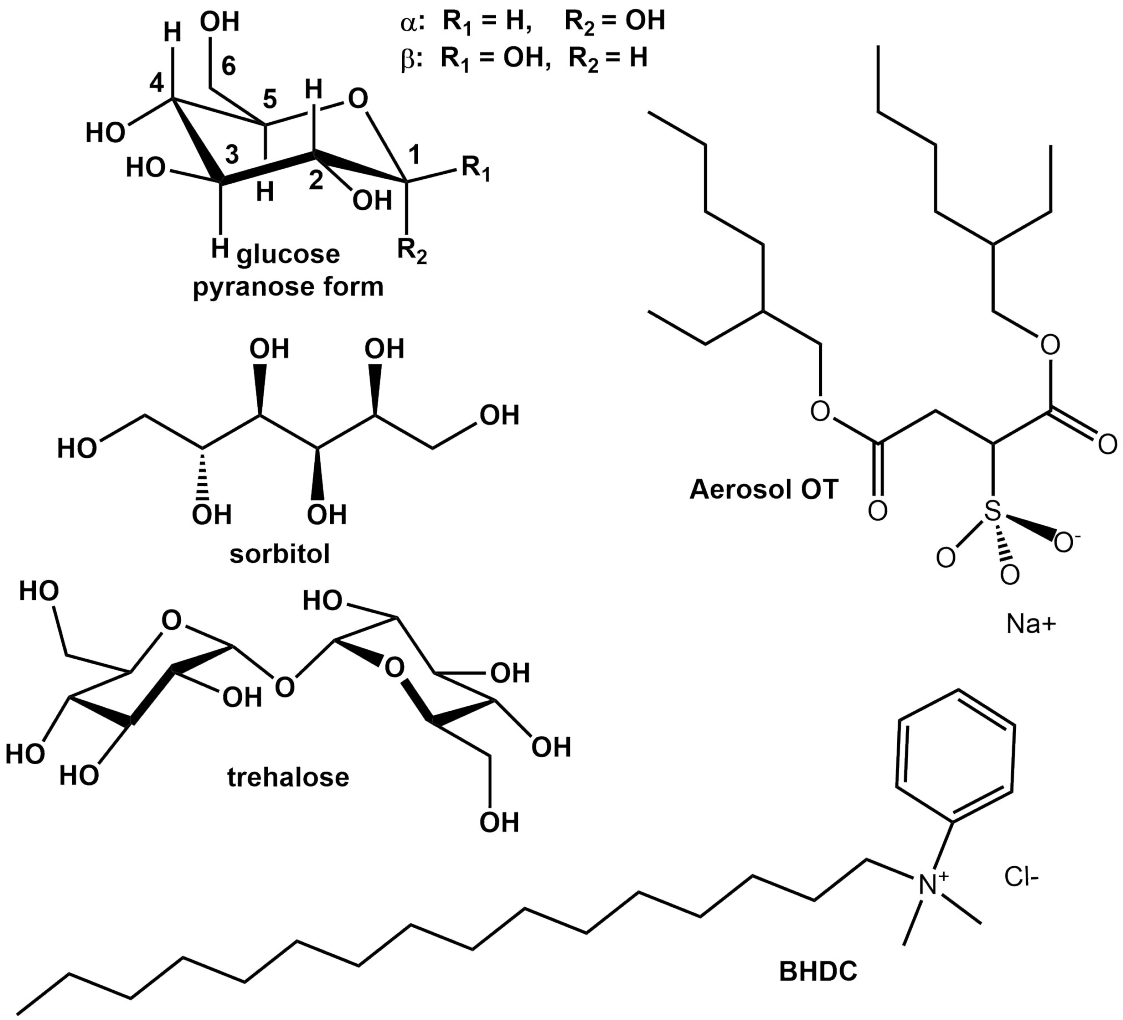

Figure 5.1: Chemical structures of the carbohydrates D-glucose, trehalose, and sorbitol as well as the surfactants AOT and BHDC. Numeric labels on glucose are used to identify signals in NMR spectra.

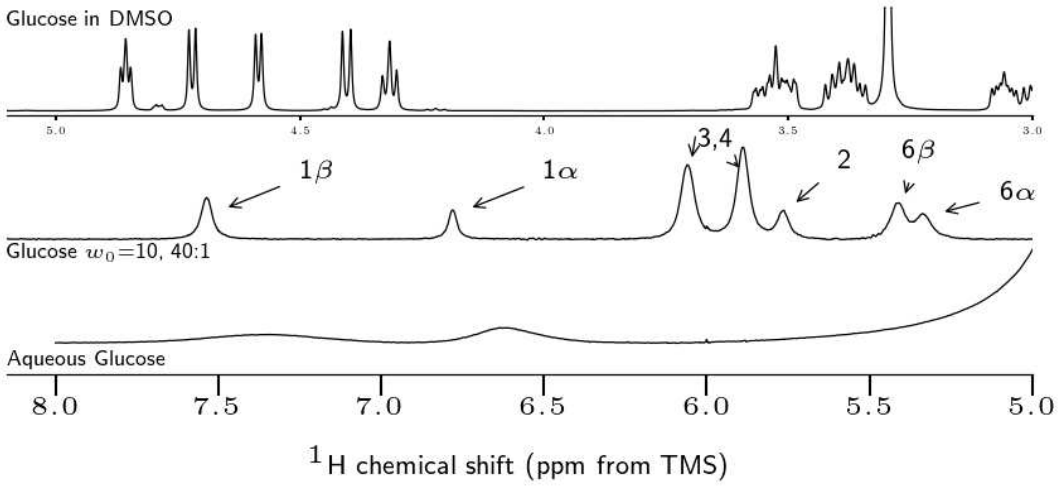

Figure 5.2: Comparison of glucose 1D-EXSY in bulk aqueous solution, encapsulated in a w_0=10 AOT RM, and in DMSO. This allows comparison of glucose in fast (AQ), slow (RM), and negligible (DMSO) exchange environments. Labels refer to hydroxyl protons according to the scheme in figure 5.1. Labels α and β designate signals arising from D-glucose α and β anomers. Hydroxyl 3 and 4 cannot be distinguished due to overlap. Integrated intensities suggest that 3,4 upfield peak obscures an additional peak associated with hydroxyl group 2. To my knowledge this is the first time individual glucose hydroxyl groups have been observed and labeled in a room temperature aqueous environment.

5.2.2 Sample preparation

Reverse micellar solutions were prepared by adding the required masses of AOT or BHDC and water to a volumetric flask and then adding a 10% cyclohexane-d_{12}/90% isooctane mixture to the final volume (e.g., 0.220 g AOT and 0.090 g H_2O for 5.00 mL of w_0=10 with [AOT]=0.10 M). The mixture was sonicated for 30-60 minutes until all solid surfactant had dissolved and no turbidity was visible. The addition of glucose was performed by adding the required mass of D-glucose into a vial and then adding reverse micelle solution by volume (e.g., 0.050 g glucose and 10 mL solution resulting in [D-glucose]$_{bulk}$ = 0.028 mM, [D-glucose]$_{RM}$ = 1.5 M, 40:1 H_2O:glucose ratio). The resulting solution was sonicated for 30-60 minutes and inspected for residual glucose or other precipitate. A 40:1 ratio was also used for sorbitol. Because trehalose is a disaccharide of glucose, an 80:1 mole ratio was used to maintain a similar H_2O:saccharide unit ratio to the a 40:1 H_2O:glucose or sorbitol ratio used in other experiments. The 40:1 ratio was chosen due to w_0=5 RMs being unable to support a higher glucose loading. w_0=10 and 20 RMs were also prepared

with a 30:1 ratio and data collected for these samples is presented. Aqueous solution was prepared with a 30:1 H_2O:glucose ratio by mixing 1.0 g of D-glucose with 3.0 g of 10% D_2O/H_2O and stirring until the D-glucose was fully dissolved. Acid and base catalyzed samples were prepared similarly to aqueous solution, except aqueous solutions of 0.01 M H_2SO_4 (pH ~ 2) and 0.05 M NaOH (pH ~ 12.7) were used instead of Millipore water. The pH of these solutions was estimated from the acid/base concentration. The acidity/basicity inside the reverse micelles differs slightly from the stock solutions used due to the nature of the reverse micelle interior[7].

5.2.3 NMR methods

All NMR experiments on aqueous and reverse micelle samples prepared with neutral water were performed on an Inova spectrometer (Varian, Inc., Palo Alto, CA) running VNMRJ software (version 4.2) and operating at 11.75 T (500 MHz for ^{1}H). Reverse micelle samples prepared with acid and base were measured using an Inova spectrometer operating at 400MHz for ^{1}H running VNMRJ software (version 4.2). The proton spectrum of aqueous glucose was a fully relaxed Bloch decay. After standard tuning and lock/shim procedures were performed, each sample was subjected to a series of NMR experiments. First, a standard 1D ^{1}H NMR spectra were collected and inspected for appropriateness (presence of glucose and AOT peaks with reasonable S/N). The 1D-EXSY experiments were performed utilizing the 1D NOESY pulse program that depends on the double pulsed field gradient spin echo (DPFGSE) to provide selective excitation of the water signal at 4.5 ppm with a 0.15 ppm (75 Hz) bandwidth and with the ZQ filter[8] disabled to allow access to short (sub 20 ms) mixing times. The mixing time for the series of EXSY spectra was systematically varied from 2 to 200 ms (2, 4, 6, 8, 10, 12, 14, 16, 18, 20, 30, 40, 50, 100, 150, 200 ms). All spectra presented here were the result of coadding 256 transients (16384 complex points) with a recovery time of 2 s. All chemical shifts are reported with respect to TMS (0.0 ppm) based on substitution from cyclohexane-d_{12} (reverse micelle), DMSO-d_6 (DMSO), or D_2O (AQ). All NMR experiments were performed at 25.0 °C on the 500 MHz spectrometer and ambient temperature on the 400 MHz.

5.2.4 Data analysis:

ACD/NMR Processor Academic Edition[9] was used to process all data. Each FID was zero filled 32768 points and apodized with a one Hz exponential weighting function. Following Fourier transformation, each spectrum was individually phased and baseline corrected. Then, each EXSY spectrum was analyzed as follows: Each NMR signal corresponding to a glucose hydroxyl proton (seven in all) was fit with a combination Gaussian-Lorentzian function with variable amplitude, width, position and shape. The estimated spectral parameters were combined to obtain the area for each signal. All signals including those lacking baseline separation (e.g., peaks 3,4 (upfield and downfield), 2, as well as 6α and 6β) were fit. For the w_0=20 data baseline separation was too poor to produce robust fit parameters so numeric integration was used instead. Sorbitol peaks had no baseline separation whatsoever and were integrated as a single unit. The kinetics regression analysis was performed with custom in-house written code using the SciPy[10] implementation of the Python programming language with the LMFIT module.[11]

5.3 Results

5.3.1 EXSY Measurement of Proton Exchange

While it was qualitatively easy to see that exchange was slowed, I wanted to measure exactly how much it was slowed by. Enter EXSY as a method of obtaining quantitative proton exchange rates; representative data are shown in figure 5.3. Here, a series of EXSY traces show hydroxyl signal strength growing in as more polarized water protons exchange onto carbohydrate hydroxyls. While the representative trace presented is of glucose in a w_0=10 AOT RM, the other systems interrogated differ only in the specifics of the NMR spectra (fig 5.4) and the rate at which peaks "grow in". Integrating the area beneath each peak allows me to produce a kinetic plot using signal intensity as an indicator of concentration as shown in figure 5.5. The resulting kinetic response of the exchange process fits well to a two-step kinetic model, equation 5.1a,

$$HOH^{\star} + COH \underset{k_{-1}}{\overset{k_1}{\rightleftharpoons}} HOH + COH^{\star} \overset{k_2}{\rightarrow} HOH + COH \tag{5.1a}$$

where $HOH^{\star}$ indicates the spin labeled water hydroxyl, $COH^{\star}$ refers to the spin excitation transferred onto a carbohydrate hydroxyl group through chemical exchange, and COH indicates the carbohydrate hydroxyl group before any polarization transfer as well as following T_1 NMR relaxation with rate constant $k_2 = \frac{1}{T_1}$. Assuming that $k_{-1} \ll k_1$, based on the carbohydrate pK_a ranging between12 and 14[12],equation 5.1a simplifies to equation 5.1b and the kinetic equation describing the generation of $COH^{\star}$ in equation 5.1b is represented by eq 5.2:

$$HOH^{\star} + COH \overset{k_1}{\rightarrow} HOH + COH^{\star} \overset{k_2}{\rightarrow} HOH + COH \tag{5.1b}$$

$$[COH^{\star}] = \frac{k_1}{k_2 - k_1} [COH]_0 \left(e^{-k_1 t} - e^{-k_2 t}\right) + C \tag{5.2}$$

where k_1 and k_2 are rate constants from equation 5.1b, $[COH]_0$ is the initial D-glucose reservoir available to accept polarization transfer, and C is a constant offset associated with the solution to the differential kinetic equation that gives us the rate law. As $k_1 \gg k_2$ i.e. $\left(k_{ex} \gg \frac{1}{T_1}\right)$ for the systems studied here, the regression analysis using this technique is very robust. Kinetic parameters extracted from regression fits appear in table 5.1. Because the exchange in aqueous solution occurs in the fast exchange regime ($k_{AQ} > 1500 s^{-1}$), quantitative rate constants for aqueous solutions are not measurable via EXSY. While the kinetic analysis method presented above references glucose, it is not specific to glucose and can be applied to other carbohydrates, such as sorbitol and trehalose (included in table 5.1).

5.3.2 Qualitative Results and Linewidths

While quantitative measurement of exchange rates is obviously preferred to qualitative data, the only reason I was led to make quantitative EXSY measurements of proton exchange for carbohydrates encapsulated in RMs was due to the qualitative observation that chemical exchange between water and glucose hydroxyl protons must be slowed; glucose peaks normally made undetectable

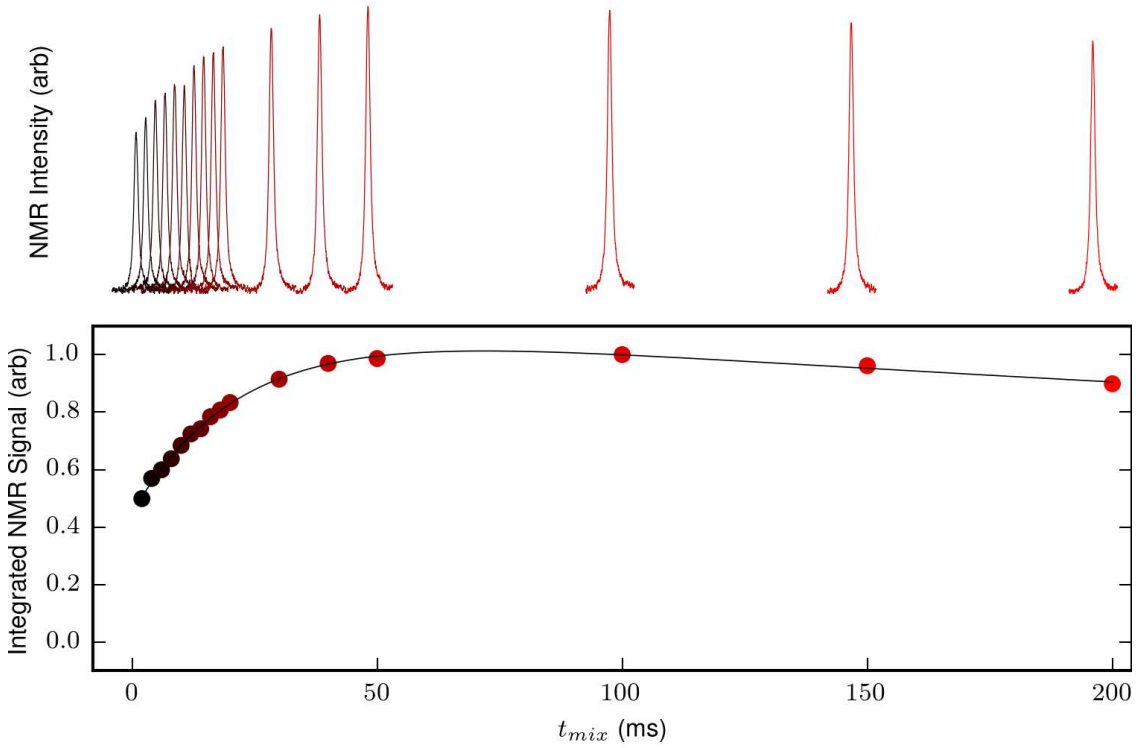

Figure 5.3: Top: Series of 1D-EXSY spectra for the 1β hydroxyl of D-glucose in w_0 =10 AOT RMs with varying t_{mix}. Showing the NMR signal intensity growing in as protons exchange from water onto glucose, and decaying away due to T_1 relaxation. Bottom: Integration of each of these peaks produces a kinetic trace similar to concentration vs time kinetic plots, which can be analyzed to determine exchange rate constants. This is a representative series, sorbitol, trehalose, and glucose in BHDC EXSY data are all similar.

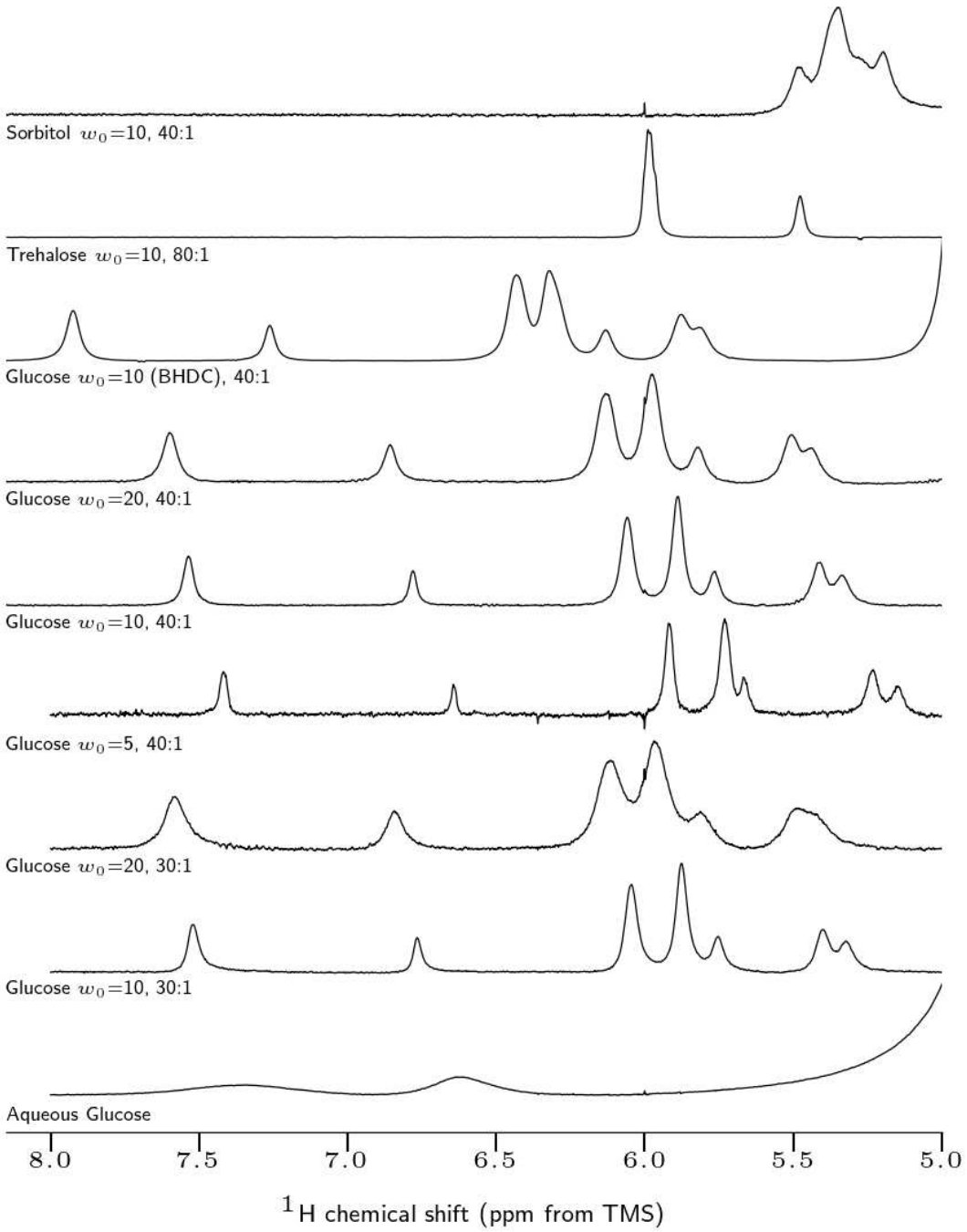

Figure 5.4: 1D-EXSY spectra (t_{mix}=14 ms) for all carbohydrate loaded RM solutions studied as well as aqueous glucose solution. This figure allows comparison of glucose behavior through different AOT RM sizess (5, 10, 20) as well as 30:1 and 40:1 water:glucose ratios in w_0 =10 and 20. It also shows the disacccharide trehalose, sugar alcohol sorbitol, and glucose in a $w_0 = 10$ BHDC RM, which cannot form h-bonds to glucose.

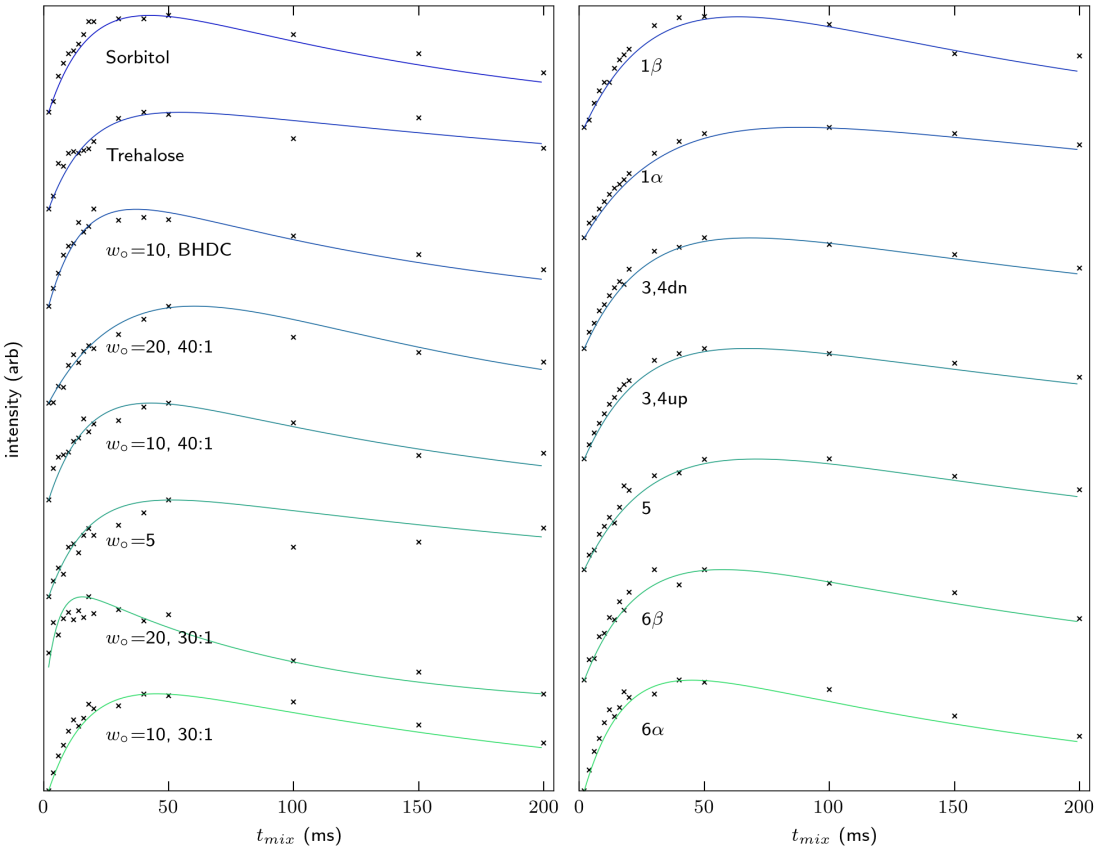

Figure 5.5: Left: Kinetic plot of most downfield peak for each carbohydrate sample (points) and regression fit (lines)
Right: Kinetic plots of all peaks for $w_0 = 10$ RM with 40:1 water:glucose ratio
Kinetic traces are normalized and offset to aid visualization.

Table 5.1: Water-Glucose Exchange Rates[a]

Exchange rate (s^{-1}) of glucose hydroxyls in reverse micelles with w_0						
hydroxyl	5[b]	10[b]	10[c]	20[b]	20[c]	10 (BHDC)[c]
6α	26 ± 3[d]	66 ± 16	49 ± 5	86 ± 8[e]	200 ± 90[e]	98±12
6β	16 ± 4	82 ± 10	38 ± 2			111±14
2	47 ± 6	71 ± 8	51 ± 4	68 ± 9	42 ± 44	87±18
3,4up	49 ± 5	54 ± 1	56 ± 1	75 ± 2	112 ± 7	68±3
3,4dn	22 ± 16	56 ± 3	49 ± 8	77 ± 3	115 ± 11	75±2
1α	27 ± 9	33 ± 2	49 ± 5	61 ± 5	85 ± 8	45±2
1β	81 ± 27	45 ± 2	49 ± 5	92 ± 12	138 ± 21	68±3
Trehalose dn[f]			28±1			
Trehalose up			20±2			
Sorbitol[g]			90±9			

[a]All rates refer to exchange between water and the identified carbohydrate hydroxyl group.
[b]40:1 water:carbohydrate ratio
[c]30:1 water:carbohydrate ratio
[d]errors represent ± one standard deviation.
[e]w_0=20 6α and 6 are integrated as a single peak.
[f]Trehalose was prepared at an 80:1 ratio, considered equivalent to a 40:1 ratio for a monosaccharide
[g]Due to complete lack of baseline separation, all sorbitol peaks were integrated as one

through exchange broadening and coalescence became distinct and identifiable when glucose was encapsulated in a RM. This exchange broadening behavior can be understood through the relationship between the exchange rate constant, k, and the NMR frequency difference between the exchanging species, F. There are two distinct exchange regimes, and an indistinct limnal region between them[13]. These regimes are:

- If both species are well defined, then exchange is slow and $k \ll F$
- If there is only one well-defined peak at the weighted average of both species, exchange is fast and $k \gg F$
- If the peaks are poorly defined with little baseline separation, then $k \approx F$

These regimes, and the transition between them, can be understood from figure 5.6 when compared to figure 5.2. In figure 5.2 I can instantly see that the distinct hydroxyl signals for RM encapsulated glucose put their exchange rate in the slow $(k \ll F)$ exchange regime while the extremely

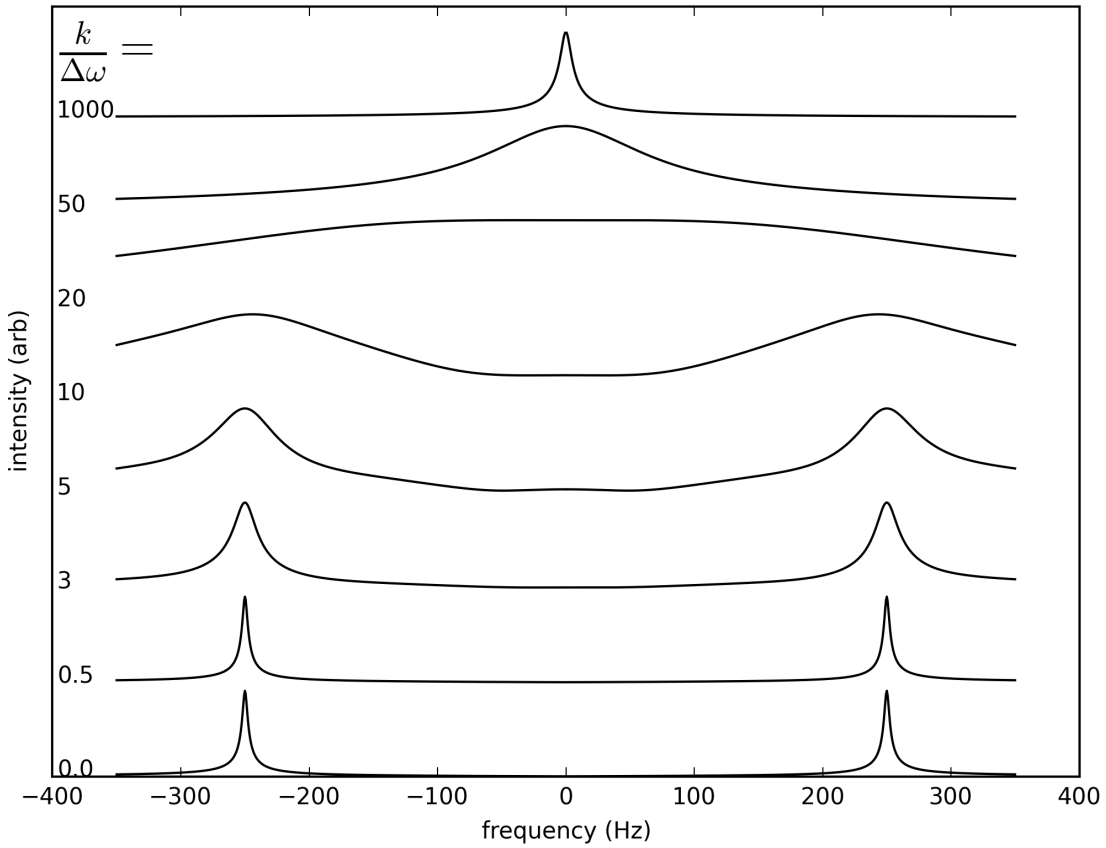

Figure 5.6: Broadening and coalescence of two exchangeable peaks as exchange rate increases from $k \ll F$, through $k \approx F$, up to $k \gg F$.

indistinct aqueous glucose hydroxyl peaks suggests that they are in fast exchange, with the slight visibility meaning they are probably at the fast edge of the limnal zone ($k \gtrapprox F$). As I know the frequency difference between all species in the NMR trace (1 ppm = 500 Hz for a 500 MHz spectrometer), I can put bounds on the maximum exchange rate for glucose in RMs and the minimum exchange rate for aqueous glucose. The frequency difference, F, between water and peak 1β is 1500 Hz, meaning aqueous glucose must exchange at a rate $k \gtrapprox 1500\ s^{-1}$, a value completely in agreement with literature values for aqueous carbohydrates and carbohydrate derivatives of around $2000\ s^{-1}$[12,14]. The minimum value for F is 400 Hz between water and 6α, giving an estimate exchange within an RM of $k \ll 400\ s^{-1}$. Again, this value is completely in agreement with exchange rates between 20 and 200 s^{-1} measured via EXSY.

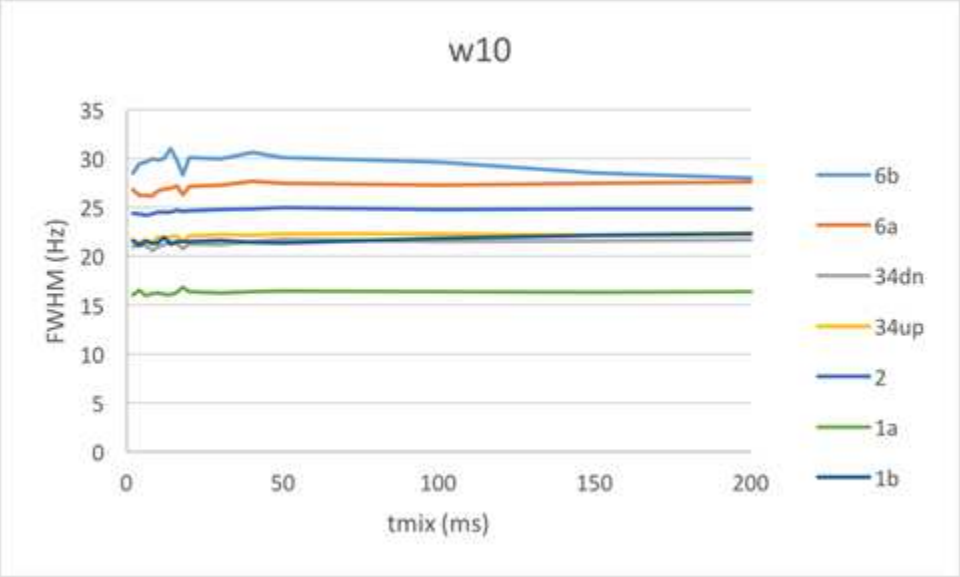

Figure 5.7: Linewidths of the hydroxyl peaks for $w_0 = 10$ during the EXSY experiment, the linewidths are constant over the experiment duration, showing that exchange is constant.

Figure 5.6 implies that NMR linewidths can be used to determine exchange rates. This is true, but unfortunately there are more contributions to line broadening than chemical exchange[13]. T_2 is constant during the entirety of an NMR experiment (a reasonable assumption, as the system is at equilibrium), then. Any change in linewidth over the course of the experiment can be attributed to a change in exchange rate. As can be seen in fig 5.7, the proton exchange rate is constant over the course of the EXSY experiment, meaning I am probing a constant exchange process and not initiating exchange via EXSY excitation. Figure 5.8demonstrates a qualitative agreement with the exchange rates observed via EXSY: that is that exchange is faster in larger RMs than in smaller ones.

5.4 Discussion

There are three mechanisms of proton exchange between water and carbohydrates: acid catalyzed, base catalyzed, and concerted. In the presence of acid or base, charge transfer catalyzes proton exchange between water and glucose resulting in rate constants far in excess of 10,000 s^{-1} at pH of 3 or 9.[3] At neutral pH the primary mechanism is concerted exchange, in which two water molecules that are part of the larger water network act in concert, one water molecule donating a

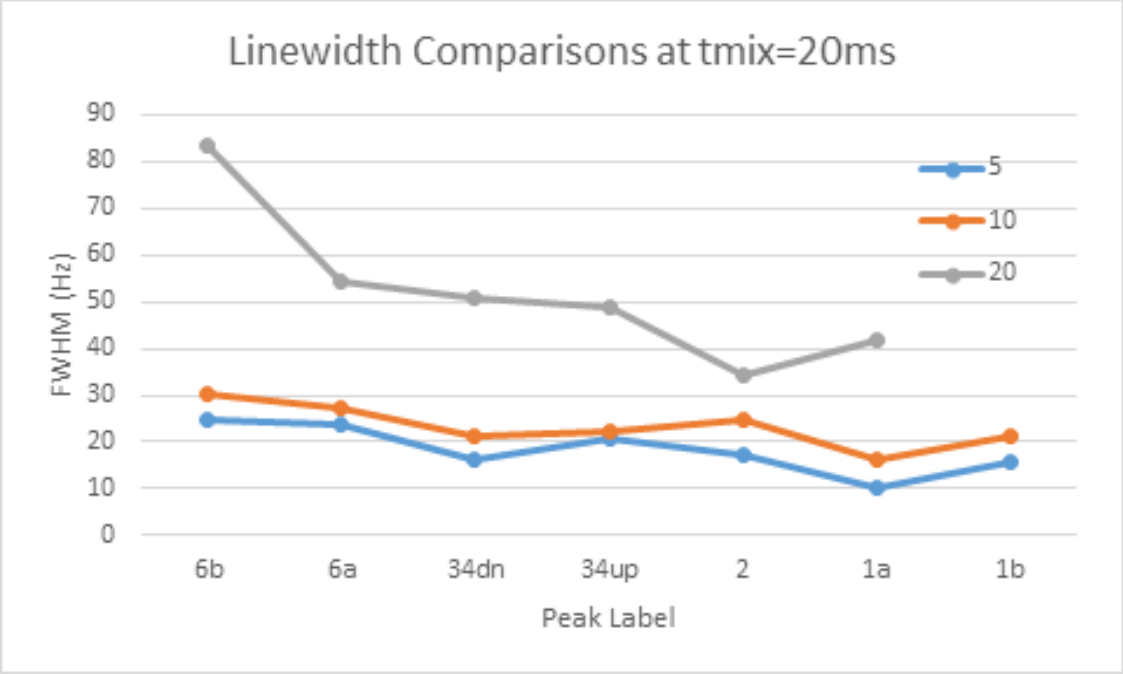

Figure 5.8: Linewidths of each hydroxyl peak for glucose in w_0= 5, 10, 20 AOT RMs at $t_{mix} = 20$ ms. the linewidths for 5 and 10 are similar, while $w_0 = 20$ RMs have consistently broader peaks. This is due to the increase in exchange rate as RMs get larger and confinement is lessened.

proton to glucose while a second water molecule simultaneously accepts a proton from glucose[14] as depicted in Fig. 5.10. The rate constants we report here arise primarily due to the concerted exchange mechanism in neutral pH RMs. As shown in Fig. 5.9, the 1D ^{1}H NMR spectra of w_0=10 glucose loaded RMs catalyzed with acid (H_2SO_4) and base (NaOH) have glucose alcohols in full coalescence with water, indicating that if these were significant contributers to exchange in neutral RMs we would not observe such slow exchange rates. Because the neutral exchange mechanism requires at least three species to act in concert (donor water, acceptor water, and glucose hydroxyl) and with specific geometry, any translational or rotational limitations on water molecules will inhibit the rate at which water molecules move into the proper intermediate position for exchange. Additionally, this demonstrates that glucose in RMs is *capable* of fast exchange, demonstrating that glucose and water are in contact with each other. This further rules out positions ③, ④, and ⑤ from Fig. 4.1 in Ch. 4.

The mobility of water molecules, especially water translation, shows significant difference between the RM environment and bulk water. Studies have shown that water translation is restricted

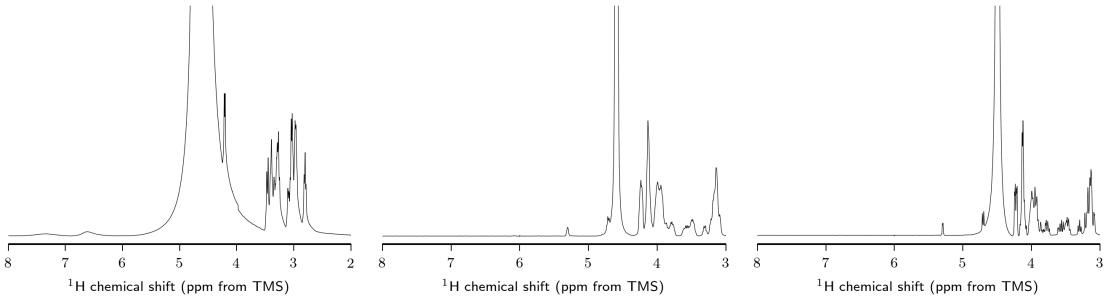

Figure 5.9: 1D H-NMR of glucose in neutral aqueous (left), acidic (middle), and basic (right) RMs. The extreme similarity of these three spectra illustrates that all have a similar exchange rate. In fact, the slight visibility of glucose hydroxyls in the aqueous spectrum shows that acid and base catalyzed exchange in RMs is, in fact, significantly faster than the concerted mechanism in bulk neutral solution.

both in aqueous carbohydrate solutions[15]and in RMs.[16] Previously, the Levinger group has found a 5-fold decrease in water translational motion in RMs through experiments and simulations of quasielastic neutron scattering.[16] This dramatic reduction in translational motion appears to lead to a similarly dramatic reduction in exchange rate. Additionally, the concerted exchange mechanism requires participation by the entire water network to move H-atoms, rather than protons, along a "water wire". It appears that the confined geometry of a RM interferes with this “water wire” formation, potentially through specific interactions of water molecules with glucose hydroxyl groups, and disrupts the 3D water network responsible for proton transfer.[17–20] Our results may indicate that the water network in aqueous solution extends significantly further than the diameter of a reverse micelle.

I considered a few different explanations to account for slowed exchange between carbohydrate and water hydroxyl groups, such as differences in ionic strength, or glucose and water being separated from each other, and glucose inserting into the aliphatic region and being shielded from contact with water at all. But the two most reasonable ones that I will consider are confinement effects on the exchange mechanism or adsorption of glucose to the interior interface changing hydroxyl chemistry and water access to hydroxyl groups. Reports of saccharides adsorbing to phospholipid monolayer[21], bilayer[22], and vesicle[23] surfaces have appeared in the literature which suggest that adsorption of glucose on AOT headgroups could account for the slow exchange rates I observe. However, if glucose adsorbed to the surfactant interface in the RMs we have measured,

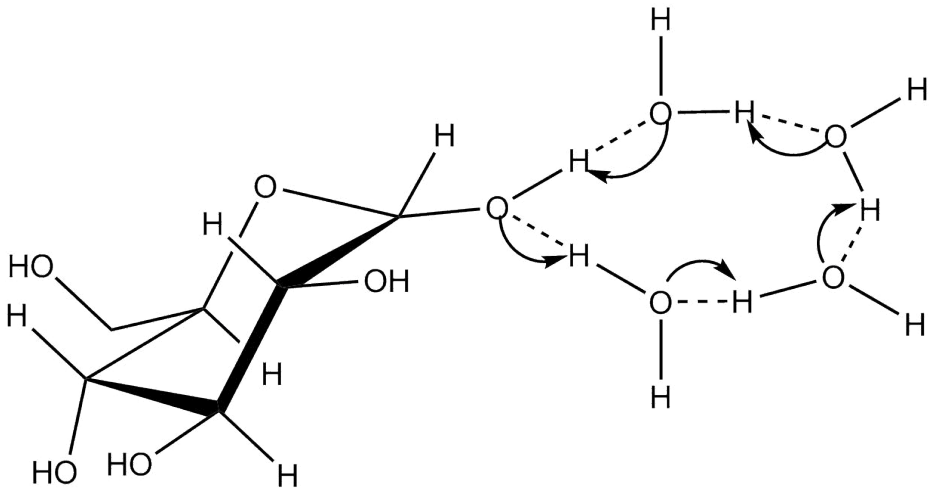

Figure 5.10: . The concerted exchange mechanism betwen water and a carbohydrate hydroxyl group.

we would expect little to no dependence of the exchange rate on w_0, which is inconsistent with the data in figure 5.4 and table 5.1. Furthermore, the environments probed in these reports are drastically different from the RM systems reported here. As an example, the monolayer, bilayer, and vescicle studies are all concerned with structures much (at least 20x, and usually more than 200x) larger than RMs. They are also studies of surfactants suspended in a polar phase of sugar solution, and are specifically probing the interface looking for adsorbed saccharides. This means they will observe adsorption to the surface if even one in a thousand sugars adsorbs, and will ignore the much larger population of free saccharide in solution.

A study by Silva et al. measured UV-vis absorption spectra of phenol compounds in AOT and BHDC RMs[24], observing that phenol ionization was inhibited in AOT RMs but not BHDC RMs. As AOT is capable of hydrogen bonding with phenol while BHDC is not, they interpreted inhibition of phenol deprotonation as evidence for phenol hydroxyl binding to the AOT polar headgroups. Significant differences exist between our work and that presented by Silva et al. For example, the concentration of the phenol probes in these experiments is $\sim 1 \times 10^{-4}$ M, or approximately one phenol for every 40 reverse micelles. At this concentration observing all the phenol molecules bound to the reverse micellar surface is significantly more likely than it would be for those presented here which contain at least 100-fold more glucose (between 1.210 and 0.17 M, depending

on w_0) with multiple glucose molecules per reverse micelle. The phenol compounds also have much lower solubility in water and much higher solubility in nonpolar solvents compared to glucose; only one hydroxyl group per phenol compared to five hydroxyls on each glucose. If glucose exchange in RMs were dominated by hydrogen bonding, I would expect far slower or no exchange of glucose hydroxyl groups. In contrast, I measured rate constants of 20-200 s^{-1}. Additionally BHDC RMs would show no exchange slowing because there is no opportunity for hydrogen bonding. Yet the exchange rate for glucose in BHDC RMs is only slightly faster than that in AOT RMs. Thus, I reject hydroxyl binding to the surfactant interface as the primary mechanism responsible for the slowed chemical exchange observed for glucose in AOT RMs.

The work by Cobo Solis et al.[25] measured a marked slowdown of the acid equilibrium process for 1-naphthol in a large unilamellar vesicle bilayer formed of the novel AOT-BHD ionic liquid surfactant. Because naphthol is significantly less polar than glucose, it has likely penetrated into the lamellar bilayer and is in a significantly different environment than the glucose molecules described in our paper. Additionally, as the authors of the paper note themselves, this observation is *"in contrast to what was observed in other large unilamellar vesicle media formed from different phospholipids and in micelles formed from different non-ionic, cationic and anionic surfactants"*. As such, the work of Cobo Solis et al. cannot explain my results of slowed exchange for carbohydrates in reverse micelles.

Placing the carbohydrates glucose, sorbitol, and trehalose in the confined environment of a reverse micelle leads to a dramatic reduction in the ability of water to exchange H-atoms with carbohydrate hydroxyl groups. The effect of confinement causes chemical exchange between water and glucose hydroxyl groups to differ significantly from the same process in a bulk H_2O:glucose solution. I can estimate the effect of the confined environment is comparable to supercooling a bulk aqueous solution to -7.15 $^{\circ}$C[2] or dissolving glucose in a 4:6 H_2O:DMSO solution at -12 $^{\circ}$C[4]. There is no reason to imagine that this slowing down of hydroxyl exchange is limited to glucose, sorbitol, and trehalose. While these three carbohydrates are glucose, reduced glucose, and a dimer of glucose, they are still distinct enough forms that there is no reason to think confined

environment should have a similar effect on H-atom exchange for any labile proton, thus affecting a wide range of processes occurring in an array of nanoconfined environments including nanoporous materials, cell organelles, and membranes. The implications for this result are widespread and may address the mechanism by which carbohydrates serve as cryo- and/or lyoprotectants for biological materials.

Bibliography

(1) Wiebenga-Sanford, B. P.; DiVerdi, J.; Rithner, C. D.; Levinger, N. E. *The Journal of Physical Chemistry Letters* **2016**, *7*, 4597–4601.

(2) Bociek, S.; Franks, F. *J. Chem. Soc., Faraday Trans. 1* **1979**, *75*, 262–270.

(3) Hills, B. P. *Mol. Phys.* **1991**, *72*, 1099–1121.

(4) Vishnyakov, A.; Widmalm, G.; Kowalewski, J.; Laaksonen, A. *J. Am. Chem. Soc.* **1999**, *121*, 5403–5412.

(5) Johnson Jr., C. S. *Advan. Magn. Resonance* **1966**, *1*, 33–102.

(6) Mittermaier, A. In *Encyclopedia of Biophysics*, Roberts, G. C. K., Ed.; Springer Berlin Heidelberg: Berlin, Heidelberg, 2013, pp 2796–2797.

(7) Crans, D. C.; Levinger, N. E. *Accounts of Chemical Research* **2012**, *45*, 1637–1645.

(8) Stott, K.; Stonehouse, J.; Keeler, J.; Hwang, T.-L.; Shaka, A. J. *Journal of the American Chemical Society* **1995**, *117*, 4199–4200.

(9) Advanced Chemistry Development, I. **2010**.

(10) Jones, E.; Oliphant, T.; Peterson, P.; others, a. SciPy: Open Source Scientific Tools for Python. http://www.scipy.org.

(11) Newville, M.; Stensitzki, T.; Allen, D. B.; Ingargiola, A. LMFIT: Non-Linear Least-Square Minimization and Curve-Fitting for Python. https://zenodo.org/record/11813 (accessed 07/01/2016).

(12) Bhattacharyya, L.; Rohrer, J. S. Wiley: Applications of Ion Chromatography in the Analysis of Pharmaceutical and Biological Products - Lokesh Bhattacharyya, Jeffrey S. Rohrer. http://www.wiley.com/WileyCDA/WileyTitle/productCd-0470467096.html (accessed 10/06/2017).

(13) Keeler, J., *Understanding NMR Spectroscopy*; John Wiley Sons: New York, 2011.

(14) Harvey, J. M.; Symons, M. C. R.; Naftalin, R. J. *Nature* **1976**, *261*, 435–436.

(15) Talon, U.; Smith, L. J.; Brady, J. W.; Lewis, B. A.; Copley, J. R. D.; Price, D. L.; Saboungi, M. L. *J. Phys. Chem. B* **2004**, *108*, 5120–5126.

(16) Harpham, M. R.; Ladanyi, B. M.; Levinger, N. E.; Herwig, K. W. *Journal of Chemical Physics* **2004**, *121*, 7855–68.

(17) Luzar, A.; Chandler, D. *Nature; London* **1996**, *379*, 55.

(18) Mei, H. S.; Tuckerman, M. E.; Sagnella, D. E.; Klein, M. L. *The Journal of Physical Chemistry B* **1998**, *102*, 10446–10458.

(19) Tuckerman, M. E.; Marx, D.; Parrinello, M. *Nature; London* **2002**, *417*, 925–9.

(20) Hassanali, A.; Giberti, F.; Cuny, J.; KÃŒhne, T. D.; Parrinello, M. *Proceedings of the National Academy of Sciences* **2013**, *110*, 13723–13728.

(21) Lambruschini, C.; Relini, A.; Ridi, A.; Cordone, L.; Gliozzi, A. *Langmuir* **2000**, *16*, 5467–5470.

(22) Kapla, J.; Wohlert, J.; Stevensson, B.; EngstrÃ¶m, O.; Widmalm, G.; Maliniak, A. *The Journal of Physical Chemistry B* **2013**, *117*, 6667–6673.

(23) Roy, A.; Dutta, R.; Kundu, N.; Banik, D.; Sarkar, N. *Langmuir* **2016**, *32*, 5124–5134.

(24) Silva, O. F.; FernÃ¡ndez, M. A.; Silber, J. J.; de Rossi, R. H.; Correa, N. M. *ChemPhysChem* **2012**, *13*, 124–130.

(25) Villa, C. C.; Moyano, F.; Ceolin, M.; Silber, J. J.; Falcone, R. D.; Correa, N. M. *Chemistry â A European Journal* **2012**, *18*, 15598–15601.